

# DANISH METEOROLOGICAL INSTITUTE

## SCIENTIFIC REPORT

02-17

### Probabilistic Analysis of Atmospheric Transport and Deposition Patterns from Nuclear Risk Sites in Russian Far East

Alexander Mahura<sup>1,2,3</sup>, Alexander Baklanov<sup>1</sup>, Jens Havskov Sørensen<sup>1</sup>,  
Frank Parker<sup>2,4</sup>, Vladimir Novikov<sup>2,5</sup>,  
Kevin Brown<sup>2</sup>, Keith Compton<sup>2</sup>

<sup>1</sup> Danish Meteorological Institute, Copenhagen, Denmark

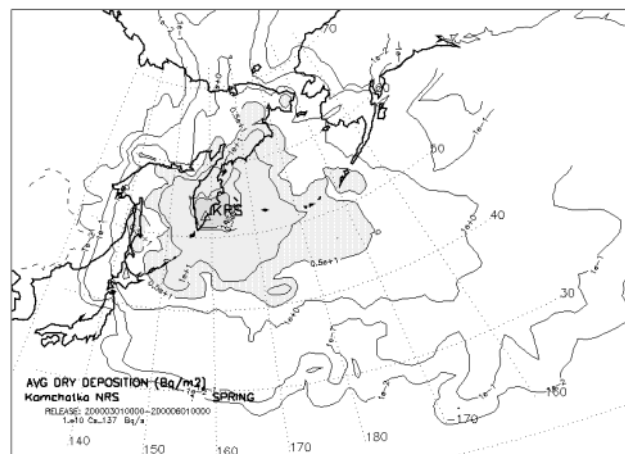
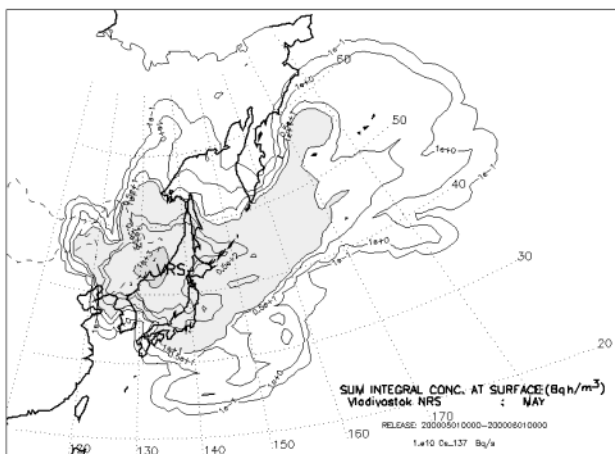
<sup>2</sup> International Institute for Applied Systems Analysis, Laxenburg, Austria

<sup>3</sup> Institute of Northern Environmental Problems, Kola Science Center, Apatity, Russia

<sup>4</sup> Vanderbilt University, Nashville, TN, USA

<sup>5</sup> Russian Research Center – “Kurchatov Institute”, Moscow, Russia

Far East Coastal Study of the Radiation Safety of the Biosphere Project  
of the International Institute for Applied System Analysis



LAXENBURG COPENHAGEN  
2002



**ISSN: 0905-3263 (printed)**  
**ISSN: 1399-1949 (online)**  
**ISBN: 87-7478-471-4**

# TABLE OF CONTENTS

<b>EXECUTIVE SUMMARY</b>	<b>2</b>
<b>INTRODUCTION</b>	<b>3</b>
<b>I. METHODOLOGICAL ASPECTS FOR PROBABILISTIC ANALYSIS OF ATMOSPHERIC TRANSPORT AND DEPOSITION PATTERNS FROM NRSs</b>	<b>5</b>
<b>1.1. APPROACHES AND RESEARCH TOOLS</b>	<b>5</b>
<b>1.2. METEOROLOGICAL DATA FOR TRAJECTORY AND DISPERSION MODELING AND COMPUTING RESOURCES</b>	<b>7</b>
<b>1.3. TRAJECTORY MODELING APPROACH</b>	<b>9</b>
<b>1.4. DISPERSION MODELING APPROACH</b>	<b>9</b>
<b>1.5. PROBABILITY FIELDS ANALYSIS FOR TRAJECTORY MODELING RESULTS</b>	<b>12</b>
<b>1.6. PROBABILITY FIELDS ANALYSIS FOR DISPERSION MODELING RESULTS</b>	<b>15</b>
<b>1.7. SPECIFIC CASE STUDIES APPROACH</b>	<b>17</b>
<b>II. ATMOSPHERIC TRANSPORT AND DEPOSITION PATTERNS FROM NRSs</b>	<b>19</b>
<b>2.1. SIMPLE CHARACTERISTICS OF THE NRS IMPACT</b>	<b>19</b>
<b>2.2. AIRFLOW AND FAST TRANSPORT PROBABILITY FIELDS</b>	<b>21</b>
<b>2.3. TYPICAL TRANSPORT TIME FIELDS</b>	<b>23</b>
<b>2.4. MAXIMUM REACHING DISTANCE AND MAXIMUM POSSIBLE IMPACT ZONE</b>	<b>25</b>
<b>2.5. PRECIPITATION FACTOR PROBABILITY FIELDS</b>	<b>28</b>
<b>2.6. NRS INDICATORS BASED ON DISPERSION MODELING: AVERAGE INTEGRAL CONCENTRATION, DRY AND WET DEPOSITION FIELDS</b>	<b>30</b>
<b>2.7. ANALYSIS OF SPECIFIC CASE STUDIES</b>	<b>39</b>
<b>CONCLUSIONS</b>	<b>46</b>
<b>RECOMMENDATIONS AND FUTURE STUDIES</b>	<b>49</b>
<b>ACKNOWLEDGMENTS</b>	<b>51</b>
<b>REFERENCES</b>	<b>52</b>
<b>APPENDIXES</b>	<b>54</b>

## EXECUTIVE SUMMARY

The probabilistic analysis is performed for atmospheric transport and deposition patterns from two nuclear risk sites (NRSs) in the Russian Far East – Kamchatka and Vladivostok. The following geographical regions of interest are considered: Japan, China, North and South Korea, territories of the Russian Far East, State of Alaska, and Aleutian Chain Islands, US. The main questions addressed are the following: Which geographical territories are at the highest risk from the hypothetical releases at NRSs? What are probabilities for radionuclide atmospheric transport and deposition on different neighbouring countries in a case of accidents at NRSs?

For analysis we applied several research tools utilized within the Arctic Risk NARP Project: 1) isentropic trajectory model to calculate a multiyear dataset of 5-day forward trajectories that originated over the site locations at various altitudes; 2) DERMA long-range transport model to simulate 5-day atmospheric transport, dispersion, and deposition of  $^{137}\text{Cs}$  for one day release (at the rate of  $10^{10}$  Bq/s); and 3) a set of statistical methods (including exploratory, cluster, and probability fields analyses) for analysis of trajectory and dispersion modeling results.

The results of trajectory and dispersion modeling are presented as a set of various indicators of the possible NRS impact on geographical regions of interest. For trajectory modeling these indicators are: 1) atmospheric transport pathways, 2) airflow probability fields, 3) fast transport probability fields, 4) maximum reaching distance, 5) maximum possible impact zone, 6) relative humidity or precipitation factor fields, and 7) typical transport time fields. Similarly, for dispersion modeling the indicators are: 1) surface air concentration, 2) integrated over time concentration at the ground surface, 3) dry deposition, and 4) wet deposition. To evaluate the temporal variability of these indicators, analyses were performed on an annual, seasonal, and monthly basis.

The results of this study are applicable for: (i) better understanding of general atmospheric transport patterns in the event of an accidental release at NRS, (ii) improvement of planning in emergency response to radionuclide releases from the NRS locations, (iii) studies of social and economical consequences of the NRS impact on population and environment of the neighbouring countries, (iv) multidisciplinary risk evaluation and vulnerability analysis, and (v) probabilistic assessment of radionuclide regional and long-range transport patterns.

The WWW-variant of this report is also available on CD (enclosed with this report with enlarged figures, if ordered) and includes archives of calculated results.

## INTRODUCTION

The risks of radioactive contamination and radiological consequences in the selected geographical region are related to nuclear risk sources located in the region of concern or adjacent territories. Once the nuclear risk sources are defined and selected for a study, it is of particular interest to answer the following questions: Which geographical territories are at highest risk from hypothetical accidental releases in a selected area? What is the probability for radionuclide atmospheric transport and deposition to neighbouring countries in case of an accident from these sources?

*Rigina & Baklanov, 2002; Baklanov & Mahura, 2001* noted that for assessment of risk and vulnerability it is important to consider various social-geophysical factors and probability indicators, which depend on the location of the area of interest and its population. They mentioned that for estimation of the potential nuclear risk and vulnerability levels for the nuclear risk sites (NRSs) it would be important to know: geographical regions most likely to be impacted; probabilities of average and fast atmospheric transport, precipitation, etc. as well as their temporal and spatial variability; analysis of worst meteorological scenarios for case studies; possible contamination and effects on the population in case of an accident; site-sensitive hazards of potential airborne radioactive release; etc. The results of such studies are applicable for further analysis of the: 1) risk, socio-economical and geographical consequences for different geographical areas and population groups applying freely available demographic databases and Geographic Information System (GIS) technology, and 2) vulnerability to radioactive deposition with a focus on the transfer of certain radionuclides into food-chains, especially for native population, and considering risks for different geographical areas. Moreover, the results of such analyses are useful for the emergency response and preparedness measures in cases of accidental releases at NRSs.

The Radiation Safety of the Biosphere Project (RAD) Project of IIASA initiated such a study for the nuclear risk sites on the Kola Peninsula, Russia in 1995 in bounds of the Kola Assessment Study (*Baklanov et al., 1996; Bergman et al., 1996; Bergman & Baklanov, 1998*).

Starting from spring 2000 the RAD Project initiated a study entitled: "Assessment of Impact of Russian Nuclear Fleet Operations on Russian Far Eastern Coastal Regions" Study (FARECS). The long-term focus of this study is to gather existing information and analyze problems associated with operations of the Russian Pacific Fleet. The research activities on this project, performed during 2000-2002, will be briefly described below.

**In 2000**, research activities were concentrated on gathering available information, evaluating data, and performing preliminary analyses. For this step, *Romanova & Takano, 2002* had considered two reactivity accidents (Chazhma Bay and hypothetical) at the nuclear submarine near the Vladivostok naval base. They stated that the accidents took place during refueling and defueling of the submarine's nuclear reactors. In their study, the worldwide version of the SPEEDI (System for Prediction of Environmental Emergency Dose Information) code (*Ishikawa, 1991; Ishikawa & Chino, 1991; Ishikawa, 1994*) was used to simulate long-range atmospheric transport of radionuclides from the accident location and estimate radiological consequences to neighbouring countries.

**In 2001**, the focus of study was an analysis of possible danger to the environment and population in neighbouring countries from the probabilistic point of view (*Mahura, 2002*). Two nuclear risk sites of concern were selected: the Kamchatka (52°55'N & 158°30'E) and Vladivostok (42°55'N & 132°25'E) NRSs, both located in the Russian Far East. The main question is to be addressed: What is the probability of the radionuclide atmospheric transport in a case of an accident at these two nuclear risk sites? The specific objectives included: 1) examination of the atmospheric

transport patterns from both NRSs, 2) evaluation of the probability of the fast transport (i.e. transport in less than one day), and 3) investigation of possible impacts of the radionuclide removal processes during atmospheric transport. The isentropic trajectory model (based on a technique by *Merrill et al., 1985*) was used to calculate trajectories for a multiyear period. Then, statistical analysis tools such as exploratory, cluster, and probability fields analyses were applied to explore the structure of calculated trajectory datasets.

**In 2002**, the main purpose of study is an attempt to combine atmospheric transport and dispersion modeling and analyses with the radiological assessment to evaluate consequences of an accidental release at the nuclear risk sites studied. The methodology by *AR-NARP, 2001-2003; Baklanov & Mahura, 2001; Baklanov et al., 2002a* includes several research tools, which could be employed for such studies. Among these tools are trajectory and dispersion modeling as well as a set of statistical methods for analysis of modeling results. Application of these research tools provides the input data for the probabilistic risk and vulnerability studies. At this step, our study consisted of two main parts: 1) continue to construct and analyze additional indicators of the NRS impact based on the trajectory modeling results, and 2) construct and analyze indicators based on the dispersion modeling results. For the first part, the main modeling tool is the isentropic trajectory model. For the second part, the main modeling tool is the operational dispersion model developed at the Danish Meteorological Institute (DMI). Probability fields analysis was applied to analyze the results of trajectory and dispersion modeling. Additionally, several specific dates, when atmospheric transport occurred towards the geographical regions of interest, were also evaluated for both NRSs.

The current report has the following structure. In the “Introduction” chapter, we briefly described the research activities of the FARECS Study completed during 2000-2002. The second chapter – methodological - provides information about research tools and approaches applied in this study. The third chapter summarizes results of trajectory and dispersion modeling used for construction and analysis of various indicators of the NRS impact. This chapter is followed by sections of “Conclusions and Recommendations”, “Acknowledgments”, “References”, and “Appendices”. The appendices include monthly and seasonal variations for indicators of the NRS impact (Appendices 1-7, as well as a short description of other suggested methods for a more detailed analysis and complex risk assessment on the local, regional, and hemispheric-scales (Appendices A, B, C). The WWW-variant of this report is also available on CD (enclosed in this report with enlarged illustrations, if ordered), including archives of calculated results.

# I. METHODOLOGICAL ASPECTS FOR PROBABILISTIC ANALYSIS OF ATMOSPHERIC TRANSPORT AND DEPOSITION PATTERNS FROM NRSs

## 1.1. APPROACHES AND RESEARCH TOOLS

The methodology by *AR-NARP, 2001-2003; Baklanov & Mahura, 2001; Baklanov et al., 2002a* mentioned several research tools and approaches, which could be applied for the probabilistic atmospheric studies. The developed methodological scheme consists of several major blocks or steps in research activities. The first block or step is data extraction and pre-processing from the available meteorological archives. The second is trajectory and dispersion modeling for the selected risk sites geographical locations. The third is statistical analysis of calculated trajectories applying various techniques. The fourth is construction and analysis of different characteristics and indicators of the nuclear risk sites impact based on trajectory and dispersion modeling results. And the fifth step is the Geographic Information System (GIS)-based risk assessment including pre-processing additional databases (e.g., administrative, population, etc) as well as GIS modeling of the nuclear risk site impact.

In this study we applied the first four steps. A short description of the last step is given in Appendix A (*by O.Rigina*) of this report. Application of the last step finalizes the probabilistic risk assessment of the NRS impact and provides a complete picture of the complex nuclear risk and regional vulnerability for geographical territories, countries, counties, groups of population, etc.

Let us briefly consider the research tools and approaches selected for this study that provide input data for the probabilistic risk and vulnerability studies, as well as allow constructing and evaluating various indicators of the NRS possible impact.

The **first research tool** is the **trajectory model**. We used an isentropic trajectory model based on a technique described by *Merrill et al., 1985*. A multiyear (1987-1996) dataset of 5-days forward trajectories originating over the NRS locations – Vladivostok and Kamchatka - at various altitudes was calculated. For the forward trajectory calculation, we used meteorological fields from the Global Tropospheric Analyses dataset (<http://dss.ucar.edu/datasets/ds082.0>) (from the National Center for Environmental Prediction, NCEP) which is one of the major gridded analyses available at the National Center for Atmospheric Research (NCAR, Boulder, Colorado, USA).

The **second research tool** is the **dispersion model**. In this study, we applied the Danish Meteorological Institute (<http://www.dmi.dk>) long-range transport model – Danish Emergency Response Model of the Atmosphere DERMA (*Sørensen, 1998; Baklanov & Sørensen, 2001*) - to simulate radionuclide atmospheric transport and deposition for hypothetical accidental releases at both NRSs. The meteorological data from the European Center for Medium-Range Weather Forecasts (ECMWF, Reading, UK) based on the ECMWF global model forecast and analysis (<http://www.ecmwf.int/services/data/archive/index.html>) were used as input data in the model simulation.

The **third research tool** is the **cluster analysis**. In this study, we did not present the results of the trajectory cluster analysis for all NRSs, because we consider this approach as the simplest of those used. The cluster analysis technique was applied in several studies related to the nuclear risk sites: at the Chukotka (*Mahura et al., 1997a; Jaffe et al., 1997a; Mahura et al., 1999b*), Kola Peninsula (*Mahura et al., 1997b; Jaffe et al., 1997b; Mahura et al., 1999a; Baklanov et al., 2001*), and Russian Far East (*Mahura, 2002*). The potential risk sources considered were the nuclear power

plants, spent nuclear fuel storage facilities, and nuclear submarine bases. In general, this technique allows identifying atmospheric transport pathways from NRSs (or any selected source points). In a similar way, cluster analysis could be applied to identify atmospheric transport pathways to the receptor points. In this case, the backward trajectories arrived at the sites will be used for clustering. This approach was applied in *Mahura et al., 1997a; Jaffe et al., 1997a; Mahura et al., 1999b*. A more detailed analysis and interpretation of the backward trajectory clustering is described in the pilot study of *Mahura & Baklanov, 2002*.

The **fourth research tool** is the **probability fields analysis**. The first attempt to use the probability fields analysis was performed by *Jaffe et al., 1997b; Mahura et al., 2001; Baklanov et al., 1998* using as an example the Kola nuclear power plant (NPP) (Murmansk region, Russia). The major focus was the airflow probability fields, which allowed testing the quality of the cluster analysis technique in identification of the general atmospheric transport pathways from the site. Such probability fields analysis provides additional information and a detailed structure of the airflow patterns from the site on a geographical map. In this study, we constructed and evaluated annual, seasonal, and monthly probability fields for airflow, fast transport, precipitation factor (or relative humidity), concentration, deposition, and other patterns. These fields allow identification of the most impacted geographical regions.

The main focus of this report is to describe the probabilistic fields analyses for use in further risk assessment of the selected nuclear risk sites in the Russian Far East. The results of probabilistic analysis for these sites are presented in the form of various indicators (Figure 1.1.1, block of the characteristics and indicators of NRS impact) of the NRS possible impact on geographical regions. These indicators are based on the results of the trajectory and dispersion modeling.

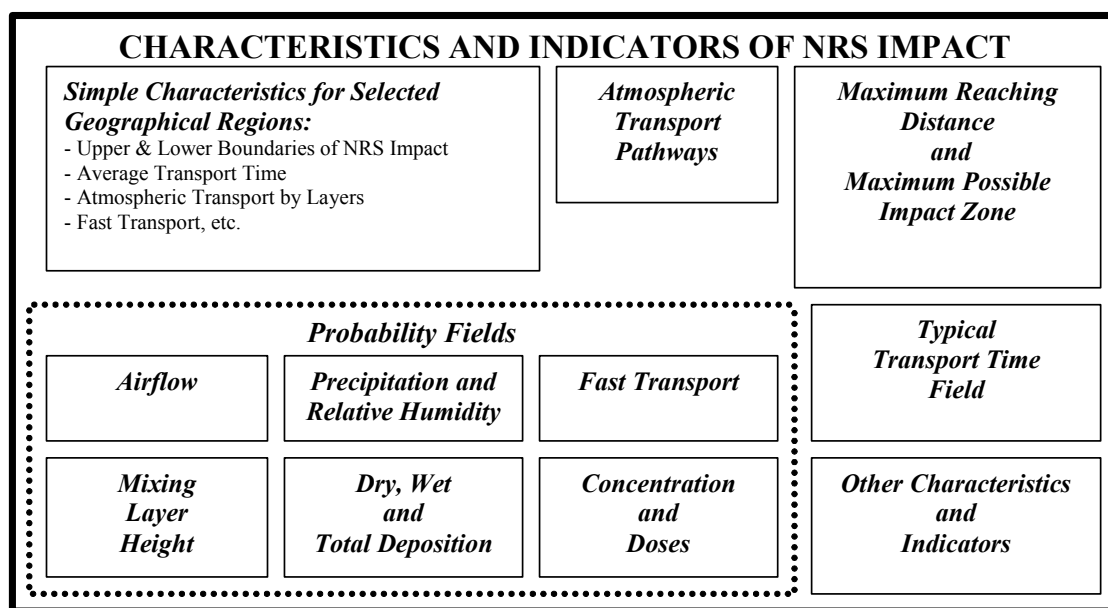


**Figure 1.1.1.** Block of the characteristics and indicators of the NRS possible impact based on trajectory and dispersion modeling approaches (adapted from Baklanov & Mahura, 2001).

In this study, among the indicators based on trajectory modeling, we should mention the following: simplest characteristics of NRS impact, atmospheric transport pathways (ATP), airflow (AF) and fast transport (FT) probability fields, precipitation factor (PF) or relative humidity (RH) fields, maximum reaching distance (MRD), maximum possible impact zone (MPIZ), and typical transport time (TTT) fields. Among the indicators based on dispersion modeling of radionuclide

transport and deposition, we should mention the following: air concentration in the surface layer (AC), integrated over time air concentration in the surface layer (IAC), wet deposition (WD), dry deposition (DD), and total deposition (TD). The monthly or seasonal variability of several indicators for both NRSs are presented in the Appendices of this report. More detailed and complete information for various NRS indicators is stored on CD (enclosed with this report if ordered).

Finally, we should note, that the indicators of the NRS possible impact are applicable for initial estimates of probability of atmospheric transport in the event of an accidental release at NRSs and for improvement in planning the emergency response to radionuclide releases from the NRS locations. These indicators are important input for the study of social and economical consequences of the NRS impact on population and environment for the neighbouring countries as well as for the multidisciplinary risk and vulnerability analysis, and the probabilistic assessment of radionuclide meso-, regional-, and long-range transport.

## **1.2. METEOROLOGICAL DATA FOR TRAJECTORY AND DISPERSION MODELING AND COMPUTING RESOURCES**

It is well known among modelers of atmospheric processes that data analysis of meteorological fields is a basis for atmospheric sciences research. Data might be represented in different forms and at different temporal and spatial scales, as well as obtained from a variety of different sources. Models, which rely on intensive usage of supercomputing resources, can produce gridded arrays for the commonly used and basic variables. Atmospheric models can calculate various variables at different levels. In our study, we considered several gridded datasets as input data. Among them were: 1) NCAR dataset - for trajectory modeling purposes, 2) ECMWF dataset - for dispersion modeling purposes, and 3) DMI-HIRLAM dataset - for selected specific case studies purposes.

### **NCAR Dataset**

The dataset DS082.0 - NCEP Global Tropospheric Analyses (from July 1976 until April 1997) is one of the major gridded analyses available at the National Center for Atmospheric Research (NCAR, Boulder, Colorado). It is a part of the operational and gridded analyses performed at the National Center for Environmental Prediction (NCEP; prior to 1995 known as the National Meteorological Center – NMC). This dataset has a resolution of 2.5° x 2.5° latitude vs. longitude (145 x 37 grids, ~3 Megabytes (Mb) per day) for both Northern and Southern hemispheres. It consists of the surface, tropospheric, tropopause, and lower stratospheric analyses at the standard levels up to 50 millibars (mb). The main analyzed variables are the following: geopotential height, temperature, components of the wind, relative humidity, sea level pressure, surface pressure and temperature, sea surface temperature, snowfall, precipitable water, potential temperature, vertical motion, tropopause pressure, and temperature. Analysis has been done on a daily basis at 00 and 12 UTC (Universal Coordinated Time) terms.

More detail information about DS082.0 dataset can be found at the WWW-address <http://dss.ucar.edu/datasets/ds082.0> and in publications by *Baker, 1992; Trenberth & Olson, 1988; Randel, 1992.*

### **ECMWF Dataset**

The meteorological data used can be obtained from the European Center for Medium-Range Weather Forecasts (ECMWF), Reading, UK based on the ECMWF global model forecast and analysis (<http://www.ecmwf.int>). The data have a resolution of 1° x 1° latitude vs. longitude and 6

hours time resolution. It consists of the temperature, u- and v-components of horizontal wind, and specific humidity at each level, plus surface fields. Analyses have been done at 00 and 12 UTC.

### **DMI-HIRLAM Dataset**

The DMI-HIRLAM high-resolution meteorological data (D-version: 0.05 $\forall$  N- and E-versions: 0.15 $\forall$  or G-version: 0.45 $\forall$  with 1 hour time resolution) are used as input data for high-resolution trajectory or dispersion simulations. The vertical model levels (31 levels in total) are presently located at 33, 106, 188, 308, etc meters for a standard atmosphere. The High Resolution Limit Area (HIRLAM) numerical weather prediction model has been run operationally by DMI for the European territory and for the Arctic region since the late 1980s. But it can be run also, after extending the grid domain, for regions including China, Afghanistan, Japan, Korea and the Russian Far East. For example, the DMI-HIRLAM was operationally used for some limited periods of time for the territory of China and surroundings, including the area of interest. The DMI 3D Lagrangian transport model (*Sørensen et al., 1994*) calculates forward and backward trajectories for any point in the area of interest. It can utilize meteorological data from the different versions of DMI-HIRLAM as well as the ECMWF global model. The present DMI weather forecasting system is based on HIRLAM 4.7 (*Saas et al., 2000*). The forecast model is a grid point model. The data assimilation is intermittent and based on the 3-D variation data assimilation (3DVAR) scheme.

### **NCAR Computing Resources**

The Scientific Computing Division (SCD, see more details at <http://www.scd.ucar.edu>) is part of the National Center for Atmospheric Research (NCAR). It is located in Boulder, Colorado, US. Its goal is to enable atmospheric research worldwide by providing and advancing high-performance computing technologies. SCD offers computing resources, various datasets, space for data storage, networking, and data analysis tools. There are several computers operated and supported by SCD: CRAY J924se, IBM SP RS/6000, SGI Origin2000, etc. Internet Remote Job Entry (IRJE) allows NCAR supercomputer users at remote sites to submit jobs directly from their local hosts and get the results delivered back to their local hosts over the Internet. It also provides an interface between the user site and Mass Storage System (MSS) to store data.

### **DMI Computing Resources**

The Danish Meteorological Institute (DMI) provides meteorological and related services for the community within the large geographical area of the Kingdom of Denmark (Denmark, the Faeroes, and Greenland), including surrounding waters and airspace as well as global services. The DMI area of activity comprises forecasting and warning services as well as continuous monitoring of weather, sea state, climate, and related environmental conditions in the atmosphere, over land, and in the sea.

In 1996, DMI in Copenhagen, Denmark, installed an NEC SX-4/16 supercomputer system. This system is being replaced with a NEC SX-6/48 supercomputer. The final system will have 224 GBytes of SDRAM main memory, 4TBytes of disk, and a peak performance of 460 Gflop/s. The first phase consisting of 2 NEC SX-6 full nodes connected with an IXS switch was installed in April 2002. NEC's SX-Series represents the highest performance offer for technical computing. The latest machine in the SX-Series, the SX-6 is based on the fastest CPU (on a single chip) in the market with a speed of 8 Gflop/s per CPU (see more details at <http://www.ess.nec.de>).

In this project, the SGI Origin scalar server was used for dispersion modeling computational purposes, and all calculated fields were stored on the DMI UniTree mass-storage device.

### **1.3. TRAJECTORY MODELING APPROACH**

Trajectory modeling is one of the approaches selected for this study. In general, each computed atmospheric trajectory represents a pathway of an air parcel motion in time and space. We consider trajectories as an estimate of the mean motion of a diffusing cloud of material. Although there are many different approaches to model atmospheric trajectories, we selected the isentropic approach. Although this approach uses the assumption of adiabatically moving air parcels and neglects various physical effects, it is still a useful research tool for evaluating common airflow patterns within meteorological systems on various scales. Some uncertainties in these models are related to the interpolation of meteorological data (which might be sparsely measured), applicability of the considered horizontal and vertical scales, assumptions of vertical transport, etc (*Merrill et al., 1985; Draxler, 1987; Stohl, 1998*).

In *Mahura, 2002* we interpolated the original National Center for Environmental Prediction (NCEP) gridded wind fields to potential temperature (isentropic) surfaces. We choose isentropic assumption in our study because isentropic trajectories are a better representation of the air parcels atmospheric transport when compared to isobaric trajectories. Additionally we should note that the quality of trajectory calculation is highly dependent on the original quality of the NCEP fields (2.5° x 2.5° latitude vs. longitude), and it may not adequately reflect the contributions of frontal passages and local terrain phenomena. However, the trajectory errors arising during a single calculation might be smoothed in further analysis due to the large number of trajectories computed for the multiyear dataset.

An interpolation procedure has been performed for a period of 10 years (1987-1996). We applied the technique described by *Merrill et al., 1985*. Then, we used the wind fields on isentropic surfaces to calculate trajectories in the model domain (2.5°N and 90°E-82.5°W) at various levels within the atmosphere. All forward isentropic trajectories from the NRS regions were computed twice per day (at 00 and 12 UTC, Universal Coordinated Time) at different potential temperature levels (or isentropic surfaces). In total, we computed more than 467 thousand trajectories for each NRS. More details concerning the trajectory calculations used in this study can be found in *Mahura, 2002*.

For both NRSs, which contain nuclear submarine reactors and radioactive storage facilities, in the case of an accidental release, the most probable release heights would be within the surface layer of the atmosphere, i.e. within the first hundred meters above the ground. Therefore, as the next step, we selected only those trajectories originating within this layer from all isentropic trajectories. Therefore, for each site, we extracted approximately 29 thousand trajectories (from more than 467 thousand original trajectories). All selected trajectories for further statistical analysis were terminated at the end of 5 days. We decided to use this limitation in duration on trajectories because: 1) the quality and accuracy of trajectory calculations after 5 days drop significantly, 2) observing development frames of the synoptic scale systems in the North Pacific region are within one week, and 3) the relative proximity of the analyzed NRS impact geographical regions to the sites of interest.

Moreover, to study altitudinal variations in the atmospheric flow patterns (in particular, within the boundary layer and free troposphere), we also considered trajectories that originated over the NRS regions at the top of the boundary layer (i.e. near 1.5 km above sea level (asl)).

### **1.4. DISPERSION MODELING APPROACH**

The dispersion modeling approach (*Baklanov et al., 2002a*) is another risk assessment approach employed in this study. It uses the long-range transport model – Danish Emergency

Response Model of the Atmosphere, DERMA (Sørensen, 1998; Baklanov & Sørensen, 2001) developed at the Danish Meteorological Institute (DMI). As input data this model can use meteorological data from the DMI-HIRLAM or European Center for Medium-Range Weather Forecasts (ECMWF) archives, and it is based on the ECMWF global model forecast and analysis. The DERMA model can simulate radionuclide atmospheric transport, dispersion, and deposition for atmospheric releases of radioactivity occurring at the selected geographical locations.

For this study, we made several assumptions. **First**, for simplicity, we selected for both NRSs the continuous “unit hypothetical release” (UHR) of radioactivity ( $1 \cdot 10^{10}$  Bq/s) with discrete emitting of puffs (every 60 minutes) during one day, i.e. the total amount of radioactivity released during one-day release is equal to  $1 \cdot 10^{10} (\text{Bq/s}) \cdot 24(\text{hour}) \cdot 60(\text{min}) \cdot 60(\text{sec}) = 8.64 \cdot 10^{14}$  (Bq). **Second**, we considered only one radionuclide of key importance -  $^{137}\text{Cs}$  - to save computational resources, although we should note that the calculation might be done for any radionuclide selected. In particular, for the specific cases studies,  $^{131}\text{I}$  and  $^{90}\text{Sr}$  will also be considered. **Third**, the simulation was performed on a daily basis considering the length of the 5-day trajectories (i.e. after release of radioactivity occurred from the site the tracking of the radionuclide cloud was limited to 5 days of atmospheric transport). **Fourth**, to minimize the computing resources used for the dispersion modeling approach, we selected only one year (1 Jan 2000 – 31 Dec 2000) in our study, although it should be noted that for the statistical analysis the multiyear period is more preferred.

Using the DERMA model, we calculated several important characteristics: 1) air concentration ( $\text{Bq/m}^3$ ) of the radionuclide in the surface layer – **surface air concentration**, 2) integrated in time air concentration ( $\text{Bq}\cdot\text{h}/\text{m}^3$ ) of the radionuclide in the surface layer – **integral concentration at surface**, 3) dry deposition ( $\text{Bq}/\text{m}^2$ ) of the radionuclide on the underlying surface – **dry deposition**, and 4) wet deposition ( $\text{Bq}/\text{m}^2$ ) of the radionuclide on the underlying surface – **wet deposition** fields. Output fields were recorded every 3 hours. The total deposition field for the radionuclide can be calculated as a sum of dry and wet deposition fields. These calculated characteristics can be represented by two dimensional fields where the value of the calculated characteristic is given in the latitude-longitude grids of the selected model grid domain. In general, the model domain covers most of the Northern Hemisphere starting from  $12^\circ\text{N}$ .

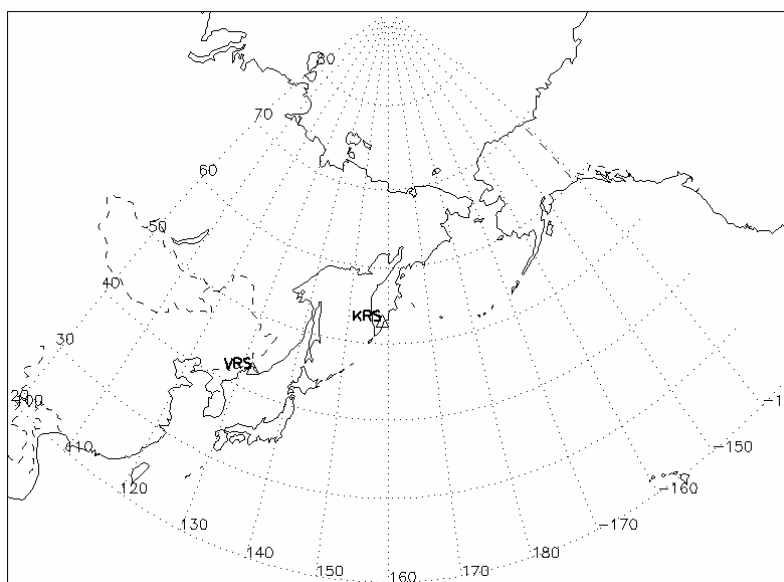
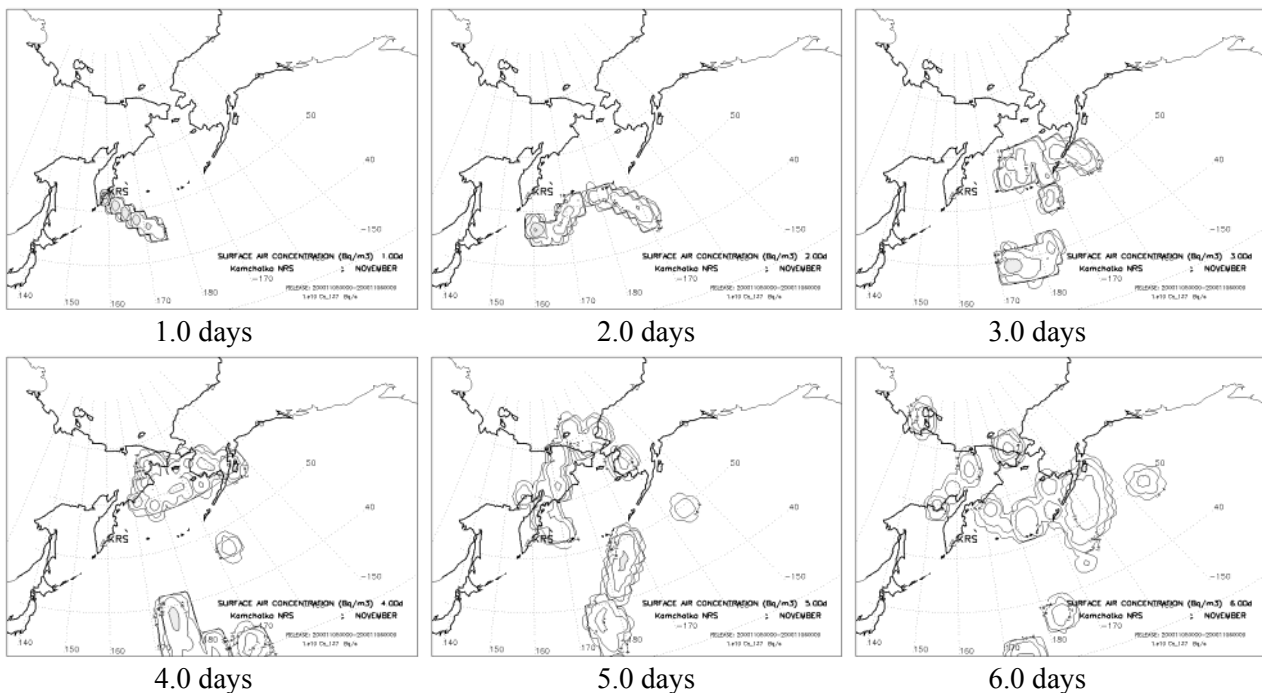


**Figure 1.4.1.** Domain for the region of interest.

From this grid domain, we extracted and incorporated data into the new grid domain in the region of interest (Figure 1.4.1), which covers territories of the North Pacific region adjacent to the

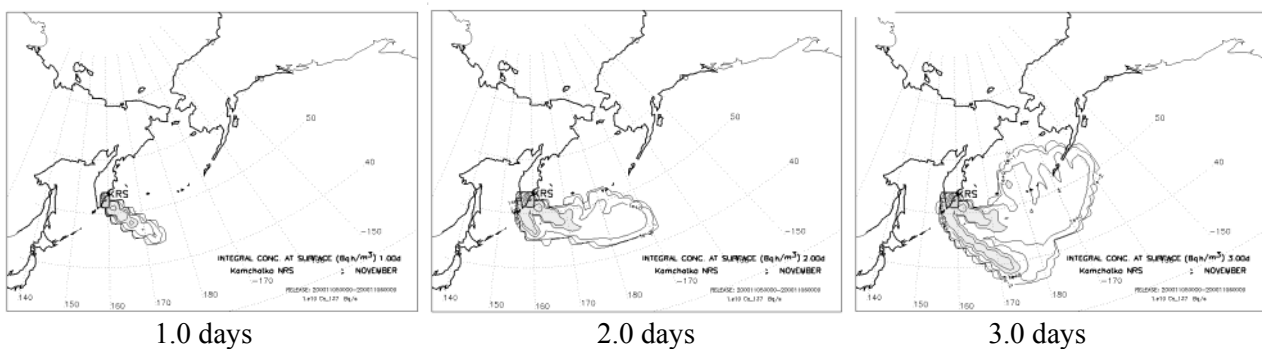
NRS locations (20-90°N vs. 100°E –140°W). This new domain had a resolution of 0.5° vs. 0.5° of latitude vs. longitude. It consisted of 241 vs. 139 grid points along longitude vs. latitude. To save storage space, the recalculated fields were re-recorded every 6 hours instead of original 3 hour intervals. Moreover, because of missing data in the archives and processing problems, we did not calculate fields for 16 days (4.4% of 366 days during the year 2000).

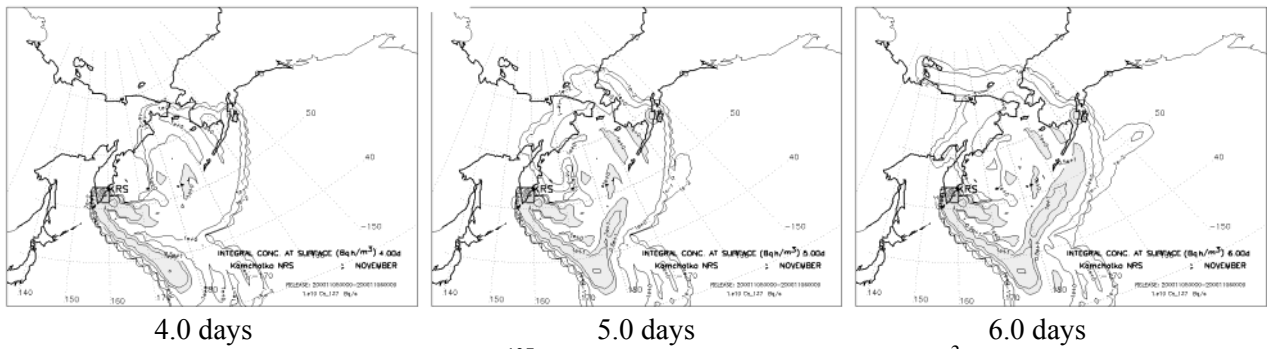
Examples of the dispersion modeling for a particular date of release at the Kamchatka NRS are shown in Figures 1.4.2-1.4.4 (see also enclosed CD with enlarged figures). Figure 1.4.2 shows the surface air concentration (Bq/m<sup>3</sup>) of <sup>137</sup>Cs within the surface layer of atmosphere after the “unit hypothetical release” (UHR) at NRS occurred during 5 Nov, 00 UTC - 6 Nov, 00 UTC, 2002. As we see (on a daily basis), as the radioactive cloud propagates from the NRS location, the concentration decreases as expected, in general, with increasing distance from the source.



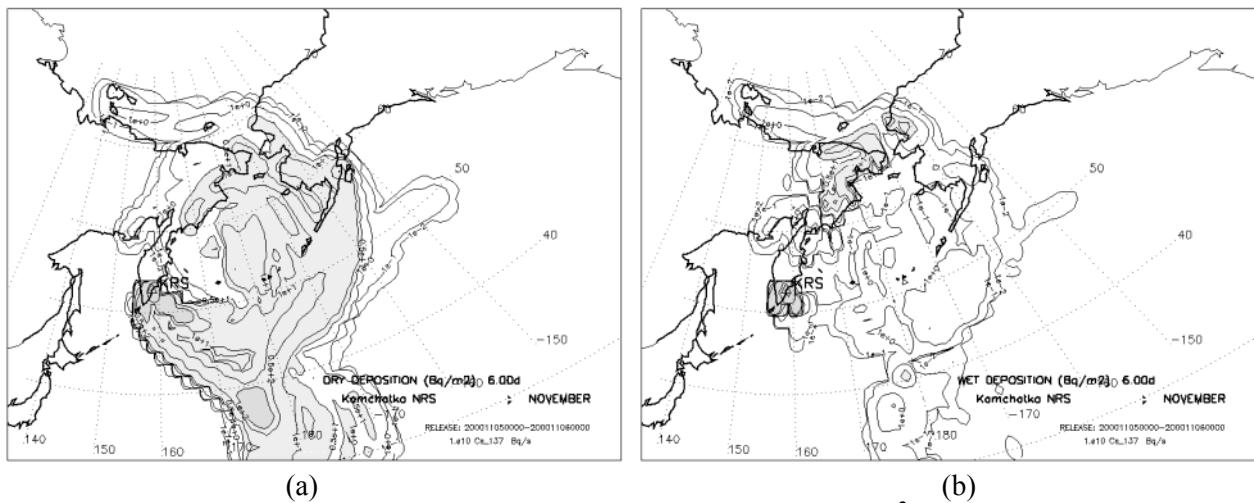
**Figure 1.4.2.** Temporal variation of the Cs<sup>137</sup> surface air concentration (Bq/m<sup>3</sup>) for the “unit hypothetical release” occurred at the Kamchatka NRS during 5-6 Nov, 2000, 00 UTC.

Figure 1.4.3 shows the integral air concentration (Bq·h /m<sup>3</sup>) of <sup>137</sup>Cs at the surface after the same UHR at NRS occurred during the same day. The integral air concentration is represented by a sum of air concentrations integrated over time through the fields at the subsequent temporal steps. Therefore, we see the accumulating concentration of <sup>137</sup>Cs at temporal steps where the areas closer to the NRS have higher magnitudes.





**Figure 1.4.3.** Temporal variation of the  $Cs^{137}$  integral air concentration ( $Bq \cdot h/m^3$ ) for the “unit hypothetical release” occurred at the Kamchatka NRS during 5-6 Nov, 2000, 00 UTC.



**Figure 1.4.4.**  $Cs^{137}$  a) dry deposition and b) wet deposition fields ( $Bq/m^2$ ) for the “unit hypothetical release” occurred at the Kamchatka NRS during 5-6 Nov, 2000, 00 UTC.

Figure 1.4.4a shows the dry deposition field for  $^{137}Cs$  ( $Bq/m^2$ ) after the same release occurred during 5-6 Nov 2000. The structure of the dry deposition field resembles the structure of the integral air concentration field (see Figure 1.4.3, at 6.0 days). Figure 1.4.4b shows the wet deposition field for  $^{137}Cs$  ( $Bq/m^2$ ) for the same release. Its structure is different due to the contribution of the wet removal processes (e.g. washout and rainout by precipitation) during the radionuclide atmospheric transport. It has a “spotted” nature, i.e. where precipitation occurred, we observe the higher values of the wet deposition at the surface.

### 1.5. PROBABILITY FIELDS ANALYSIS FOR TRAJECTORY MODELING RESULTS

Probabilistic analysis is one of the ways to estimate the likelihood of occurrence of one or more phenomena or events. As mentioned in this study, we calculated a large number of trajectories that passed over various geographical regions. Each calculated trajectory contained information about longitude, latitude, altitude, pressure, temperature, relative humidity, and other variables at 12 hour intervals. The probability fields for these characteristics, either individual or combined, can be represented by a superposition of probabilities for the air parcels reaching each grid region in the chosen domain or on the geographical map.

Let us consider several common approaches to construct probability fields based on trajectory modeling results (Baklanov & Mahura, 2001; Mahura et al., 2002c). Initially, we construct a

gridded domain having  $M_{lat} \times M_{lon}$  latitude vs. longitude grid points with a size of  $\Delta Y \times \Delta X$  degrees latitude vs. longitude.

The **first approach** to construct such fields (an example is shown in Figure 1.5.1a) considers the number of trajectory intersections with each cell of the gridded domain ( $N_{CELL_{ij}}$ ):

$$N_{CELL_{ij}} = \frac{N_{tr} \cdot M_{lat} \cdot M_{lon}}{k|1 \cdot j|1 \cdot i|1} n_{ijk} \quad \text{where:} \quad n_{ijk} = \begin{cases} 0 & \text{if } \left[ \begin{array}{l} X_i \leq \Omega X_{k,t} \leq X_{i+1} \\ Y_j \leq \Omega Y_{k,t} \leq Y_{j+1} \end{array} \right. \\ 1 & \text{if } \left[ \begin{array}{l} X_i < \Omega X_{k,t} < X_{i+1} \\ Y_j < \Omega Y_{k,t} < Y_{j+1} \end{array} \right. \end{cases}$$

where:

$X_{k,t}, Y_{k,t}$  – longitude and latitude of  $k$ -trajectory at time  $t$  (where:  $t = 0,5$  days;  $\Delta t = 12$  hours);

$X_i, X_{i+1}$  – longitudinal boundaries of the grid cells of domain;

$Y_j, Y_{j+1}$  – latitudinal boundaries of the grid cells of domain;

$N_{tr}$  – total number of trajectories during the multiyear period studied (number days per year \* 8 trajectories per day \* number of years);

$M_{lat}, M_{lon}$  – number of the grid points in domain along latitude and longitude.

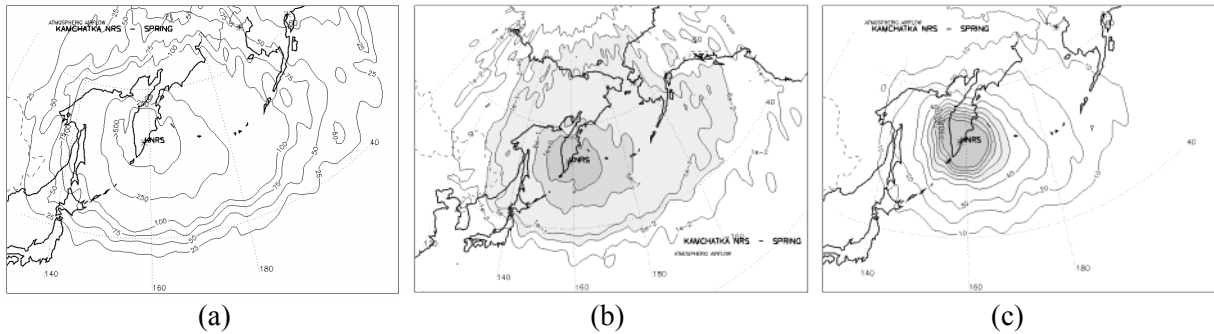


**Figure 1.5.1.** Examples of airflow probability fields for the Kamchatka NRS using the a) first, b) second, and c) third approaches to construct probabilistic fields based on trajectory modeling results.

The **second approach** for construction of probabilistic fields (an example is shown in Figure 1.5.1b) uses an assumption that the total sum of contributions from all individual grid cells of domain is equal to 100%. Hence, the contribution or probability that a given trajectory might reach the geographical boundaries of the individual cell could be estimated as follows:

$$P_{i,j} = \frac{N_{CELL_{ij}}}{N_{tot}} \approx 100\%, \quad N_{tot} = \sum_{i|1}^{M_{lat}} \sum_{j|1}^{M_{lon}} N_{CELL_{i,j}}$$

where:

$P_{i,j}$  – probability of trajectory intersections with a particular cell of the gridded domain;

$N_{tot}$  – total number of trajectory intersections with all cells of the gridded domain.

The **third approach** for construction of probabilistic fields (an example is shown in Figure 1.5.1c) uses an assumption that for an individual NRS there is always an area where there is the highest probability of the maximum possible impact due to atmospheric transport. The borders of such an area (or more precisely, the cells included in such area) could be estimated by comparing the number of trajectory intersections with the cells (adjacent to NRS location) with the cell where the maximum number of intersections occurred:  $N_{AMC} = \max(N_{CELL_{1,1}}, \dots, N_{CELL_{M_{lat}, M_{lon}}})$ . Among all grid cells, the cell where the absolute maximum of intersections occurred will be identified as an “absolute maximum cell” (AMC). Because all trajectories start near the NRS region, to account for

the contribution into the flow at larger distances from the site, we extended the area of maximum to cells adjacent to the AMC. We compared the number of intersections in cells adjacent to AMC and then assigned additional cells, which had difference of less than 10% between cells. Therefore, this new “area of maximums”, if isolines are drawn, will represent the area of the highest probability of the possible impact (AHPPI) from NRS. Assuming a value of 100% for this area, the rest could be re-calculated as percentage of the area at the highest probability of the possible impact, or:

$$P_{AHPMI_{i,j}} = \frac{N_{CELL_{ij}}}{N_D} \cdot 100\% , \quad N_D = N_{tot} - 4 N_{AHPMI} ,$$

$$N_{AHPMI} = \sum_{j=1}^{M_{lat}} \sum_{i=1}^{M_{lon}} n_{ij} \quad \text{where:} \quad n_{ij} = \begin{cases} 0 & \text{if } N_{CELL_{i,j}} \geq 0.9 N_{AMC} \\ N_{CELL_{i,j}} & \text{if } N_{CELL_{i,j}} < 0.9 N_{AMC} \end{cases}$$

where:

$P_{AHPMI_{i,j}}$  - probability of NRS impact with respect to the area of the highest probability of the possible impact (AHPPI) of the nuclear risk site;

$N_D$  - total sum of trajectory intersections with cells from the gridded domain, except the cells located in the boundaries of AHPPI for the nuclear risk site;

$N_{AHPMI}$  - total sum of trajectory intersections with cells from the gridded domain located within the boundaries of AHPPI for the nuclear risk site.

In our study, we selected the third approach to construct the probabilistic fields as the most representative to evaluate the NRS possible impact. We should note that the most interest for the further analysis would be the following types of probabilistic fields (*Baklanov & Mahura, 2001*): a) airflow, b) fast transport, c) precipitation factor or relative humidity, d) maximum reaching distance, and e) maximum possible impact zone.

The first type of probabilistic fields (**airflow probability fields**) shows the common features in the atmospheric transport patterns, i.e. it may provide a general insight on the possible main direction of the radioactive cloud’s transport as well as the probability that it will reach or pass any geographical area. The result of this analysis is an appropriate test to support or disprove results of the cluster analysis. This is because the atmospheric transport pathways (or mean trajectory clusters) show only the common direction of airflow away from the site. However, information between these pathways (or clusters) is missing.

The second type of probabilistic fields (**fast transport probability fields**) indicates the probability of the air parcels movement during the first day of transport. It is important information, especially, for estimating the radionuclides - such as iodine and cesium isotopes - impact. These fast transport fields show those territories that may be reached after the first day, and those areas that are at the most danger due to fast transport probability.

The third type of probabilistic fields (**relative humidity or precipitation factor probability fields**) describes the possibility for removal processes to impact the contaminated air mass as it passes over the particular geographical area. Such an analysis, a simple approximation, was used in *INTAS, 2000*; *OCB, 2000* and *AR-NARP, 2001-2003*. In our study, we used a better representation of possible contribution of the possible removal processes during radionuclide atmospheric transport. We constructed the wet deposition fields – summary and averaged (see §1.6) - from the “unit hypothetical releases” at the NRS locations.

The fourth type of probabilistic fields indicates the farthest boundaries on the geographical map that might be reached during the first day by, at least, one trajectory originating over the NRS location (**maximum reaching distance**) as well as shows boundaries of areas with the highest probability of being reached by trajectories during the first day of transport (**maximum possible impact zone**).

## 1.6. PROBABILITY FIELDS ANALYSIS FOR DISPERSION MODELING RESULTS

The dispersion modeling results might be analyzed in a similar manner to those for the trajectory modeling results. Further, we analyze the following calculated characteristics: integral concentration at surface, dry deposition, and wet deposition of  $^{137}\text{Cs}$  (see §1.4). Let us consider two approaches to construct probability fields for each of these characteristics (*AR-NARP, 2001-2003; Baklanov et al., 2002a; Baklanov et al., 2002b*). It should be noted that in both approaches for calculation of fields only data with “valid dates” were used (i.e. when original meteorological data were available for computation and the dispersion simulation was performed without any computational problems). All characteristics’ values are given in a gridded domain having  $M_{lat} \times M_{lon}$  latitude vs. longitude grid points with a size of  $\Delta Y \times \Delta X$  degrees ( $0.5^\circ \times 0.5^\circ$ ) latitude vs. longitude for each day during January-December 2000. As an example, let us select only one characteristic - integral air concentration of radionuclide, although similar steps in the construction of fields could be applied for all other characteristics.

The **first approach** to construct fields based on the results of dispersion modeling (an example is shown in Figure 1.6.1a) considers the distribution of the total sum of daily continuous discrete releases of radioactivity at the site during the time period of interest (for instance: month, season, or year). Let us call this field the **summary field** for one of the chosen characteristics, and note that it is a field integrated over a given time period. For example, for integral air concentration, at any grid point -  $(i,j)$  - the total sum ( $C_{i,j}$ ) is equal to the sum of integral air concentrations ( $c_{ijk}$ ) at the end of the 6<sup>th</sup> day of atmospheric transport from the site for each daily release of radioactivity during the time period of interest:

$$C_{i,j} = \sum_{k=1}^{TP} c_{ijk}, \quad i \in \{1, M_{lon}\}; \quad j \in \{1, M_{lat}\};$$

where:

$TP$  – number of valid dates in the selected time period of interest.

$M_{lat}, M_{lon}$  - number of the domain grid points along latitude and longitude.

This type of field shows the most probable geographical distribution of the radionuclide’s integral air concentration at the surface if the release of radioactivity occurred during the time period of interest.

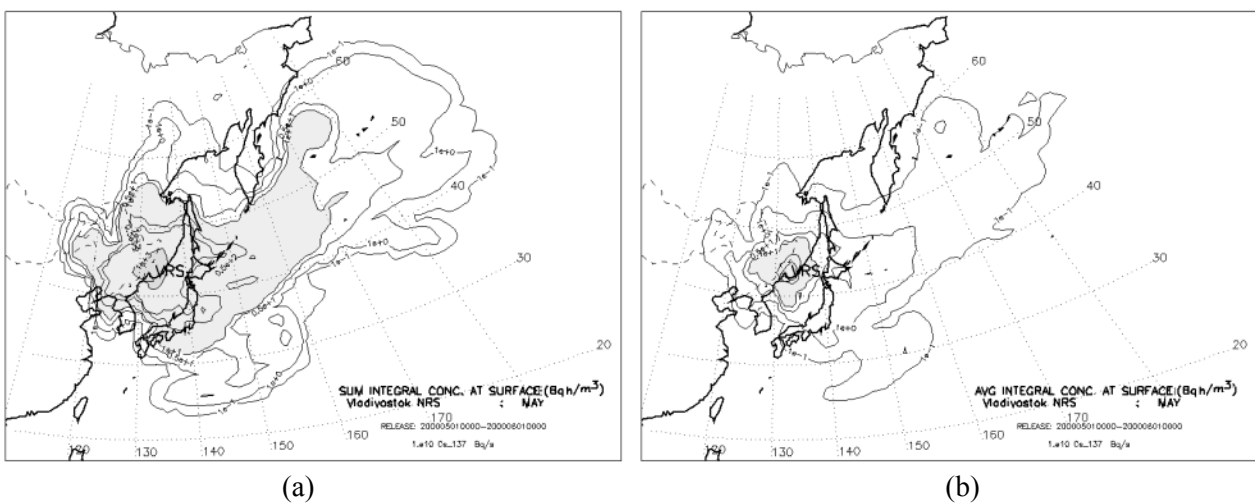


**Figure 1.6.1.**  $\text{Cs}^{137}$  a) summary and b) average fields of integral concentration at surface for the “unit hypothetical release” occurred at the Vladivostok NRS during 1-31 May, 2000, 00 UTC.



## 1.7. SPECIFIC CASE STUDIES APPROACH

The specific case study is one of the approaches selected for this project. We should note that this approach is computationally less expensive when compared to dispersion modeling for a multiyear period, although it does provide less reliable output and allows us to consider further risk and vulnerability analysis only on particular dates. Alternatively, this approach provides possibility of seeing potential consequences of an accident for worst-case meteorological situations. In this study, we followed several ways suggested by *Baklanov et al., 1994; INTAS, 2000; OCB, 2000* (for local scale) and *Bergman et al., 1998; Baklanov et al., 2001; Baklanov et al., 2002a; Mahura et al., 2002a* (for regional scale) on examples of the Kola NPP as well as nuclear submarines and spent nuclear fuel facilities in the northern latitudes.

The selection of specific cases with typical or worst-case scenarios can be based on results from trajectory modeling and probability fields analysis. In general, several criteria could be used for specific case selection. First, the main direction of atmospheric transport of radioactive cloud of an accidental release at NRS should be toward the region of interest. In our study, these regions are Japan, Korea, Northeast China, Aleutian Chain Islands, State of Alaska, and populated territories of the Russian Far East). Second, the possibility of precipitation during atmospheric transport of the radioactive cloud over the region of interest should be taken into account. In our study it could be inferred from the dispersion modeling of wet deposition patterns. Third, the relatively short travel time of the radionuclide cloud from the NRS location toward the region of interest (consideration of which depends on the fast transport probability fields patterns) will be important. Fourth, the relatively large coverage of the regions of interest by the radioactive cloud during atmospheric transport should be considered. And finally, preferably, although not crucial, for the regional scale analysis, the stable boundary layer conditions and atmospheric transport is limited by the boundary layer height as well as for cold and warm seasons. Based on these criteria, we selected several specific cases with worst-case scenarios for both NRSs shown in Table 1.7.1.

**Table 1.7.1.** Selected specific cases for Kamchatka and Vladivostok NRSs.

#	Specific Case	Dates & Duration of Release	NRS	Regions of Interest
1a	15 Nov 2000	15 Nov, 00 UTC, 2000 – 16 Nov 00, UTC, 2000	KRS	State of Alaska, Chukotka Region
1b	15 Nov 2000	15 Nov, 00 UTC, 2000 – 16 Nov 00, UTC, 2000	VRS	Japan, North & South Korea, Aleutian Chain Islands
2	05 Aug 2000	05 Aug, 00 UTC, 2000 – 06 Aug 00, UTC, 2000	KRS	State of Alaska, Chukotka Region
3	10 Aug 2000	10 Aug, 00 UTC, 2000 – 11 Aug 00, UTC, 2000	VRS	Japan, North & South Korea, North-East China, Chukotka Region
4	17 Aug 2000	17 Aug, 00 UTC, 2000 – 18 Aug 00, UTC, 2000	VRS	North & South Korea, North-East China, Primorskiy Krai
5	05 Apr 2000	05 Apr, 00 UTC, 2000 – 06 Apr 00, UTC, 2000	KRS	Aleutian Chain Islands, Magadan & Chukotka Regions
6	26 Apr 2000	26 Apr, 00 UTC, 2000 – 27 Apr 00, UTC, 2000	KRS	Japan

For the specific case studies, it is important also to consider common parameters of accidental radionuclide releases. Among these factors are the following: 1) duration of accidental release at

selected location, 2) altitudes of initial plume rise, 3) distribution of particle sizes for considered radionuclides, and 4) reference deposition velocities. In this study, we selected three radionuclides -  $^{137}\text{Cs}$ ,  $^{131}\text{I}$ , and  $^{90}\text{Sr}$  – as a major dose-contributing radionuclides. The major characteristics for each radionuclide used in dispersion modeling are shown in Table 1.7.2. It should be noted that for  $^{131}\text{I}$  we used an average of the gaseous and particulate forms. During these specific dates, the releases at NRSs are the continuous “unit hypothetical releases” of radioactivity ( $1 \cdot 10^{10}$  Bq/s) with the discrete emitting of puffs (every 60 minutes) during 24 hours, and a simulation of release in the boundary layer for the following 5 days of atmospheric transport after the accidental release occurred.

Our detailed analysis for both NRS worst-case scenarios is shown in §2.7 of this report. However, it should be noted that specific case analysis for the Vladivostok NRS for the typical synoptic situations (in August) was performed by *Romanova & Takano, 2002*.

**Table 1.7.2.** Characteristics of radionuclides selected for dispersion modeling.

<b>Radionuclide</b>	$^{137}\text{Cs}$	$^{131}\text{I}$	$^{90}\text{Sr}$
<b>Characteristics</b>			
Half Life (s)	$9.50428 \cdot 10^8$	$6.94800 \cdot 10^5$	$9.17640 \cdot 10^8$
Dry Deposition Velocity (m/s)	0.0015	0.006	0.002
Average Particle Size ( $\mu\text{m}$ )	0.3	0.325	1.25

## II. ATMOSPHERIC TRANSPORT AND DEPOSITION PATTERNS FROM NRSs

In this chapter we will present and discuss some results based on application of the methodology for the complex probabilistic assessment of the nuclear risk sites impact suggested by *Baklanov & Mahura, 2001; Baklanov et al., 2002c*. The risk sites of concern in this study are the Kamchatka and Vladivostok NRSs located in the Russian Far East.

For this purpose we used calculated trajectories (during 1987-1996) originated over two NRSs - Vladivostok and Kamchatka – to construct and estimate various indicators of the NRS impact based on the trajectory modeling approach (*Baklanov & Mahura, 2001*). We also used calculated fields of the air concentration, integral air concentration, wet and dry deposition patterns for  $^{137}\text{Cs}$  (as a result of a continuous hypothetical release at both NRSs with a discrete emitting of radionuclide particles) – to estimate other indicators of the NRS impact based on the dispersion modeling approach (*Baklanov et al., 2002a*).

*Mahura, 2002* presented some simple characteristics of the Vladivostok and Kamchatka nuclear risk sites impact, atmospheric transport pathways as well as airflow and fast transport patterns for the areas of interest. In this report we will briefly summarize them in §2.1 and 2.2. In further sections, additional indicators of the NRS impact, such as typical transport time (§2.3), maximum reaching distance and maximum possible impact zone (§2.4), and precipitation factor or relative humidity (§2.5) fields based on the trajectory modeling are considered. Another set of NRS impact indicators, such as integral air concentration, and wet and dry deposition fields based on the dispersion modeling, will be presented in §2.6. In §2.7, following an approach for specific case studies suggested by *Baklanov et al., 2001; Baklanov & Mahura, 2001; Baklanov et al., 2002a*, we will evaluate several cases when atmospheric transport has occurred to the territories of interest (Japan, Korea, China, State of Alaska, and Aleutian Chain Islands). The geographical locations of the names used further in data analysis and interpretation are shown in Figure 2.1.

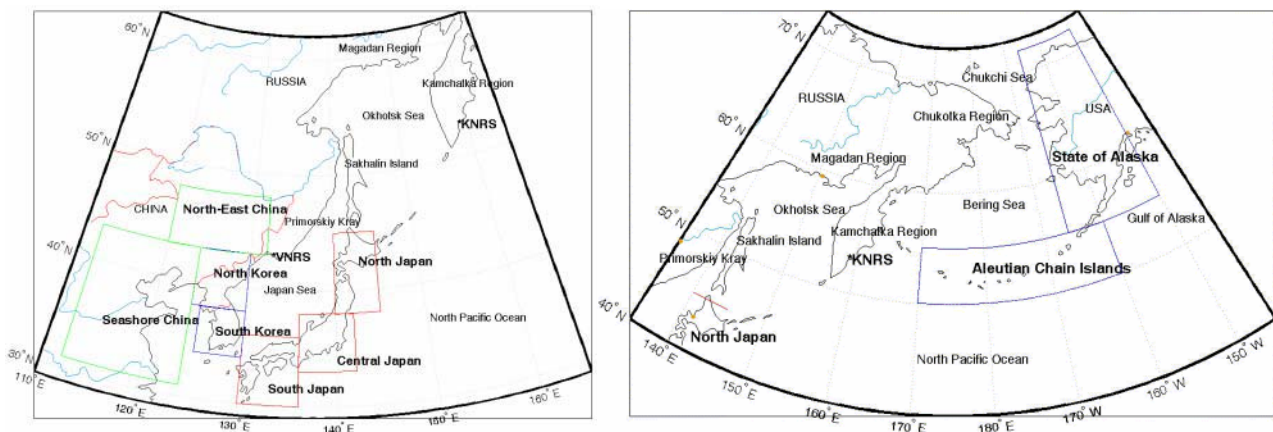


**Figure 2.1.** Geographical names and selected geographical regions of interest (VNRS – Vladivostok NRS, KNRS – Kamchatka NRS).

### 2.1. SIMPLE CHARACTERISTICS OF THE NRS IMPACT

Among the **simple characteristics of the nuclear risk sites impact**, we could suggest the following. First, it is the number and percentage of trajectories reaching the boundaries of the chosen geographical regions. Second, it is the number and percentage of days that at least one trajectory had reached the region. Third, it is the average transport time of air parcels to reach these regions. Fourth, it is the probability of transport within different atmospheric layers (boundary layer

and free troposphere). Fifth, it is the likelihood of very rapid (fast) transport of air parcels, i.e. transport in one day or less. All these characteristics can be evaluated over a multiyear dataset of calculated trajectories, by individual year, season, and month. Such analysis allows investigation of possible temporal and spatial variation in the airflow patterns from the NRS locations to selected geographical regions of interest.

Evaluation of these characteristics is based on the following. As a first approximation, trajectories can be separated into groups by altitude of the initial trajectory points. The boundaries of geographical regions can be selected depending on political borders, climatic regimes, areas of research interest, etc. For simplicity, we assumed that any trajectory, which crosses into the boundaries of the chosen geographical region, might bring air parcels containing pollutants. Therefore, trajectories crossing boundaries of these regions could be selected in the further evaluation of the simple characteristics of the NRS impact.

Another approach in the simple analysis is to apply, as a research tool, a cluster analysis technique for trajectories originated at each site. As a result of this analysis, the mean trajectories for each cluster will be produced. These mean trajectories are **atmospheric transport pathways from the nuclear risk sites**, and they can be explained based on existing synoptic features and peculiarities in the studied regions. These pathways show the general direction of atmospheric transport from the site region as well as probability of such transport (examples are shown in Figure 2.1.1). The mean trajectory for each cluster is given with points indicating 12-hour intervals. Two numbers were used for each cluster. The first is the identifier of a cluster. The second is the percentage of trajectories within a cluster. The cluster numbers are arbitrary and only used to separate the possible types of transport.

We should note that a detailed evaluation of the simple characteristics of the nuclear risk sites' impact and atmospheric transport pathways from the nuclear risk sites' locations in the Russian Far East, based on the exploratory and cluster analyses of trajectories, are discussed by *Mahura et al., 1999b; Mahura, 2002*. The focus of this study is two NRSs –Vladivostok and Kamchatka.

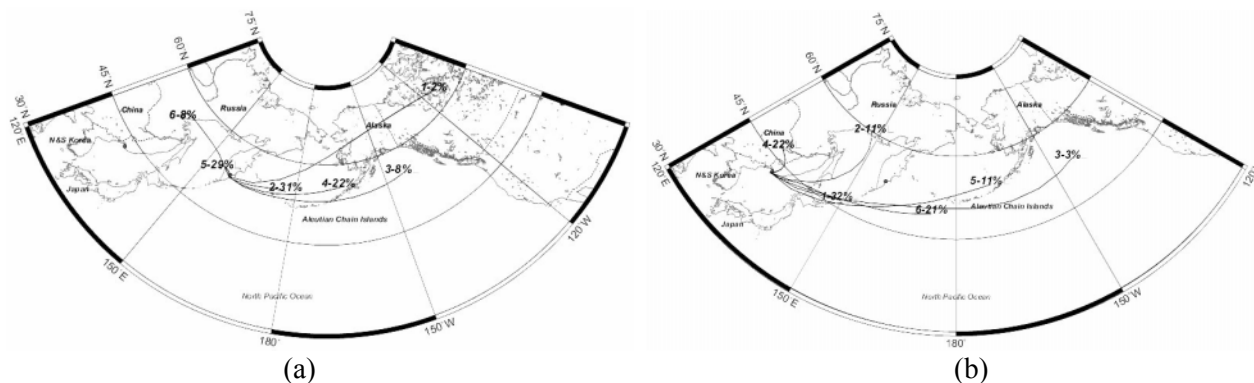


**Figure 2.1.1.** Annual atmospheric transport pathways (cluster mean trajectories) from the a) Kamchatka NRS and b) Vladivostok NRS regions.

**For the Kamchatka NRS**, *Mahura, 2002* identified six clusters for the trajectories originating over the NRS region within the boundary layer (Figure 2.1.1a). Four of them (#1, 2, 3 and 4 with 2, 31, 8 and 22% of occurrence, respectively) show westerly flow. These were observed about 63% of the time. Cluster #1 was used to show the possibility of the relatively rapid westerly flow toward the State of Alaska and Canadian territories. Cluster #6 (8%) shows easterly flow toward the continent both within the boundary layer and free troposphere. Cluster #5, which occurred 29% of the time, represents transport to the west, but it is significantly slower when compared to cluster #6. Throughout the year, westerly flow is predominant for the Kamchatka NRS.

Transport from the west varies from 63% (in winter) to 87% (in spring) of the time. Transport from the east occurs from 15% (in fall) to 37% (in winter) of the cases. Transport in the northward direction is only apparent during fall, and it is equal to 17% of the cases.

**For the Vladivostok NRS**, the same number of clusters - six - were identified for the trajectories originating within the boundary layer over the NRS region (Figure 2.1.1b). Four of them (#1, 3, 5 and 6 with 32, 3, 11 and 21% of occurrence, respectively) also show westerly flow. These were observed about 67% of the time. Among these clusters, cluster #3 represents the possibility of the relatively rapid westerly flow toward the North America territories. Cluster #4 (22%) shows easterly flow. Cluster #2, which occur 11% of the time, is transport with a northward component of the flow through the Okhotsk Sea. Throughout the year, westerly flow is also dominant for the Vladivostok NRS. Transport from the west varies from 68% (in fall) to 82% (in summer) of the time. Transport from the east occurs only during winter-spring and varies from 7% (in spring) to 10% (in winter) of the cases. Transport with the northward component is a peculiarity of the Vladivostok NRS. It is reflected in each season throughout the year and varies from 14% (in winter) to 32% (in fall) of the time.

Although results of cluster analysis are useful, they are not complete, because information between mean trajectories (or transport pathways) is “missing”. Therefore, another research tool – probability fields analysis - is required to extract this information.

## **2.2. AIRFLOW AND FAST TRANSPORT PROBABILITY FIELDS**

As we mentioned, probabilistic analysis is one of the ways to estimate the likelihood of occurrence of one or more phenomena or events. In this study, we calculated a large number of trajectories that passed over various geographical regions for each NRS. Each calculated trajectory contains information about longitude, latitude, altitude, pressure, temperature, relative humidity, etc. at each 12 hours interval. The probability fields for these characteristics, either individual or combined, can be represented by a superposition of probabilities for air parcels reaching each grid area in the chosen domain or on a geographical map. The most interest for the further analysis would be the following probabilistic fields: airflow and fast transport probability fields.

The first type of probabilistic field – **airflow probability field** - shows the most common features in the atmospheric transport patterns from NRSs. It could provide a general insight on the possible main direction of the radioactive plume transport as well as the probability that it will reach or pass a given geographical area. The result of this analysis is an appropriate test to support or reject the results from the cluster analysis, which also could be applied to identify the general atmospheric transport pathways from the site.

For the Kamchatka and Vladivostok nuclear risk sites, the annual airflow probability fields within the boundary layer, based on 5-day trajectories calculated during 1987-1996, are shown in Figure 2.2.1. Monthly variability of the airflow probability fields within the boundary layer for both sites is shown in Appendix 1. *Mahura, 2002; Mahura et al., 2002b* noted that **for the Kamchatka NRS**, the airflow is concentrated along the major tracks of the high and lower pressure systems. These systems are always under the influence of the Aleutian Low and Siberian High. During fall, the airflow reaches the North America continent. During May-November the possibility for the air masses to pass over the North Japan region is the lowest. November is a time when air masses have the ability to reach the Arctic shore territories, and it is a time for the Arctic front to move northward at the Russian Far East. During August, the airflow can pass over some parts of the State of Alaska.

**For the Vladivostok NRS**, the similar dominance of the westerly flow can be identified. During summer, the northward component of the airflow became evident. At the end of the spring,

the airflow passes over the northern parts of the continental areas of the Russian Far East. During August-November, the airflow can reach the northern areas of the Okhotsk Sea and seashore of the Magadan Region. In September, the airflow pattern can be observed in the Seashore China region reaching the lower 30°N latitudes.

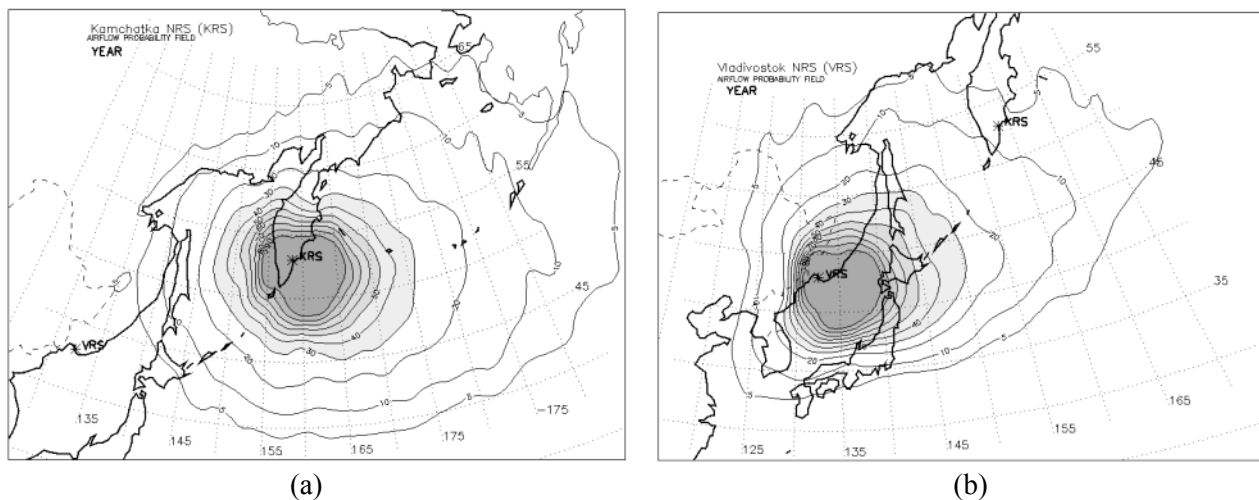


**Figure 2.2.1.** Annual airflow probability field within the boundary layer for the trajectories, originated over the a) Kamchatka NRS and b) Vladivostok NRS regions.

The second type of probabilistic fields – **fast transport probability field** - indicates the probability of air parcels movement during the first day of transport (Figure 2.2.2 show probability fields at 24 hours of atmospheric transport). In particular, these fields can be calculated after the first 12 and 24 hours of atmospheric transport. It is important information, especially, for estimation of the short-lived radionuclide impact such as the iodine isotopes. These fast transport fields show those territories that may be reached after the first half of the day or after one day, and those areas that are at the most danger due to fast transport.

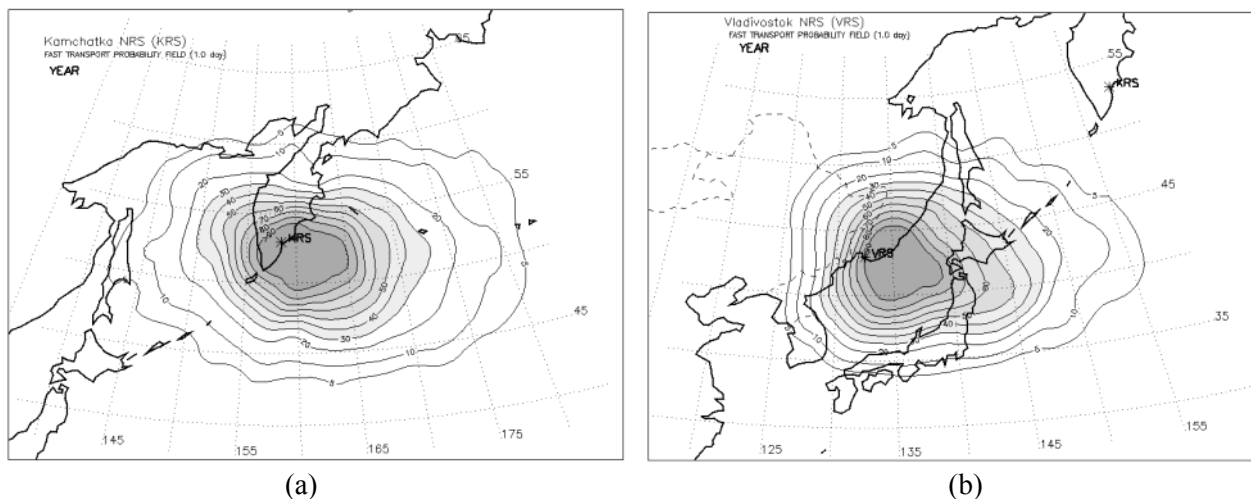


**Figure 2.2.2.** Annual fast transport probability field within the boundary layer for the trajectories, originated over the a) Kamchatka NRS and b) Vladivostok NRS regions.

Our analysis of the fast transport probability fields showed that the westerly flow is dominant for both NRSs. Monthly variability of the fast transport probability fields within the boundary layer for both sites is shown in Appendix 2. **For the Kamchatka NRS**, the area of the highest probability of the possible impact (AHPPI) from the NRS is located southeast of the site, except during summer. During winter, there is a possibility of fast transport toward the Sakhalin Island. During

fall and spring, air mass could reach the Magadan Region territories during the first day. In summer, due to lower wind speeds, it is concentrated around the NRS region. During December-April, the fast transport field indicates the possibility of reaching the Sakhalin Island and Magadan Region territories. During September-October, it almost reaches the territories adjacent to the Magadan city. In November, there is a possibility of it reaching the Primorskiy Kray. The AHPPI is located to the east and south of the NRS during November-December. In October, it is to the north, and during February-March – to the west of the site. Starting in May, the total area of the AHPPI, which is under influence of the fast transport pattern, decreases, but in August, it will start again to increase.

**For the Vladivostok NRS**, the AHPPI is also to the east and south of the site. Although in winter it is located far from NRS, and in summer it is in the proximity of the site. During fall, AHPPI is over the Japan Sea territories. During December-April, it passes over the North and Central Japan regions. In May, which might be considered as a transition period, there are two AHPPIs – above the Japan Sea and to the north of the Vladivostok NRS in the Russian Far East. During June-August and October-November, the AHPPI is situated above the Japan Sea. In September, the southward component prevails. During September-November, there is a possibility to reach the North and South Korean regions.

### **2.3. TYPICAL TRANSPORT TIME FIELDS**

In the emergency response systems for nuclear accidents, the estimation of the radionuclide transport time to a particular territory, region, county, city, etc. is one of the important input parameters in the decision-making process. We extracted this information from the calculated isentropic trajectories and constructed fields called the **typical transport time** (TTT) fields. These fields show: first, how long it will take for an air parcel to reach a particular geographical area from the NRS location, and second, what areas would be at the highest risk during the first few days of radionuclide cloud transport after an accidental release at NRS.

To visualize the TTT fields, at the first step, we construct a new polar grid domain having 36 sectors ( $10^\circ$  each) with NRS in the center. At the second step, in the same way as in the probability fields analysis, we count the number of trajectory intersections in each grid cell of new domain. Then, we select along each sector a grid cell with absolute maximum of trajectory intersections and construct an isoline of typical transport time. A similar procedure is repeated for each temporal term of 0.5, 1, 1.5, 2, and 2.5 days. More detailed information can be found in *Mahura, 2002*. Seasonal variability of the typical transport time fields for both sites is shown in Appendix 3.

**For the Kamchatka NRS** (as shown in Figure 2.3.1a), on an annual scale, only the territories of the Kamchatka Region and islands in the adjacent seas, and in particular, the Komandor Islands (Russia) and the far western islands of the Aleutian Chain Islands (USA), can be reached during the first 2.5 days.

Some differences can be observed on a seasonal scale (see Appendix 3). During spring and fall, the Sakhalin Island (Russia) could be reached typically in 2 days. The populated areas of the Magadan Region as well as northern areas of the Kamchatka Peninsula can be reached in 2.5 days. During summer, especially during the first 2 days, only the Kamchatka Peninsula and surrounding seas territories can be typically reached by atmospheric flow. During winter, the northern areas of Japan (Hokkaido Island) will be reached in 2 days as well as the southern territories of the Chukotka Region. After 1.5 days, it can be seen that there are two flow components which dominate – transport in the eastern (toward the region of the Aleutian Chain Islands) and northeastern directions (Chukotka Region seashore and western parts of the Bering Sea). It should

be noted also that after 1.5 days the transport paths cross significantly into the Western Hemisphere (cross 180°E over the North Pacific Ocean).

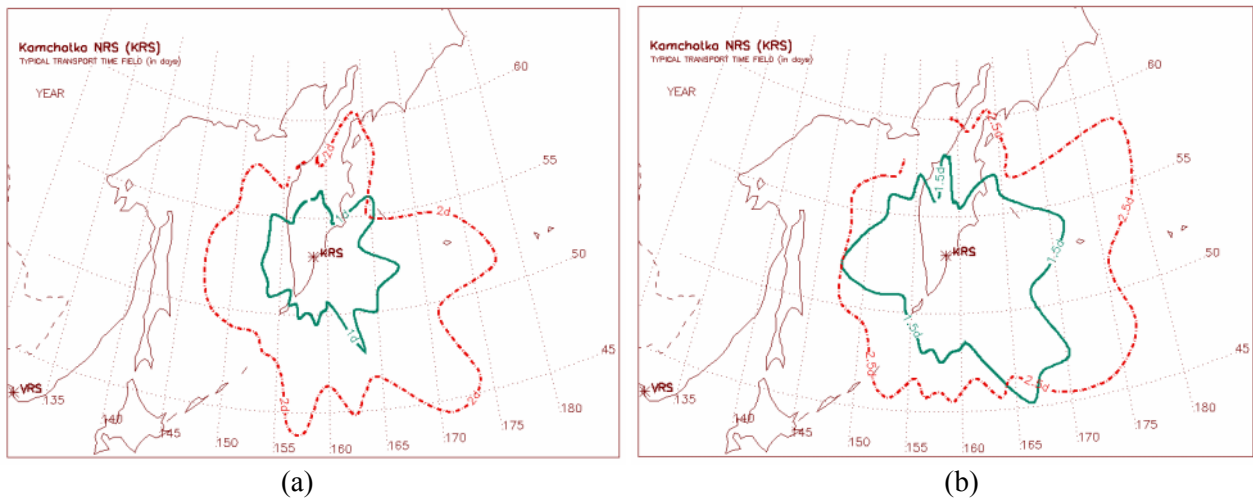


**Figure 2.3.1.** Annual typical transport time field for a) 1 & 2 days and b) 1.5 & 2.5 days of atmospheric transport from the Kamchatka NRS.

**For the Vladivostok NRS** (as shown in Figure 2.3.2), on an annual scale, the typical transport time from the site to reach the northern seashore areas of Japan is 1 day. Further, during 1-2.5 days the air parcels will pass over the Northern Japan. Typical transport time to reach the North and South Korea is about 1.5 and 2 days, respectively. We should note that the pattern of these fields depends strongly on the dominance of the westerly flows. Therefore, it is extended toward the main tracks of the cyclones traveling to the Bering Sea and Gulf of Alaska.

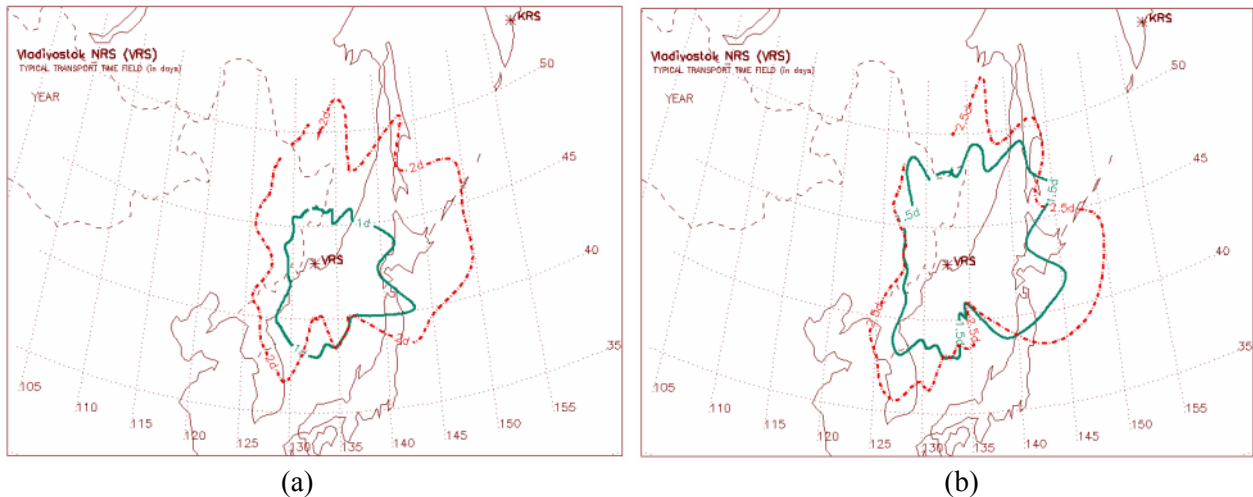


**Figure 2.3.2.** Annual typical transport time field for a) 1 & 2 days and b) 1.5 & 2.5 days of atmospheric transport from the Vladivostok NRS.

Some differences could be observed on a seasonal scale (see Appendix 3). During fall, the southern part of the Kamchatka Peninsula can be reached typically after 2.5 days of atmospheric transport. The Korean Peninsula will be first reached after 1.5 days. After 2.5 days, the air mass has traveled over both Korea. The northern areas of Japan can be reached after the first day of transport. During winter, the northern territories of Japan will be reached in less than 1 day, and central Japan - in 1.5 days, with an air mass propagating further toward the northeastern direction. During spring, similarly to winter, the central and northern territories of Japan will be reached

typically in 1-1.5 days, the southern territories – in 2.5 days. After 2-2.5 days of transport, it can reach the seashore of China. Typically transport to the Sakhalin Island occurs in 1.5 days, and it reaches the middle parts of the Okhotsk Seas after 2.5 days. During summer, the transport pattern is minimized, i.e. it will require more time to reach the geographical region of interest considered in our study. In particular, the Korea could be reached only after 2 days of transport, as well as transport to the northern territories of Japan may be minimized because of the dominating pattern of transport toward the north-north-east.

#### 2.4. MAXIMUM REACHING DISTANCE AND MAXIMUM POSSIBLE IMPACT ZONE

Let us introduce two additional fields, which will be indicators of the nuclear risk sites impact, and are based on the results of trajectory modeling. The indicator - **maximum reaching distance (MRD)** - shows the farthest boundaries on the geographical map, which might be reached during the first day, at least, by one trajectory originated over the NRS location. To visualize the MRD indicator, we used all endpoints of calculated trajectories at the end of the first day of atmospheric transport. An isoline of MRD had been drawn through the grid boxes where at least one trajectory intersected with the grid's boundaries. We should note also, that although the likelihood that an air parcel will reach these boundaries is low, it is still a possible case of transport.

The indicator - **maximum possible impact zone (MPIZ)** - as an integral characteristic shows areas as well as boundaries with the highest probability of being reached by trajectories during the first day of transport. To visualize the MPIZ indicator, we counted all endpoints of calculated trajectories during the first day of transport. Then, a similar approach for the construction of probability fields (as was used for the fast transport and airflow probability fields) was used to construct the MPIZ field. An isoline of MPIZ was drawn through the areas with the highest occurrence of trajectory intersections.

The annual MPIZ and MRD indicators are shown in Figure 2.4.1 (seasonal variability – in Figure 2.4.2 and 2.4.3 for the Kamchatka and Vladivostok NRSs, respectively; and monthly variability – in Appendix 4 of this report). The analyses are performed and presented annually, seasonally, and then monthly.

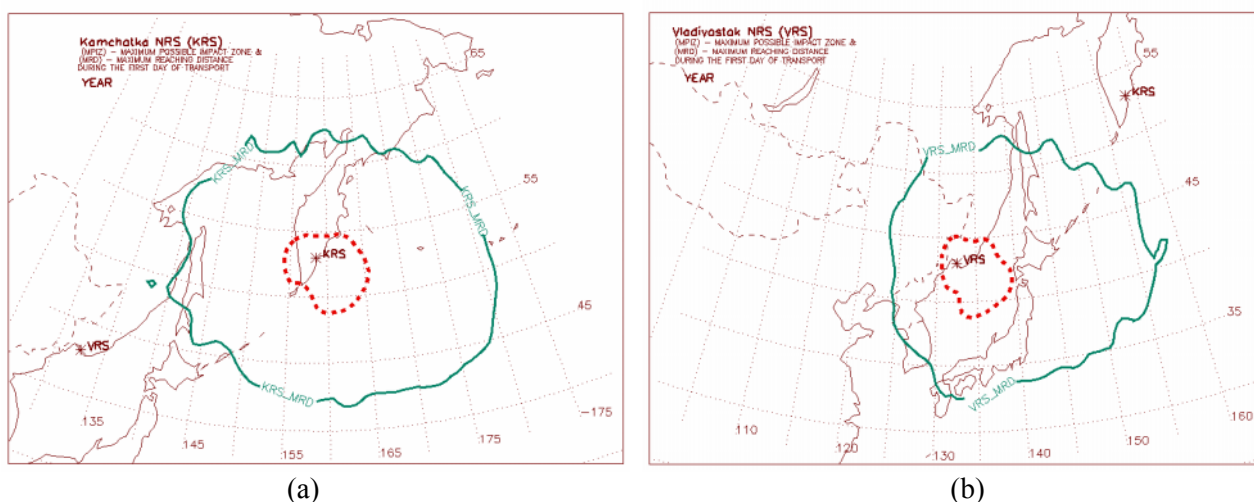


**Figure 2.4.1.** Annual maximum possible impact zone (MPIZ ---) and maximum reaching distance (MRD —) indicators for the a) Kamchatka NRS and b) Vladivostok NRS.

**For the Kamchatka NRS** (Figure 2.4.1a), on an annual scale, the areas under the MPIZ and MRD isolines are equal to  $29.8 \cdot 10^4 \text{ km}^2$  and  $676.2 \cdot 10^4 \text{ km}^2$ , respectively. It should be noted that the MRD area also includes the MPIZ area. Let us interpret these results. First, the total maximum area,

which might be potentially affected during the first day after an accidental release occurs, is more than 6762 thousand km<sup>2</sup>. Second, from this potentially affected area, an area of about 298 thousand km<sup>2</sup> is a territory with the highest probability of the NRS possible impact might be observed.

Further analysis of seasonal (Figure 2.4.2) and monthly (Appendix 4) variability of these indicators showed the following. The area of MRD varies greatly throughout the year, especially comparing summer vs. winter. In particular, during November-April, it is almost twice as high as in June-August. The area of MRD is a maximum in December ( $867.2 \cdot 10^4$  km<sup>2</sup>) and a minimum in June ( $389.3 \cdot 10^4$  km<sup>2</sup>). The MRD indicator shows that during January-March at least one trajectory during the first day of atmospheric transport can reach the northern areas of Japan. During June-September, it is practically impossible for the air mass to reach the Sakhalin Island and seashore of the Primorskiy Kray (Russia) at the end of the first day. The MRD indicator indicates that the Magadan Region territories are reachable throughout the year, although the large areas will be covered by transported air masses during November-April.

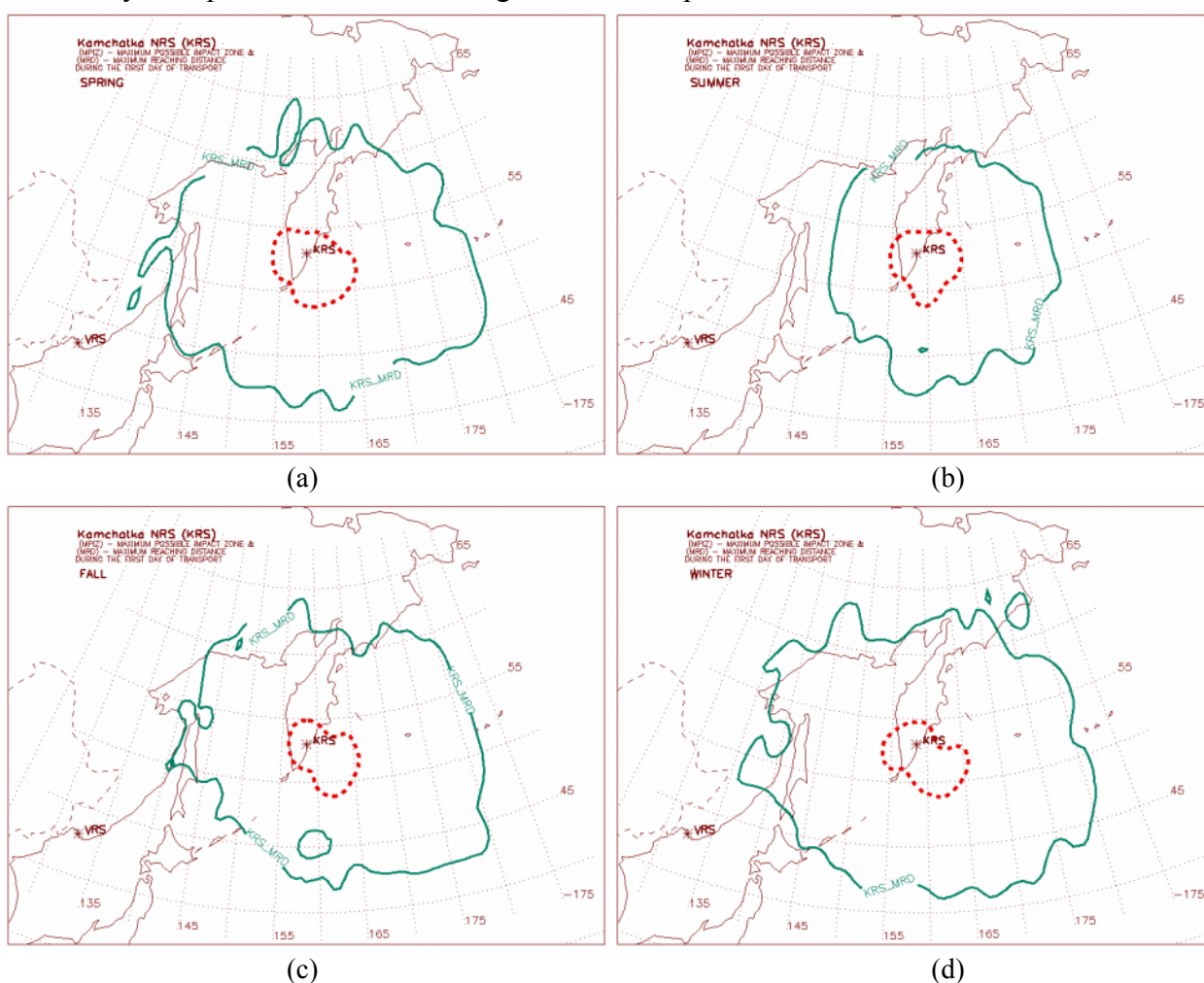


**Figure 2.4.2.** Seasonal variability of the maximum possible impact zone (MPIZ ---) and maximum reaching distance (MRD —) indicators for the Kamchatka NRS: a) spring, b) summer, c) fall, and d) winter.

The boundaries of the MPIZ are extended mostly in the southeastern direction from the site. The area of MPIZ varies throughout the year. It reaches a maximum in May ( $33.8 \cdot 10^4$  km<sup>2</sup>) and appears higher during June-September in comparison with other months. The lowest MPIZ areas are observed during October-February with an absolute minimum in January ( $18.8 \cdot 10^4$  km<sup>2</sup>). In general, the populated, southern territories of the Kamchatka Peninsula are inside the MPIZ.

For the Vladivostok NRS (Figure 2.4.1b), on an annual scale, the areas under the MPIZ and MRD isolines are equal to  $25.4 \cdot 10^4 \text{ km}^2$  and  $505.8 \cdot 10^4 \text{ km}^2$ , respectively. Both areas are smaller in comparison with the Kamchatka NRS, and at first, it depends on the characteristic wind regimes for both sites. Interpretation of values will be similar: during the first day after an accidental release the total maximum area of potentially affected territory is 5058 thousand  $\text{km}^2$ . Moreover, 254 thousand  $\text{km}^2$  of this territory are within the area of the highest probability of the NRS possible impact.

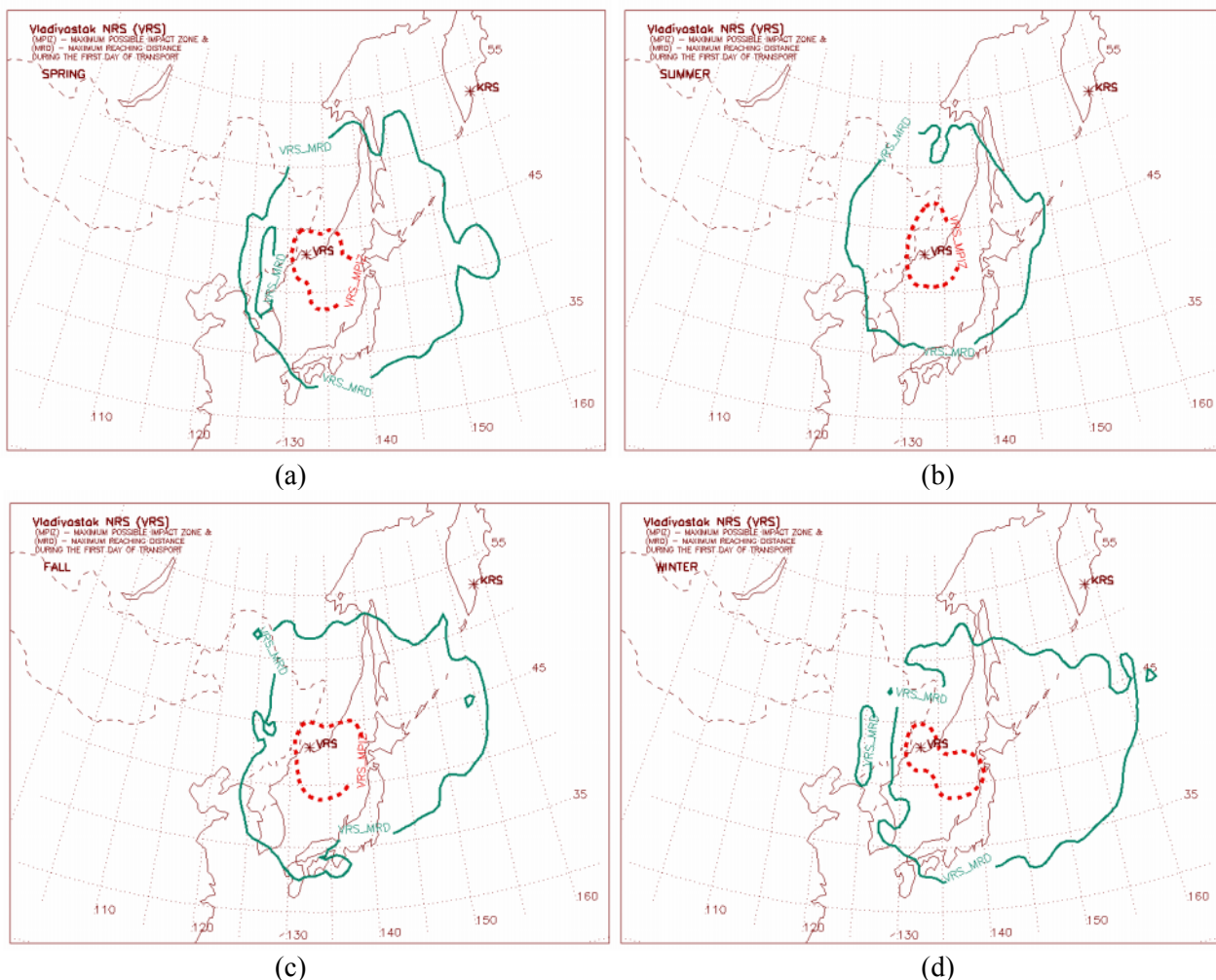


**Figure 2.4.3.** Seasonal variability of the maximum possible impact zone (MPIZ ---) and maximum reaching distance (MRD —) indicators for the Vladivostok NRS: a) spring, b) summer, c) fall, and d) winter.

Further analysis of seasonal (Figure 2.4.3) and monthly (Appendix 4) variability for these indicators showed the following. The area of MRD varied significantly throughout the year; it has a maximum in May ( $692.8 \cdot 10^4 \text{ km}^2$ ) and a minimum in July ( $296.7 \cdot 10^4 \text{ km}^2$ ). The MRD indicator showed, that throughout the year at least one trajectory during the first day of atmospheric transport could pass over Japan, although the southern territories are less reachable during summer. During January, it will be practically impossible for an air mass to reach the Korea by the end of the first day. During May-August, in comparison with other months, the MRD boundary extends further toward the west from the site almost reaching  $120^\circ\text{E}$  - Chinese northeastern territories.

The boundaries of the MPIZ are extended mostly in the southeastern direction from the site, except, during June-August when the north-south directions are dominant. In general, the populated southern territories of the Primorskiy Krai as well as northeast territories of the Russian-Chinese border are inside the MPIZ. During October-April, the isolines of MPIZ almost reach the northern

territories of Japan, and during June-August – the northern territories of the North Korea. The area of MPIZ varies throughout the year. It reaches a maximum in October ( $29.0 \cdot 10^4 \text{ km}^2$ ) and appears high during spring and fall in comparison with other seasons. The lower MPIZ areas are observed during summer and winter where an absolute minimum is found in January ( $15.7 \cdot 10^4 \text{ km}^2$ ).

## 2.5. PRECIPITATION FACTOR PROBABILITY FIELDS

During the transport of any kind of pollutants, including radionuclides, within the atmosphere, many different processes may influence the distribution of substances. In general, the temporal change of the radionuclide concentration during atmospheric transport will depend on the following factors. The dispersion, in all directions, due to horizontal advection by a wind velocity vector and turbulent diffusion are the most important factors. All radionuclides during transport are subject to dry deposition of gaseous and particulate nuclides from the atmosphere by vegetation, biological, or mechanical processes; and wet removal by precipitation, rain, and snow. Other factors are radioactive decay and resuspension (i.e. lifting of already deposited material again back into the atmosphere). Although the contributions of all factors are important, there is always a possibility to ignore some of them depending on the scale of analysis and each term's contribution to a particular problem. There are several approaches, which may be used to evaluate possible contributions to radionuclide removal by precipitation (AR-NARP, 2001-2003; Baklanov & Mahura, 2001; Mahura, 2002).

The **first approach** is based on the evaluation of precipitation as well as relative humidity climatology patterns for a particular geographical area of interest. Such climatological maps (on a multiyear, seasonal, or monthly basis for large scale domains) might be obtained from the meteorological weather services or constructed from the climatological data archives. These maps would reflect the accumulated precipitation or relative humidity measured near the surface for each interval of time. It may be used for identification of the large areas having common precipitation and relative humidity patterns. For example, NOAA-CIRES Climate Diagnostic Center (<http://www.cdc.noaa.gov>) allows, based on their data archives, to construct the relative humidity fields for different temporal intervals as shown in Figure 2.5.1.

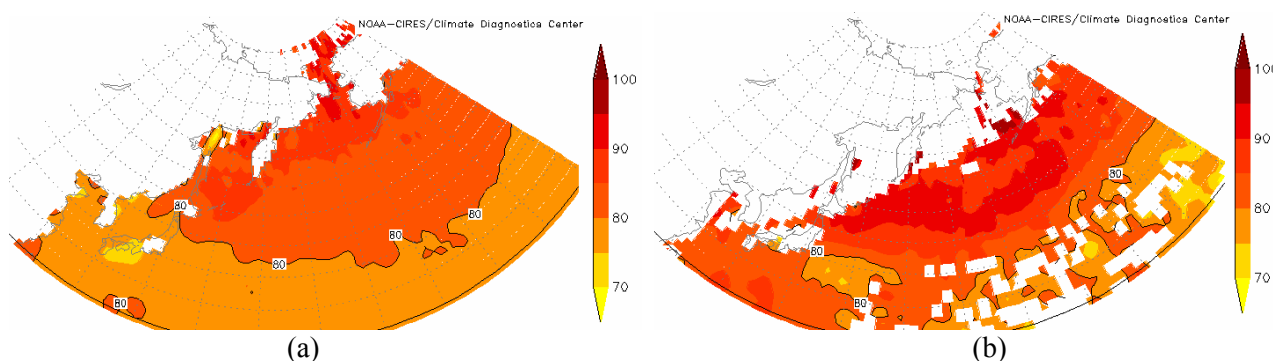


**Figure 2.5.1.** Relative humidity field for the North Pacific region based on a) 1985-1996 and b) August 1985 data (Source: NOAA-CIRES CDC).

The **second approach** is based on the evaluation of the probabilistic fields for the “precipitation factor” (INTAS, 2000; Mahura et al., 2001). Relative humidity “plays the role” of a precipitation factor. It is one of the factors, which will determine the possibility of radionuclide removal during transport. Increasing relative humidity in the atmosphere is one of the signals of the water vapor's increasing presence, and it may, in the presence of the cloud condensation nuclei (CCN), lead to the formation of cloud cover. After clouds develop and form, under certain

conditions there is a possibility of precipitation, and hence, radionuclide removal. Construction of the relative humidity fields is similar to the first steps in the probability field analysis. In this case we calculate an average value of the relative humidity in each grid cell. Both the precipitation and relative humidity fields have a cellular structure in comparison with the airflow pattern. A pitfall in this analysis is the fact that all relative humidity values are directly related to the existing flow pattern. So, each field is valid only with respect to a particular NRS. Nevertheless, it is a more realistic pattern of the possible removal during transport than calculating rainfall climatological maps used in the first approach, because it includes processes above the surface.

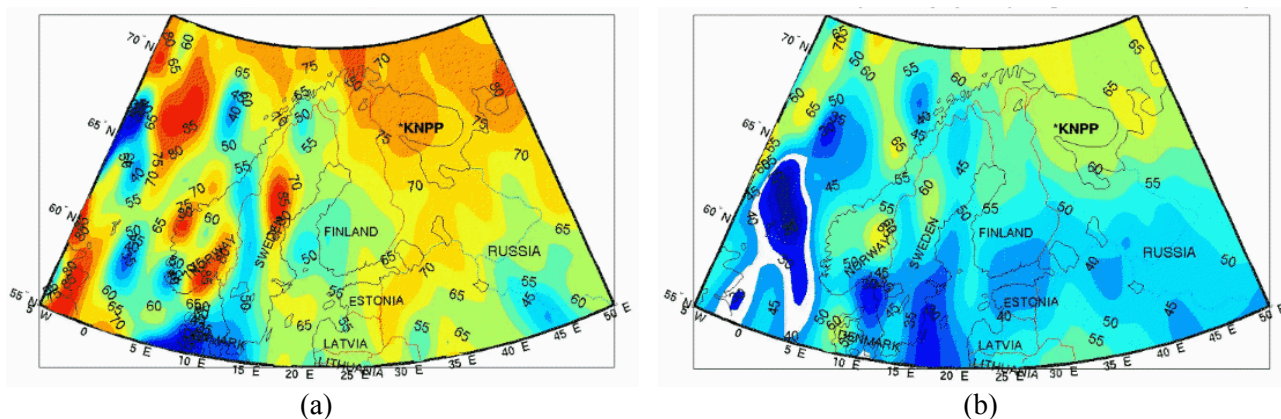


**Figure 2.5.2.** Spring relative humidity (or precipitation factor) probability field for the Kola NPP in the layer of a) surface – 1.5 km asl and b) 1.5-3 km asl.

Although we did not apply the second approach in our study, we would like to mention a possible output of such application. For example, *Mahura et al., 2001; INTAS, 2000* to account for the contribution of radionuclide wet removal during atmospheric transport, the temporal and spatial distribution of relative humidity was calculated by constructing the relative humidity probability fields over the geographical areas of concern. Several atmospheric layers - surface - 1.5, 1.5-3, 3-5, and above 5 km asl - were examined to determine altitudinal differences in the possible removal processes (see examples in Figure 2.5.2). As a first approximation, it was assumed that areas with relative humidity above 65% were areas, where water vapor could be condensed and later removed in the form of precipitation. The limitation is how we might resolve precipitation processes during air parcels transport (for example, to resolve it we might need a finer meteorological data resolution). Analysis of relative humidity fields for the Kola NPP showed that the precipitation factor's contribution dominates in the low troposphere layers, and areas associated with the Icelandic Low activity and along the main tracks of the cyclone systems.

The **third approach** is based on the direct evaluation of the wet deposition fields at the surface (*AR-NARP, 2001-2003; Baklanov et al., 2002a*). In this approach, assuming a unit continuous discrete release of puffs occurred at NRS every selected time interval (for example, every 60 minutes, or every 3 hours, etc.), we can run a model of atmospheric transport, dispersion, and deposition (both dry and wet) of the radioactive material. As a result of such simulation, we can produce a field for the wet deposition patterns accumulated during a selected time period (for example, month, season, year, or multiyear period). Analysis of such field allows one to estimate: what would be accumulated wet deposition patterns if a continuous release of radioactivity took place at NRS. Moreover, analysis of such field also allows identification of the geographical areas (presumably of the cellular nature) where the wet deposition is observed. These areas are territories where the greatest removal of radionuclides is possible during atmospheric transport from NRS. It

should be noted that such fields are also valid (as in the second approach mentioned) with respect to a particular NRS of interest. The results of the third approach are shown in §2.6.

## **2.6. NRS INDICATORS BASED ON DISPERSION MODELING: AVERAGE INTEGRAL CONCENTRATION, DRY AND WET DEPOSITION FIELDS**

As mentioned in Chapter 1, we calculated and constructed two types of fields - summary and average - for  $^{137}\text{Cs}$  for several characteristics. The summary field is a sum of fields after 5 days of atmospheric transport for a one-day discrete continuous release of radioactivity at the site during the time period of interest (for instance: month, season, or year). The average field is simply based on calculation of an average value from the summary field. That is in each latitude vs. longitude grid point the average value will be equal to the summary value divided by the number of days within the period of interest. In this study, we first constructed both types – summary and average - of fields for the integrated over time air concentration ( $\text{Bq}\cdot\text{h}/\text{m}^3$ ) of  $^{137}\text{Cs}$  in the surface layer and denoted them the **summary** and **average integral concentration at surface fields**. Second, fields constructed for the  $^{137}\text{Cs}$  dry deposition ( $\text{Bq}/\text{m}^2$ ) on the underlying surface we called the **dry deposition fields**. Third, fields constructed for the  $^{137}\text{Cs}$  wet deposition ( $\text{Bq}/\text{m}^2$ ) on the underlying surface we called the **wet deposition fields**.

In this chapter we will omit using abbreviation -  $^{137}\text{Cs}$  - assuming that all three considered fields (integral concentration, dry and wet deposition) were constructed for this particular radionuclide. Moreover, in this chapter we will consider only average fields of characteristics, although the summary fields are stored on CD (enclosed with this report if ordered).

To study temporal variability of these fields the summing and averaging of fields was performed on monthly, seasonal, and annual basis. The scaling with similar magnitude isolines starting from the lowest of  $10^{-2}$  ( $1\text{e}-2$  in Figures) is used to simplify interpretation and comparison of fields, although another scale might be selected and fields re-plotted based on the original archived data. Let us analyze annual fields using an isoline of  $10^{-2}$ , and seasonal and monthly fields with an isoline of  $10^{-1}$ .

Some important comments should also be taken into account. **First**, it should be noted that using average and summary fields it is possible to interpolate data to a particular geographical area of interest (enclosed by geographical boundaries) or for a particular geographical location (for example, a city). **Second**, the summary fields of these characteristics might be used further to calculate doses accumulated over the considered time period (month, season, year) – i.e. monthly doses, seasonal doses, or annual doses. These summary fields will be more representative if the routine discharges of radioactivity from NRS are considered. **Third**, the average fields of these characteristics might be used further to calculate doses accumulated during one day averaged over the considered time period (month, season, year) – i.e. average daily doses for a particular month, season, or year. These average fields will be more useful if the accidental short-term releases of radioactivity from NRS are considered. **Fourth**, the summary fields of characteristics will have larger areas enclosed by the isolines and the characteristic's magnitudes will be higher in comparison with average fields. **Fifth**, because all fields were calculated for the unit hypothetical release, it is possible to recalculate or rescale these fields for another accidental release of radioactivity at different magnitude rates. **Sixth**, in calculating atmospheric transport and deposition of radioactivity releases (with a duration of one day) at NRSs, we limited our calculation to 5 days after the release is completed at the site. As uncertainties in the modeling of atmospheric transport after 5 days became too great, the calculated fields for a one-day release were assumed to be unchangeable, i.e. we did not apply any loss processes after that 5 day term. Hence, once material

was deposited on the surface, the radioactive decay was not considered, although it should be accounted for the further risk and vulnerability analyses.

### **<sup>137</sup>Cs Integral Concentration Pattern**

The integral concentration of radionuclide is input data to calculate doses due to inhalation. It is an air concentration of radionuclides accumulated during a selected time interval. Therefore, for example, for a particular month, the average monthly field might be used to calculate an average dose due to inhalation at any selected geographical location at any given day of a particular month. The summary monthly field might be used to calculate the monthly dose due to inhalation at any selected geographical location.

Let us mention some common peculiarities. First, integral concentration fields have a distribution type of isolines around the site, which is closer to elliptical than circular. The shape of these fields, in some way, reflects the presence of dominating airflow patterns throughout the year. These airflow patterns could also be obtained from the results of trajectory modeling, cluster analysis, and probability fields analysis of 5-day trajectories. Second, the larger magnitudes of the integral concentration are observed near the sites, and they decrease significantly with distance, as expected.

Temporal variability of the average <sup>137</sup>Cs integral concentration fields for both sites is shown in Figure 2.6.1 (annual), Figure 2.6.2-2.6.3 (seasonal), and Appendix 5 (monthly).

**For the Kamchatka NRS** (as shown in Figure 2.6.1a), on average annually, the area from the western parts of the Kamchatka to 180°E is enclosed by the isoline of 10<sup>0</sup> Bq·h/m<sup>3</sup>. This area includes territories of the Kamchatka Peninsula as well as the farthest western islands of the Aleutian Chain Islands. The highest integral concentration (10<sup>1</sup> Bq·h/m<sup>3</sup>) is observed in the southern parts of the Kamchatka Peninsula.

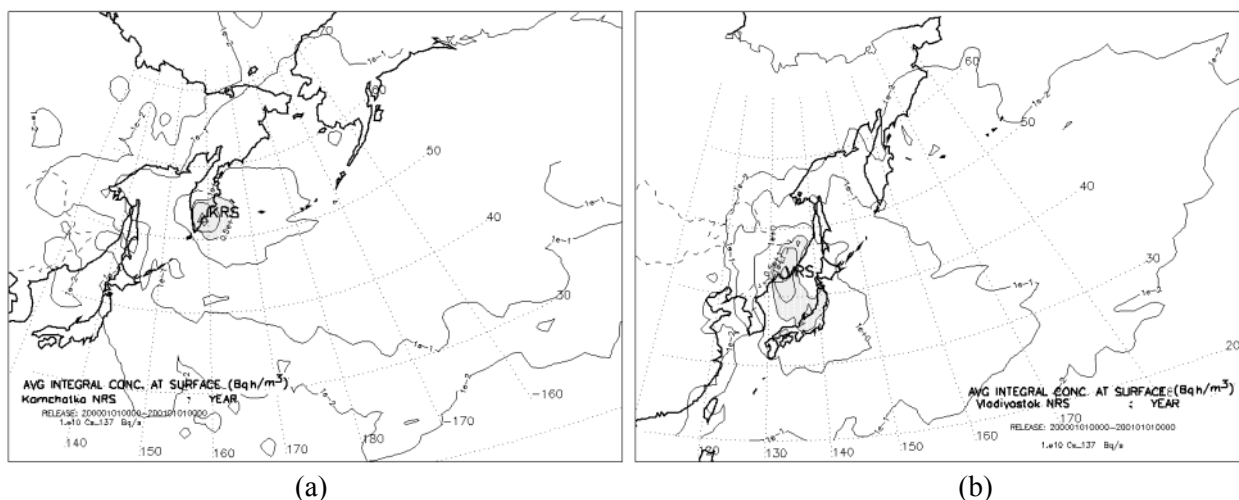


**Figure 2.6.1.** Annual average <sup>137</sup>Cs integral concentration at surface field for the “unit hypothetical release” from the a) Kamchatka NRS and b) Vladivostok NRS.

Seasonally (Figure 2.6.2), the area enclosed by the isoline of 10<sup>-2</sup> Bq·h/m<sup>3</sup> is larger, except summer, during all seasons. This selected isoline crosses into the 20-25°N-latitudinal belt during all seasons, except in summer (30°N). The continental parts of Asia are more affected during winter in comparison with other seasons, although the integral concentration does not exceed 10<sup>-2</sup> Bq·h/m<sup>3</sup> over northeast China and Primorskiy Krai, and 10<sup>-1</sup> Bq·h/m<sup>3</sup> over the Magadan and Chukotka regions. Moreover, the integral concentration pattern is a good indicator of atmospheric transport patterns. In particular, the westerly flows are dominant. The same result might be seen from the

atmospheric transport pathways (§2.1) and airflow probability fields (§2.2), both based on trajectory modeling approach.

The integral concentration pattern varies significantly temporally (considering monthly variability) and spatially (considering a distance from the site during different months) (as indicated in Appendix 5). In general, it depends on the variability of airflow patterns throughout the year: the wind speed is lower during summer and is higher in winter. Therefore, the total area of the integral concentration field (enclosed by the lowest selected isoline of  $10^{-1}$  Bq·h/m<sup>3</sup>) is lower during June-August in comparison with September-May. Moreover, the highest values are observed near the site. During October-March and August, the isoline of  $10^0$  Bq·h/m<sup>3</sup> crosses the western shore of the State of Alaska. During January-May and September, the highest integral concentration over the northern territories of Japan might reach  $10^{-1}$  Bq·h/m<sup>3</sup>, although in other months the territory remains unaffected.

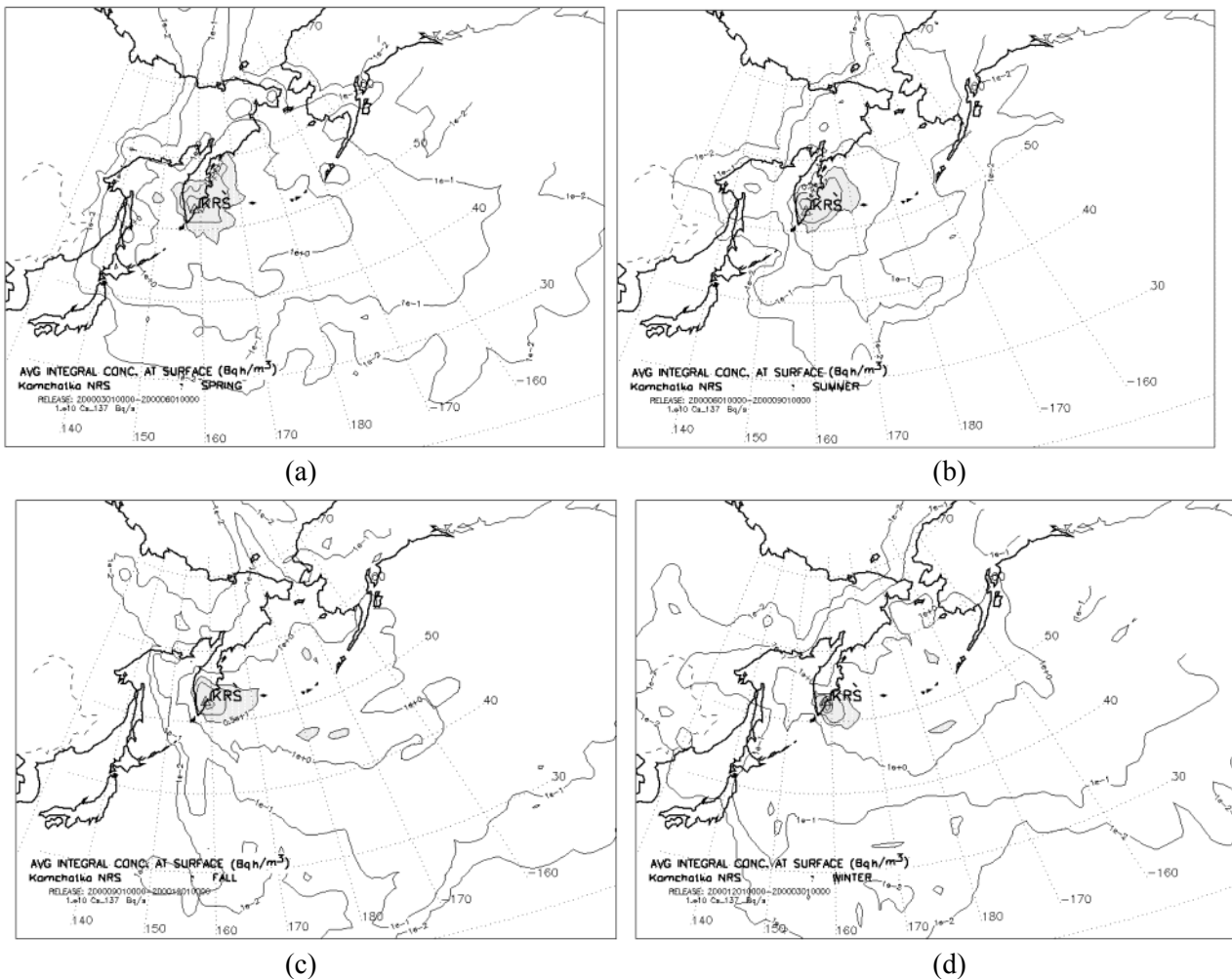


**Figure 2.6.2.** Seasonal variability of the average <sup>137</sup>Cs integral concentration at surface field for the “unit hypothetical release” from the Kamchatka NRS: a) spring, b) summer, c) fall, and d) winter.

**For the Vladivostok NRS** (as shown in Figure 2.6.1b), on average annually, the area from 130 to 150°E and from 30 to 50°N is enclosed by the isoline of  $10^0$  Bq·h/m<sup>3</sup>. This area includes the populated territories of the Primorskiy Krai, northeast China, Japan, and eastern seashore of both Koreas. Moreover, although atmospheric transport occurs in eastern direction toward the Aleutian Chain Islands, the <sup>137</sup>Cs integral concentration there does not exceed  $10^{-2}$  Bq·h/m<sup>3</sup>.

Seasonally (Figure 2.6.3), the area of the integral concentration field, enclosed by an isoline of  $10^{-2}$  Bq·h/m<sup>3</sup>, is minimal during summer with the highest values within the 130-140°E and 40-50°N geographical area. The highest integral concentrations are observed near the site throughout the year. Although the westerly flows dominated, there is a distinctive pattern of transport in the southwestern direction from the site during fall-winter, and in particular, the boundaries ( $10^{-1}$  Bq·h/m<sup>3</sup>) of the integral concentration field reached the eastern seashore of China during fall.

The structure of the average integral concentration field varies significantly throughout the year (Appendix 5). During June-September, the total area enclosed by the  $10^{-1}$  Bq·h/m<sup>3</sup> isoline is smaller in comparison with other months. It does not even reach the Kamchatka Peninsula. During October-November and March, the integral concentration at the seashore of China (below 30°N) is  $10^{-1}$  Bq·h/m<sup>3</sup>. Westerly flows dominate atmospheric transport from this site, which is also seen from the structure of the integral concentration fields. During March-April and October-December, the integral concentration along the Aleutian Chain Islands is about  $10^{-1}$  Bq·h/m<sup>3</sup>, although in other months it does not reach this magnitude. During October-April, the integral concentration of <sup>137</sup>Cs over the Japanese territories will be higher than  $10^{-1}$  Bq·h/m<sup>3</sup>.

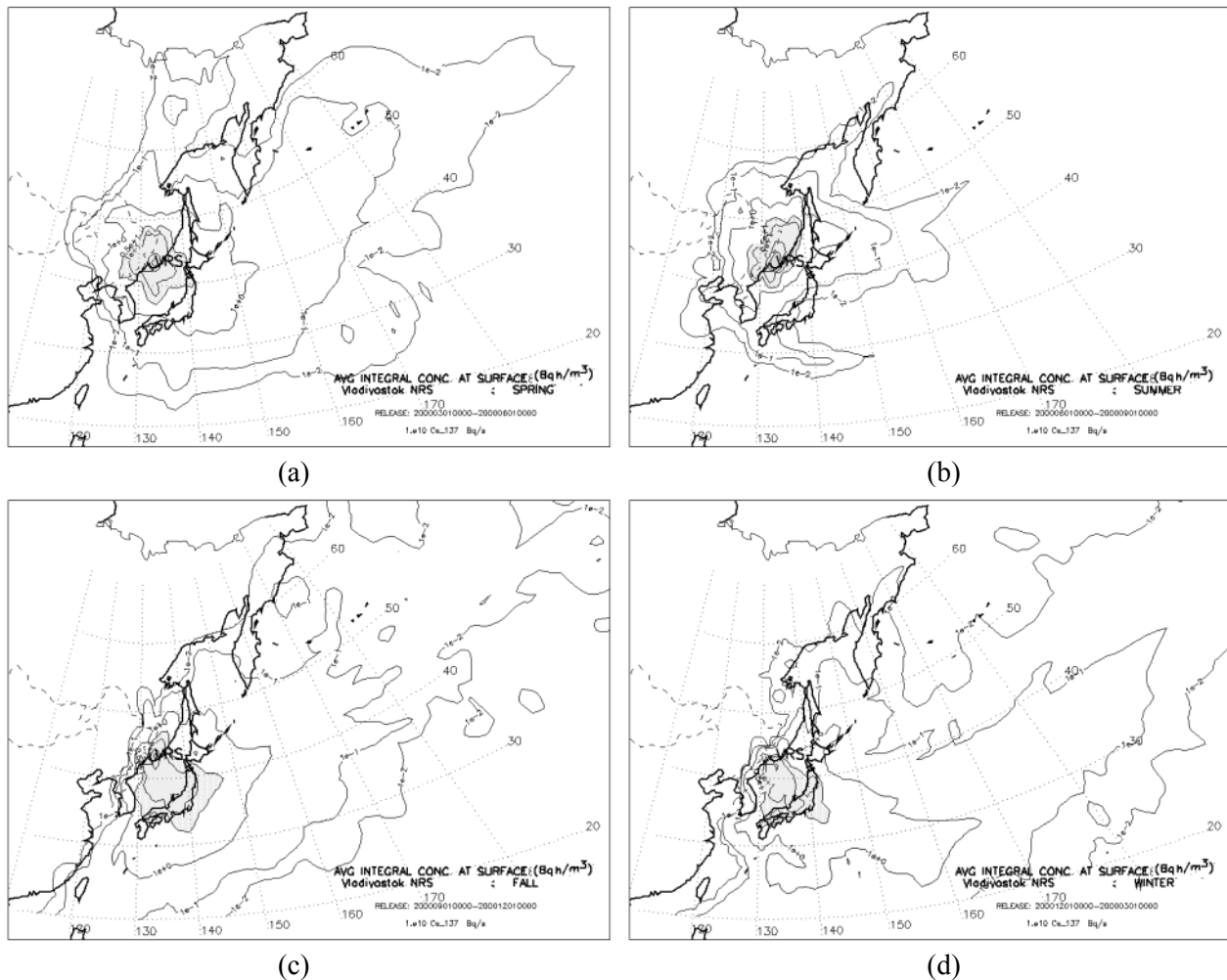


**Figure 2.6.3.** Seasonal variability of the average <sup>137</sup>Cs integral concentration at surface field for the “unit hypothetical release” from the Vladivostok NRS: a) spring, b) summer, c) fall, and d) winter.

### <sup>137</sup>Cs Dry Deposition Pattern

The dry deposition of a radionuclide is input data, as a first approximation, to calculate doses from the underlying surface. Dry deposition reflects the concentration of radionuclide deposited at

the surface due to the dry deposition process. Doses should include contribution of both – dry and wet – depositions processes, although as a first approximation, it is possible to use only dry deposition. In this case, doses would be underestimated because wet deposition is also an important contributor.

Similar to integral concentration, for a particular month, the average monthly field might be used to calculate an average dose from the underlying surface at any selected geographical location at any given day of a particular month. The summary monthly field might be used to calculate the monthly dose from the underlying surface at any selected geographical location.

The dry deposition patterns reflect in some way a structure of the integral concentration patterns. Therefore, the elliptical configuration of both fields is very similar. The dry deposition reaches its highest values in vicinity of the site. Dry deposition fields are as reliable an indicator of the prevailing atmospheric transport patterns as an airflow probability field. In particular, for both NRSs there is a clear tendency of atmospheric transport by westerly flows.

Temporal variability of the average  $^{137}\text{Cs}$  dry deposition fields for both sites is shown in Figure 2.6.4 (annual), Figure 2.6.5-2.6.6 (seasonal), and Appendix 6 (monthly).

**For the Kamchatka NRS** (as shown in Figure 2.6.4a), on average annually, the area from the western parts of the Okhotsk Sea to the middle parts of the State of Alaska (in the west-east direction), and from the Bering Strait to 35°N (in the north-south direction) is enclosed in the isoline of  $10^0 \text{ Bq/m}^2$ . This area includes the populated territories of the Kamchatka, Magadan, and Chukotka Regions as well as the Aleutian Chain Islands and western regions of the State of Alaska.

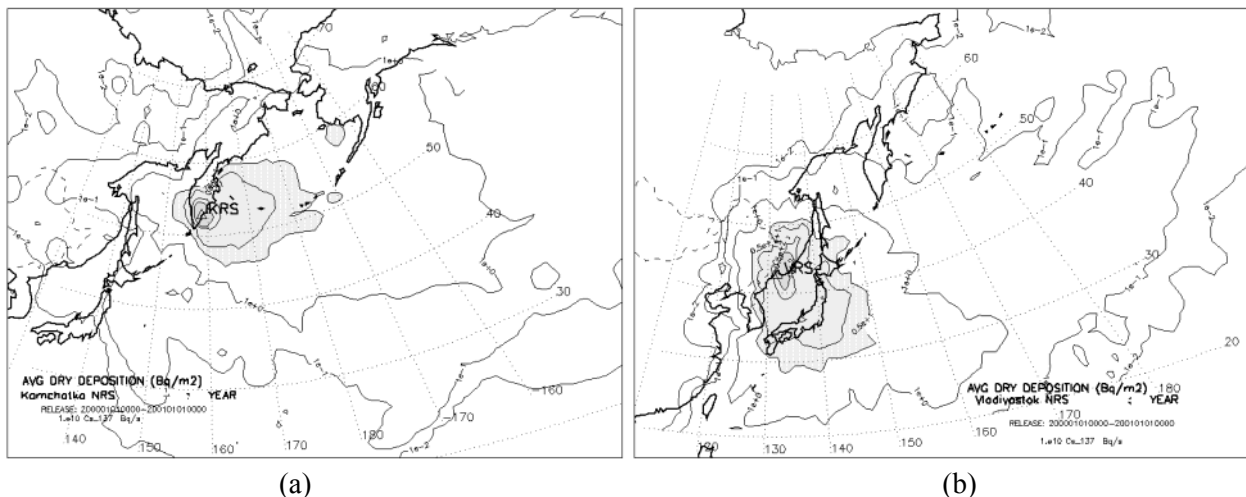


**Figure 2.6.4.** Annual average  $^{137}\text{Cs}$  dry deposition field for the “unit hypothetical release” from the a) Kamchatka NRS and b) Vladivostok NRS.

Seasonally (Figure 2.6.5), the dry deposition is lowest during summer, and it is extended in the northeastern direction, reaching the Chukchi Sea. It also shows that Japan is unaffected during summer and fall, and dry deposition there is equal to 0 because there is a low probability of atmospheric transport as seen from the airflow probability fields. During fall-winter, the boundary of  $10^0 \text{ Bq/m}^2$  isoline is extended significantly in the eastern direction from the site, reaching 140°W. During fall, the same isoline crosses the 30°N latitude line. The northeastern territories of China are more affected by dry deposition patterns during winter than in other seasons.

The configuration of the dry deposition field varies significantly throughout the year (Appendix 6). It is highly dependent upon the variability of airflow patterns. During October-May, the total area enclosed by  $10^{-1} \text{ Bq/m}^2$  isoline is larger in comparison with other months. The domination of westerly atmospheric transport could be also seen from the structure of the dry deposition fields. Therefore, the elliptical configuration of fields is extended toward the prevailing

direction of atmospheric transport. During all months, the deposition field propagates in the eastern direction from the site, except in August when there is a northeastern component. During March, July, and September, the western shore of the State of Alaska is crossed by  $10^{-1}$  Bq/m<sup>2</sup> isoline of dry deposition pattern. During June-August and October-November, the territory of Japan remains unaffected by the dry deposition, although in other months there might be deposited up to  $0.5 \cdot 10^{+1}$  Bq/m<sup>2</sup> of <sup>137</sup>Cs on the surface on average on any given day of a month. Both Korea are practically unaffected by the dry deposition field throughout the year. During January, dry deposition over the northeastern territories of China reaches  $10^1$  Bq/m<sup>2</sup>.

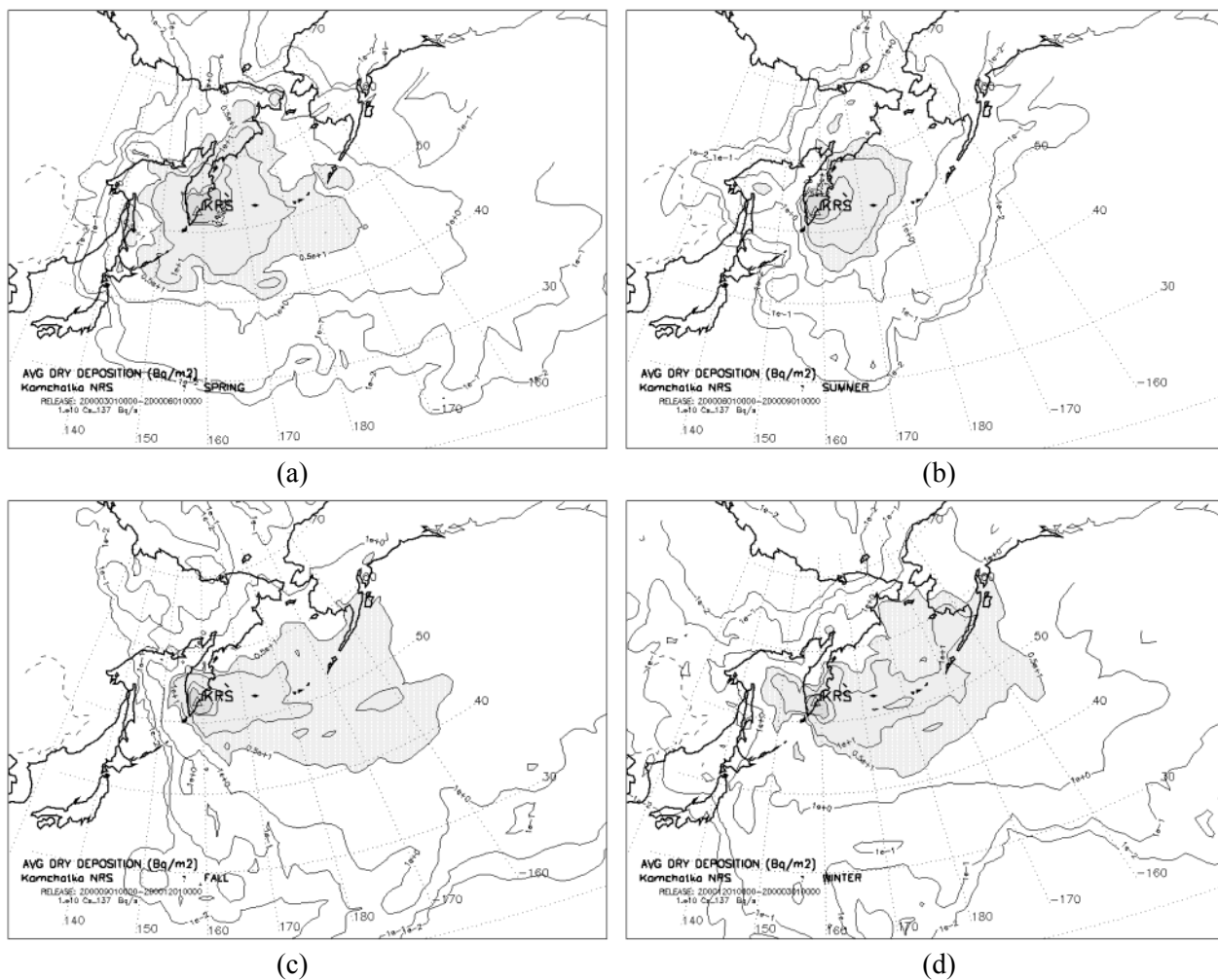


**Figure 2.6.5.** Seasonal variability of the average <sup>137</sup>Cs dry deposition field for the “unit hypothetical release” from the Kamchatka NRS: a) spring, b) summer, c) fall, and d) winter.

**For the Vladivostok NRS** (as shown in Figure 2.6.4b), on average annually, the area from 125 to 170°E and from 20 to 50°N is enclosed by the isoline of  $10^0$  Bq/m<sup>2</sup>. This area includes the populated territories of the Primorskiy Krai and Sakhalin Island, North-East China, Japan, and both Korea. Moreover, although atmospheric transport occurs in the eastern direction toward the State of Alaska and Aleutian Chain Islands, the <sup>137</sup>Cs dry deposition there does not exceed  $10^{-2}$  Bq/m<sup>2</sup>.

Seasonally (Figure 2.6.6), the area of the dry deposition field, enclosed by the  $10^{-2}$  Bq/m<sup>2</sup> isoline is minimal during summer. Two distinctive patterns might be observed. First, the highest deposition rates are observed near the site. Second, although the dominating transport is by westerlies, there are three separate outflows from the site – in eastern, southeastern, and northeastern directions. There is also a significant deposition pattern spreading from the site in the

southern and southwestern directions during winter and fall, respectively. Moreover, during fall the  $10^{-2}$  Bq/m<sup>2</sup> isoline almost reaches the seashore of China along the 120°E longitudinal line.

The configuration of the average dry deposition field varies significantly throughout the year (Appendix 6). During July-August, the total area enclosed by  $10^{-1}$  Bq/m<sup>2</sup> isoline is lower in comparison with other months. In July, it does not reach even the Kamchatka Peninsula. Westerly flows dominate atmospheric transport from the site, which is also seen from the structure of the dry deposition fields. During October-November, the dry deposition of  $10^1$  Bq/m<sup>2</sup> occurs also in the southwestern direction from the site, and during December-February – in the southeastern direction. During October-March, the dry deposition of <sup>137</sup>Cs over the Japanese territories will be higher than  $10^{+2}$  Bq/m<sup>2</sup>. During July-September and February, the dry deposition over the Kamchatka Peninsula is negligible in comparison with  $10^{-1}$  Bq/m<sup>2</sup> isoline.

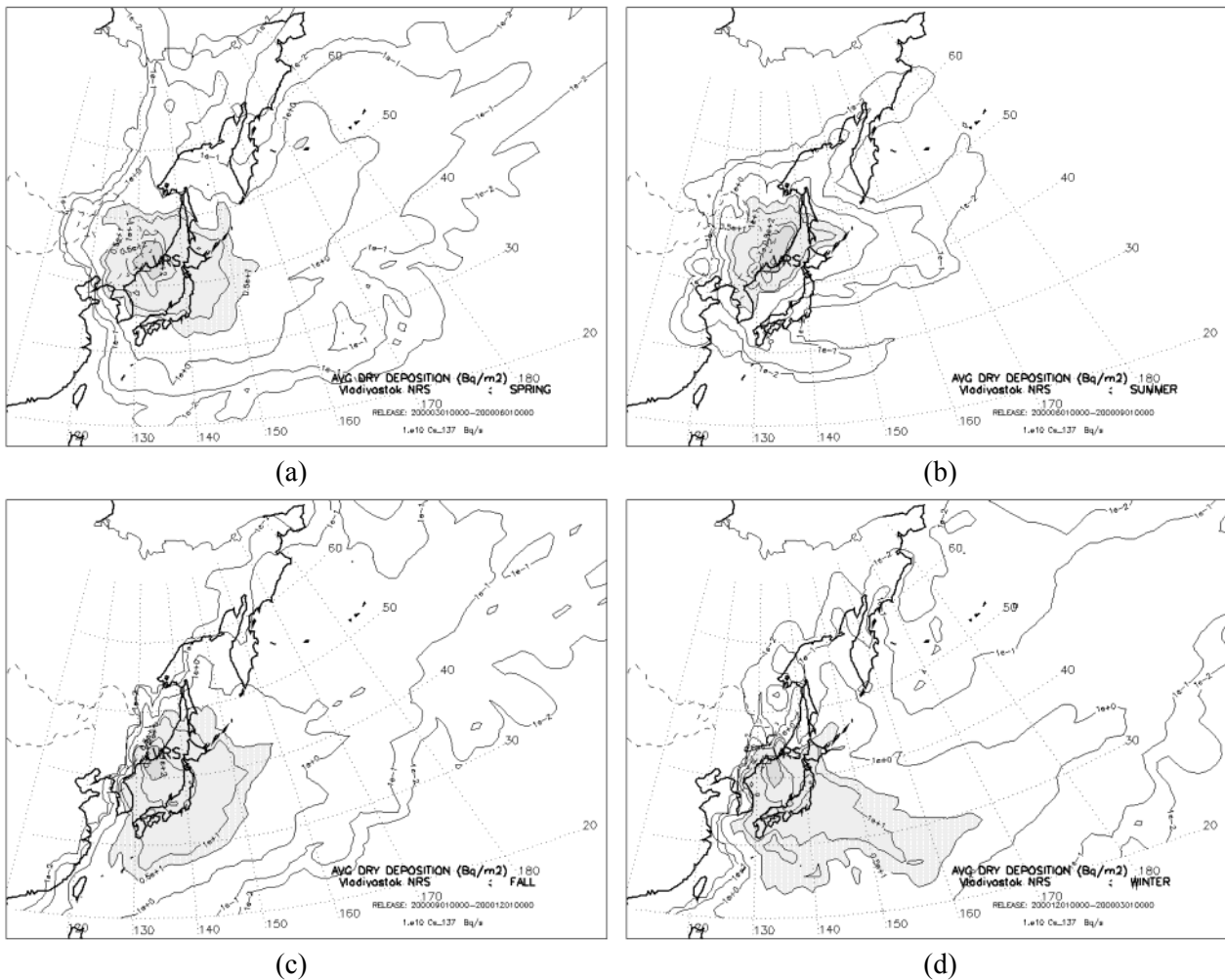


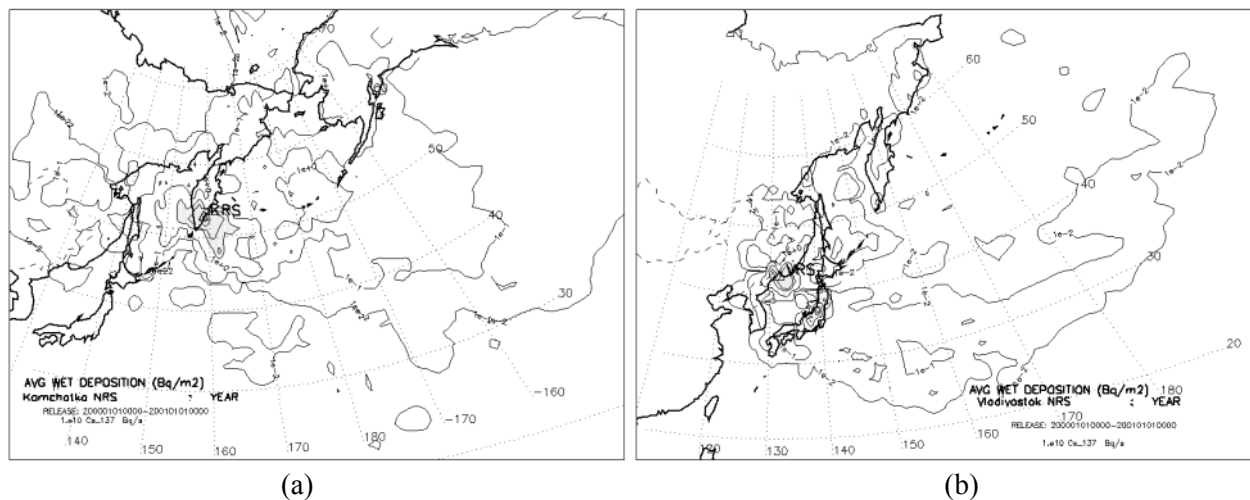
**Figure 2.6.6.** Seasonal variability of the average <sup>137</sup>Cs dry deposition field for the unit “hypothetical release from” the Vladivostok NRS: a) spring, b) summer, c) fall, and d) winter.

### <sup>137</sup>Cs Wet Deposition Pattern

The wet deposition patterns are different than the integral concentration and dry deposition patterns. The wet deposition fields are less smooth and have a cellular structure, because they reflect irregularity of the rainfall patterns. It is a concentration of radionuclide deposited at the surface due to wet deposition processes. The total deposition is a sum of dry and wet depositions, and it is also input data to calculate doses from the underlying surface.

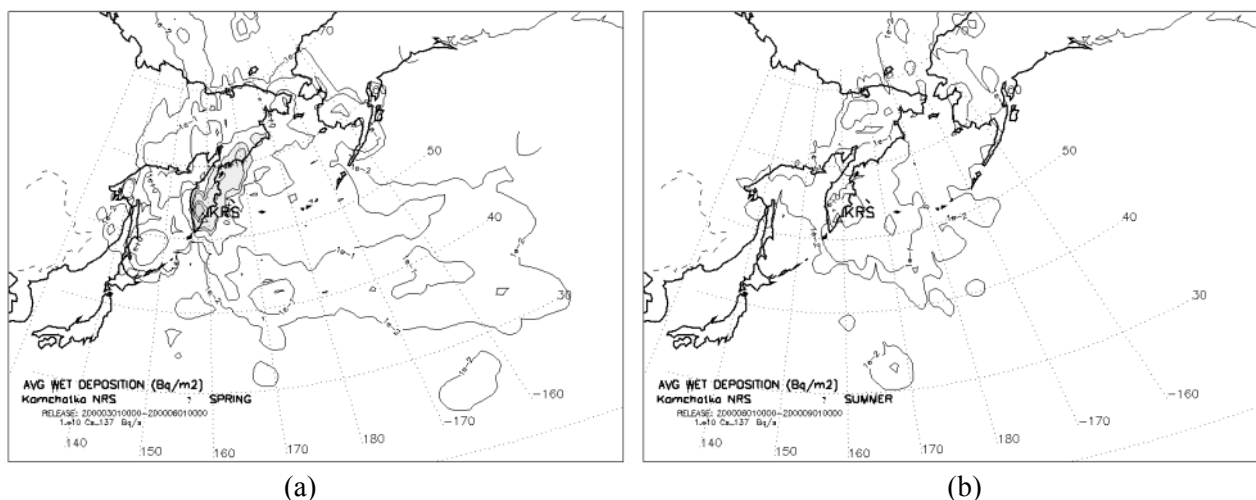
Temporal variability of the average  $^{137}\text{Cs}$  wet deposition fields for both sites is shown in Figure 2.6.7 (annual), Figure 2.6.8-2.6.9 (seasonal), and Appendix 7 (monthly). It is interesting to note, that over some geographical areas the wet deposition is higher by an order of magnitude in comparison with dry deposition, which is also a reflection of irregularity in the rainfall patterns. The wet deposition reflects a general tendency of airflow propagating in the eastern direction by westerly flows, although this tendency is less in comparison with integral concentration and dry deposition fields.

**For the Kamchatka NRS** (as shown in Figure 2.6.7a), on average annually, the area from the middle of the Okhotsk Sea to the northern parts of the Bering Sea is enclosed in the isoline of  $10^0 \text{ Bq/m}^2$ . This area includes the populated territories of the Kamchatka Peninsula, Aleutian Chain Islands, and State of Alaska. Moreover, the wet deposition reaches highest magnitude in the close proximity of the site.



**Figure 2.6.7.** Annual average  $^{137}\text{Cs}$  wet deposition field for the “unit hypothetical release” from the a) Kamchatka NRS and b) Vladivostok NRS.

Considering seasonal (Figure 2.6.8) variability of wet deposition areas enclosed by  $10^2 \text{ Bq/m}^2$  isoline, the total area is the highest during winter, and decreases throughout the year, reaching a minimum in summer. During winter, there are local maxima of wet deposition over the Russian Far East and Alaska territories. During summer, the wet deposition field is extended more toward the northeastern direction, although in other seasons it propagates in the east and east-east-south directions.



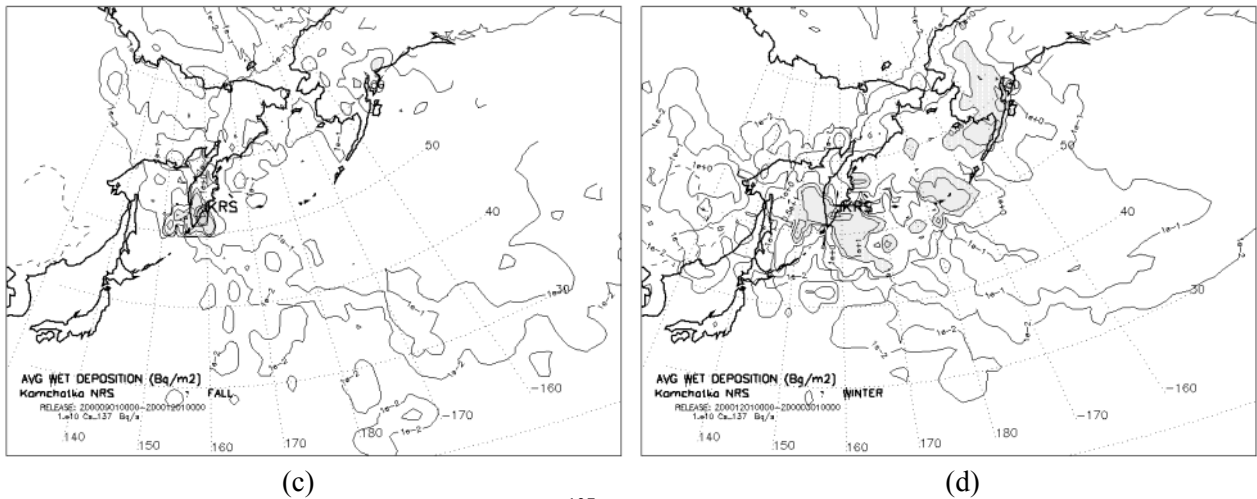
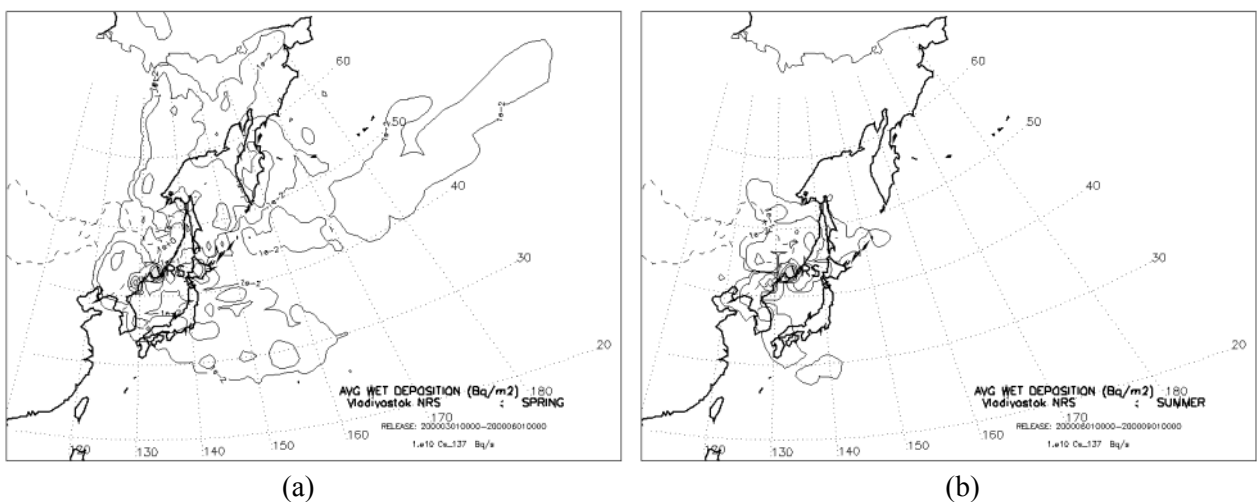


**Figure 2.6.8.** Seasonal variability of the average  $^{137}\text{Cs}$  wet deposition field for the “unit hypothetical release” from the Kamchatka NRS: a) spring, b) summer, c) fall, and d) winter.

The wet deposition pattern diminishes during June-September (Appendix 7). The area where wet deposition is occurring increases significantly during November-February with a maximum in December. The seashore territories of the Russian Far East including the Sakhalin Island are under influence of wet deposition during December-January and March-April. During January, a significant area of the continental Asian part of Russia is also covered by wet deposition pattern.

**For the Vladivostok NRS** (as shown in Figure 2.6.7b), on average annually the area between 130-140°E is enclosed in the isoline of  $10^0$  Bq/m<sup>2</sup>. This area includes partially the populated territories of the Primorskiy Kray, central Japan, and northeast China. Moreover, wet deposition reaches highest magnitude in the vicinity of the site as well as over the central territories of Japan. The configuration of wet deposition field shows the dominance of the westerly flows, which is similar to airflow patterns.

Considering seasonal (Figure 2.6.8) variability of areas enclosed by  $10^{-2}$  Bq/m<sup>2</sup> isoline (similar to the Kamchatka NRS), the total area is the highest during winter, and decreases throughout the year, reaching a minimum in summer. During winter, there are two major directions for the distribution of wet deposition pattern. The first is toward the populated territories of the Japan, both Koreas, and Russian Far East. The second is toward the maritime areas of the Pacific Ocean along the 30°N latitude line.



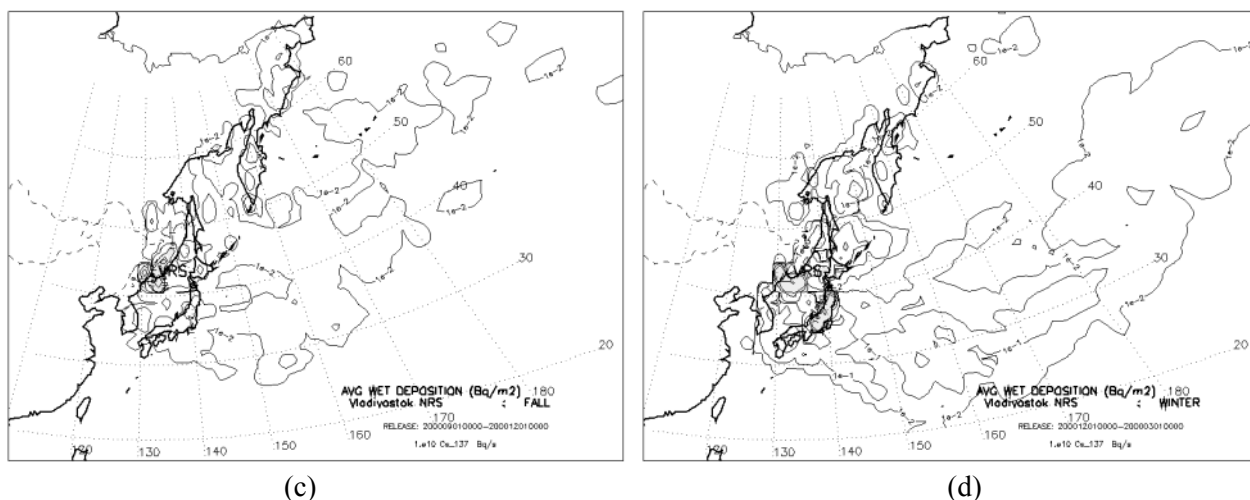


**Figure 2.6.9.** Seasonal variability of the average  $^{137}\text{Cs}$  wet deposition field for the “unit hypothetical release” from the Vladivostok NRS: a) spring, b) summer, c) fall, and d) winter.

During summer, the wet deposition field is limited to an approximately 1500 km circle around the site. It reflects the higher values in the vicinity of the site. On a monthly scale (Appendix 7), the area covered by the wet deposition field is higher during November-April in comparison with other months. During July, Japan is minimally affected by wet deposition, but it is highly affected during September-April in comparison with other months.

## 2.7. ANALYSIS OF SPECIFIC CASE STUDIES

In this section of report, we will consider in more detail the selected specific cases mentioned in §1.7. Among these cases are: a) 15<sup>th</sup> November 2000 (described in §2.7), and b) 5<sup>th</sup> and 26<sup>th</sup> April, 5<sup>th</sup>, 10<sup>th</sup>, and 17<sup>th</sup> August of 2000 (stored on CD; enclosed with this report if ordered). Any of selected cases showed atmospheric transport toward the selected regions of interest. For all these specific cases, we considered atmospheric transport, dispersion, and deposition of three radionuclides ( $^{137}\text{Cs}$ ,  $^{131}\text{I}$ , and  $^{90}\text{Sr}$ ) for the discrete continuous “unit hypothetical release” (UHR) with a fixed rate of  $1 \cdot 10^{10}$  Bq/s. The total amount of radioactivity released during one-day in this case is equal to  $1 \cdot 10^{10} (\text{Bq/s}) \cdot 24 (\text{hour}) \cdot 60 (\text{min}) \cdot 60 (\text{sec}) = 8.64 \cdot 10^{14}$  (Bq). This amount is same for all three radionuclides.

### Specific Case: Kamchatka NRS - 15 November 2000

For this specific case of 15 November 2000, we analyzed atmospheric transport of three radionuclides ( $^{137}\text{Cs}$ ,  $^{131}\text{I}$ , and  $^{90}\text{Sr}$ ) for the “unit hypothetical release” (UHR) occurred during 24 hours (15-16 Nov 2000, 00 UTC) simultaneously at both NRSs. For UHR occurred at the Kamchatka NRS, we consider atmospheric transport toward the State of Alaska and Chukotka region territories. For UHR occurred at the Vladivostok NRS we consider atmospheric transport toward the Aleutian Chain Islands, Japan, and both Korea.

Following the subsequent temporal daily snapshots of the  $^{137}\text{Cs}$  surface air concentration field (Figure 2.7.1), it is possible to identify the development of the atmospheric transport from the site. For example, for the Kamchatka NRS, at the end of 1<sup>st</sup> day (16 Nov 2000, 00 UTC) after release started (15 Nov 2000, 00 UTC), the radioactive cloud extended in the southwestern and eastern directions passing over the southern areas of the Kamchatka Peninsula into the Okhotsk Sea and reaching 170°E.

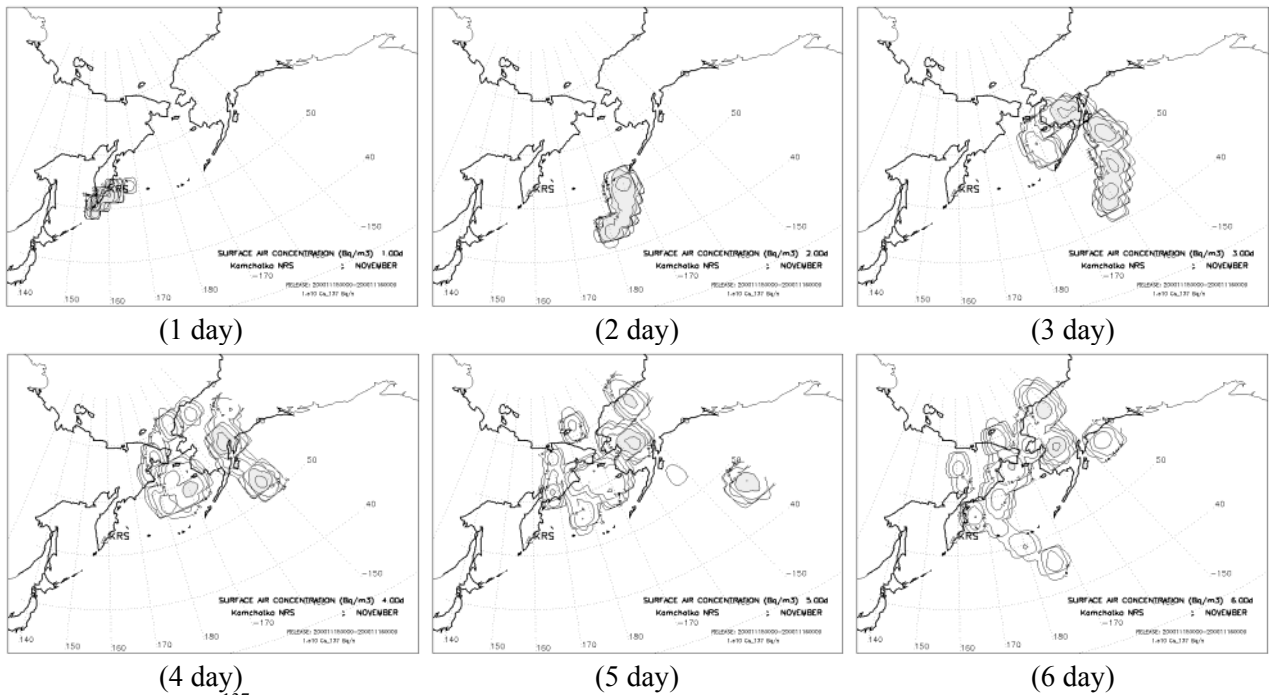


**Figure 2.7.1.**  $^{137}\text{Cs}$  surface air concentration field for the “unit hypothetical release” occurred at the Kamchatka NRS during 15-16 Nov, 2000, 00 UTC.

During 2<sup>nd</sup> day it is relatively fast transported and dispersed by the westerly flows toward the Aleutian Chain Islands almost reaching 40°N and 170°W. By the end of 3<sup>rd</sup> day, the cloud passed over the southwestern territories of the State of Alaska and moved into the Bering Sea aquatoria as well as partially continued to propagate in the eastern direction (150°W). During 4<sup>th</sup> day, it continued atmospheric transport in the northern directions passing over the Chukotka region, northern and central parts of the State of Alaska and Bering Sea into the Chukchi Sea. During 5<sup>th</sup> and 6<sup>th</sup> days it circled around the same area expanding in the latitudinal and longitudinal directions, finally almost reaching the Kamchatka Peninsula, where the release occurred.

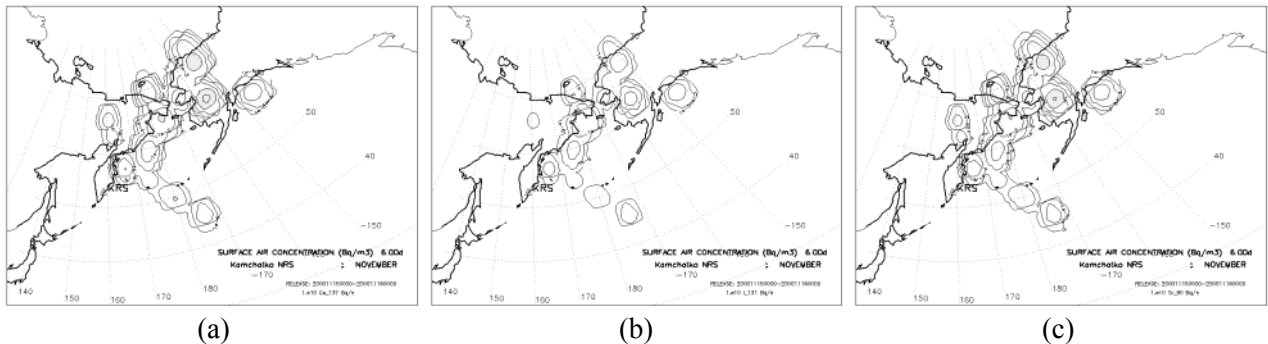
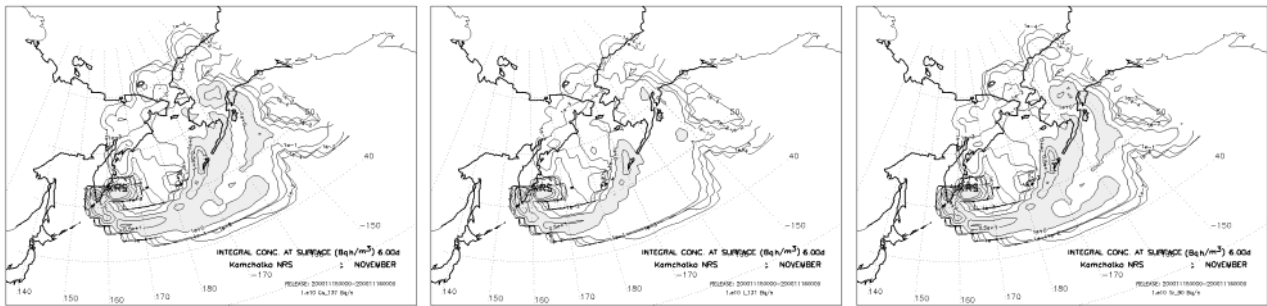


**Figure 2.7.2.** Surface air concentration fields of a)  $^{137}\text{Cs}$ , b)  $^{131}\text{I}$ , and c)  $^{90}\text{Sr}$  for the “unit hypothetical release” occurred at the Kamchatka NRS during 15-16 Nov, 2000, 00 UTC.

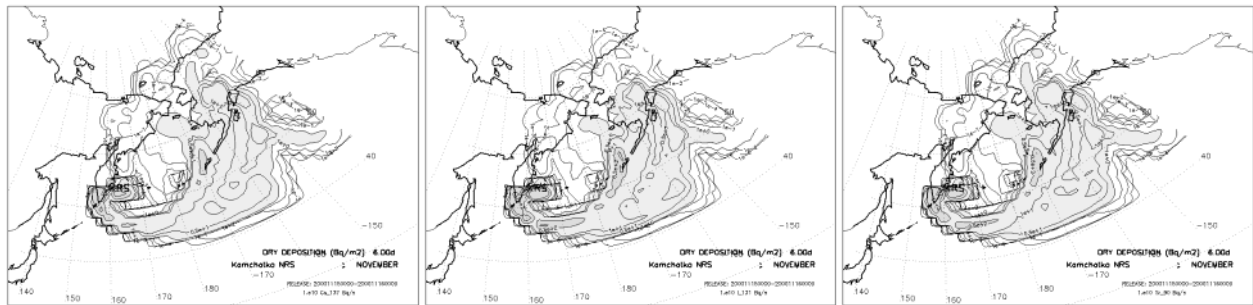
For this specific case, we analyzed four characteristics: surface air concentration, integral concentration, dry and wet deposition. Figures 2.7.1-2.7.5 shows 2-dimensional fields plotted at the end of the 6<sup>th</sup> day of atmospheric transport after the release had started at the Kamchatka NRS.

Analysis of fields (shown in Figures 2.7.1-2.7.5) allows us to identify several features for this specific case. First, it should be noted that for  $^{137}\text{Cs}$  and  $^{90}\text{Sr}$  the shape and magnitude of isolines are similar for all characteristics, which is due to almost the same half lifetimes and reference dry deposition velocities for these radionuclides (see Table 1.7.2) in comparison with  $^{131}\text{I}$ . Second, for

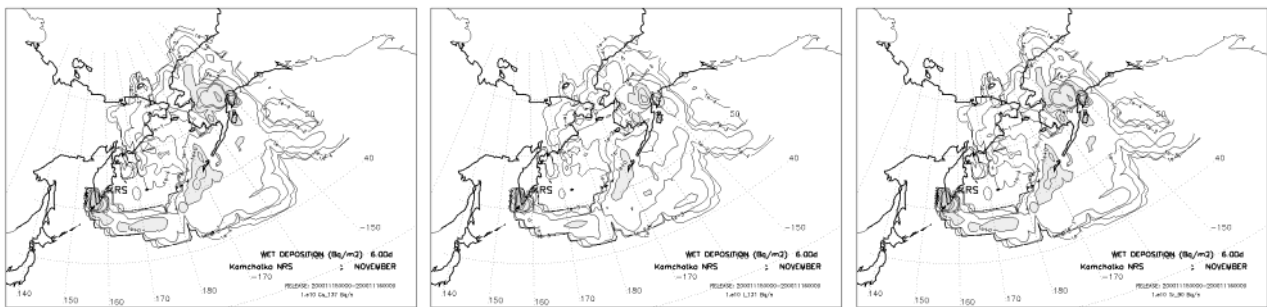
$^{131}\text{I}$ , the surface air concentration decreases faster with distance from the site; similar to other calculated characteristics, although the rate of decrease is slower.



(a) (b) (c)  
**Figure 2.7.3.** Integral concentration fields of a)  $^{137}\text{Cs}$ , b)  $^{131}\text{I}$ , and c)  $^{90}\text{Sr}$  for the “unit hypothetical release” occurred at the Kamchatka NRS during 15-16 Nov, 2000, 00 UTC.



(a) (b) (c)  
**Figure 2.7.4.** Dry deposition fields of a)  $^{137}\text{Cs}$ , b)  $^{131}\text{I}$ , and c)  $^{90}\text{Sr}$  for the “unit hypothetical release” occurred at the Kamchatka NRS during 15-16 Nov, 2000, 00 UTC.



(a) (b) (c)  
**Figure 2.7.5.** Wet deposition fields of a)  $^{137}\text{Cs}$ , b)  $^{131}\text{I}$ , and c)  $^{90}\text{Sr}$  for the “unit hypothetical release” occurred at the Kamchatka NRS during 15-16 Nov, 2000, 00 UTC.

Third, the territory between 160-180°E and 50-55°N was not significantly affected by precipitation, and therefore, the wet deposition over this region is smaller compared with the dry deposition contribution. The integral concentration and dry deposition showed similarities when the air mass had traveled over this region. Moreover, the wet deposition field for this particular case has a pattern in some way similar to dry deposition, although, in general, it has an irregular form.

Additionally, the area under a particular order of magnitude isoline could be calculated similarly to estimation of areas enclosed by isolines of the maximum reaching distance and maximum possible impact zone indicators (based on results of trajectory modeling). If several geographical locations of interest are selected (i.e. its latitude and longitude are known) then exact

values of the integral concentration, dry deposition, and wet deposition can be calculated by interpolation from the original fields.

**Table 2.7.1.** Selected geographical locations/sites by countries.

Country	Locations/Sites	Latitude vs. Longitude
USA	Anchorage	61.2°N, 150.0°W
	Barrow	71.3°N, 156.8°W
	Fairbanks	64.8°N, 147.9°W
	Nome	64.5°N, 165.4°W
	Kodiak	57.8°N, 152.5°W
	Shemya	52.7°N, 174.1°E
Japan	Fukuoka	33.6°N, 130.5°E
	Sapporo	43.1°N, 141.4°E
	Tokyo	35.7°N, 139.8°E
Korea	Pyongyang	39.0°N, 125.7°E
	Seoul	37.6°N, 127.0°E

Let us evaluate orders of magnitude for the integral concentration, and dry and wet deposition after 5 days of atmospheric transport from NRSs at selected geographical locations or sites (Table 2.7.1) and selected regions of interest (shown in Figure 2.1). For locations/sites, we estimated a magnitude of characteristics at exact latitude vs. longitude point on a map. For geographical regions of interest, we estimated a maximum and an average (in Tables 2.7.2 and 2.7.3 this value is shown in paratheses) magnitudes of the same characteristics within latitudinal vs. longitudinal boundaries of regions (shown in Figure 2.1).

**Table 2.7.2.** Calculated characteristics for the selected geographical regions of interest and locations/sites for the “unit hypothetical release” occurred at the Kamchatka NRS during 15-16 Nov, 2000, 00 UTC.

Characteristic Units Radionuclide	Integral Concentration			Dry Deposition			Wet Deposition		
	Bq·h/m <sup>3</sup>			Bq/m <sup>2</sup>			Bq/m <sup>2</sup>		
	Cs <sup>137</sup>	<sup>131</sup> I	<sup>90</sup> Sr	Cs <sup>137</sup>	<sup>131</sup> I	<sup>90</sup> Sr	Cs <sup>137</sup>	<sup>131</sup> I	<sup>90</sup> Sr
<b>Regions</b>									
<i>Alaska State</i>	0(-1)	0(-1)	0(-1)	+1(0)	+1(0)	+1(0)	+1(0)	+1(-1)	+1(0)
<i>Aleutian Islands</i>	+1(0)	0(-1)	+1(0)	+1(0)	+2(+1)	+1(+1)	+1(-1)	0(-1)	0(-1)
<b>Sites</b>									
<i>Kamchatka NRS</i>	+2	+2	+2	+2	+3	+3	+2	+2	+2
<i>Anchorage</i>	0	-1	0	0	0	+1	0	0	0
<i>Barrow</i>	-3	-5	-3	-2	-4	-2	-3	-5	-3
<i>Fairbanks</i>	-3	-4	-3	-2	-3	-2	-3	-4	-3
<i>Nome</i>	-1	-2	-1	-1	-1	-1	-2	-3	-2
<i>Kodiak</i>	-1	-1	-1	0	0	0	-2	-2	-2
<i>Shemya</i>	-3	-4	-4	-3	-3	-3	-6	-7	-6

For the Kamchatka NRS, as shown in Table 2.7.2, the order of magnitude for the integral concentration and wet deposition is +2, and for dry deposition it varies between +2 and +3. For Anchorage, all characteristics have the highest order of magnitudes in comparison with other sites. Shemya has the lowest wet deposition. For regions of the Aleutian Chain Islands and State of Alaska, for the integral concentration and dry deposition, there is only one order of magnitude difference between maximum and average (given in paratheses) values, although for wet deposition it is two.

### **Specific Case: Vladivostok NRS - 15 November 2000**

Similarly, the temporal variability of the atmospheric transport from the Vladivostok NRS could be analyzed. Let us follow the subsequent temporal daily snapshots of the surface air concentration field (stored on CD; enclosed with this report if ordered). At the end of 1<sup>st</sup> day (16 Nov 2000, 00 UTC) after release started (15 Nov 2000, 00 UTC), the radioactive cloud extended in the southeastern and eastern directions passing over Japan into the Pacific Ocean along 35–40°N belt. During 2<sup>nd</sup> day the radioactive cloud was divided into two parts. The first part was transported over both Korea due to a newly arrived cyclone from the continental Asia. The second part was transported in the southern direction over the southern Japanese territories. By the end of 3<sup>rd</sup> day: the first part passed again over Japan, and the second continued transport in the southwestern direction crossing 20°N. During 4<sup>th</sup> day, the second part of the cloud continued slow atmospheric transport in the southwestern direction almost reaching seashore of China. In the same time, the first part of the cloud was transported by westerlies through the Pacific Ocean reaching 170°E. During 5<sup>th</sup> and 6<sup>th</sup> days, both parts of original cloud continued transport in the same directions. The first part reached slowly the seashore of China. The second part passed rapidly south of the Aleutian Chain Islands into the Gulf of Alaska and reached the southern territories of the State of Alaska.

Similarly to analysis of the Kamchatka NRS release at specific date, for selected geographical locations or sites (Table 2.7.1), we estimated a magnitude of characteristics at exact latitude vs. longitude point on a map. For geographical regions of interest, we also estimated a maximum and an average (in Table 2.7.3 this value is given in paratheses) magnitudes of the same characteristics within latitudinal vs. longitudinal boundaries of regions (shown in Figure 2.1).

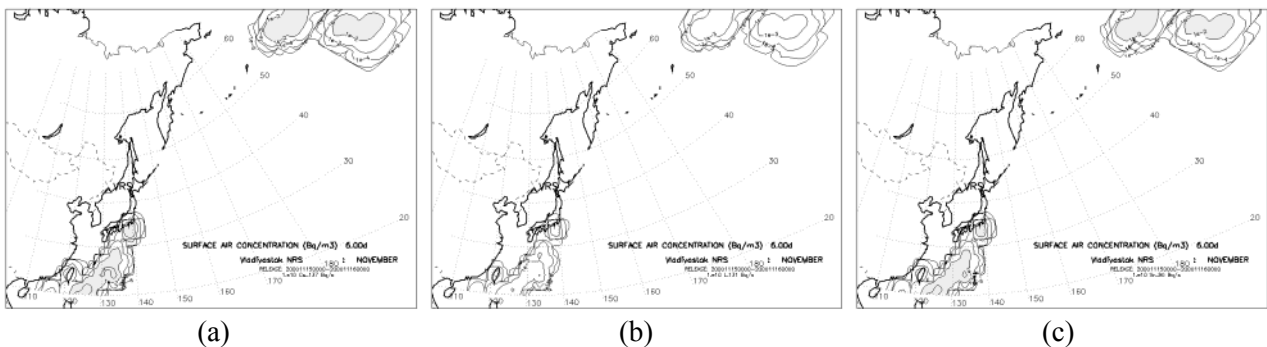


**Figure 2.7.6.** Surface air concentration fields of a)  $\text{Cs}^{137}$ , b)  $\text{I}^{131}$  and c)  $\text{Sr}^{90}$  for the “unit hypothetical release” occurred at the Vladivostok NRS during 15-16 Nov, 2000, 00 UTC.

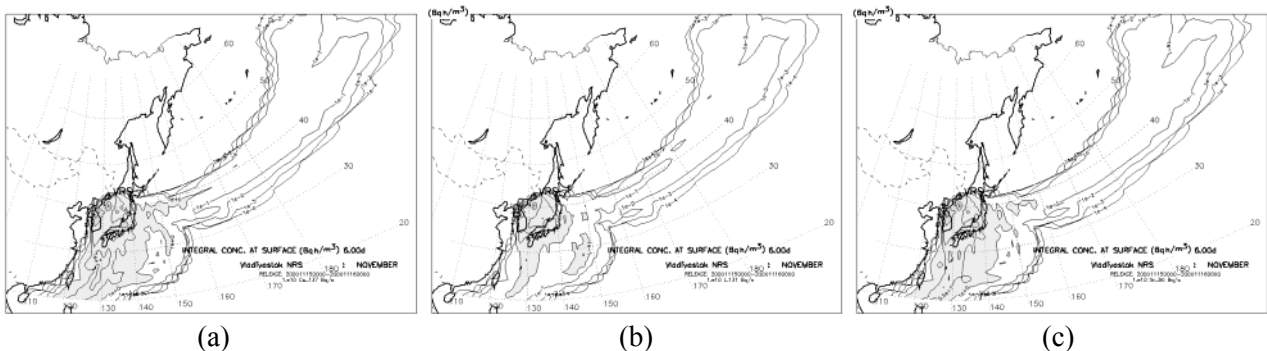


**Figure 2.7.7.** Integral concentration fields of a)  $\text{Cs}^{137}$ , b)  $\text{I}^{131}$  and c)  $\text{Sr}^{90}$  for the “unit hypothetical release” occurred at the Vladivostok NRS during 15-16 Nov, 2000, 00 UTC.

For this specific case, we analyzed four characteristics: surface air concentration, integral concentration, dry and wet deposition. Figures 2.7.6-2.7.9 shows 2-dimensional fields plotted at the end of the 6<sup>th</sup> day of atmospheric transport after the release had started at the Vladivostok NRS.

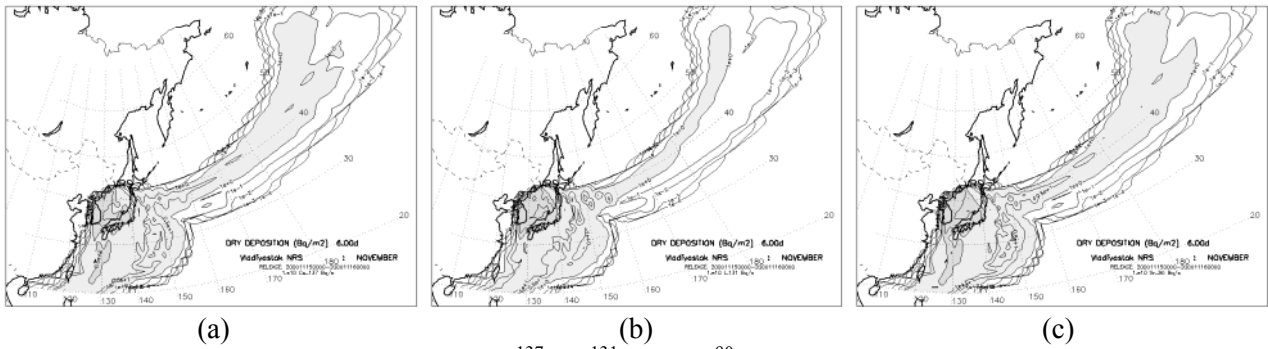


**Figure 2.7.8.** Dry deposition fields of a)  $\text{Cs}^{137}$ , b)  $^{131}\text{I}$  and c)  $^{90}\text{Sr}$  for the “unit hypothetical release” occurred at the Vladivostok NRS during 15-16 Nov, 2000, 00 UTC.

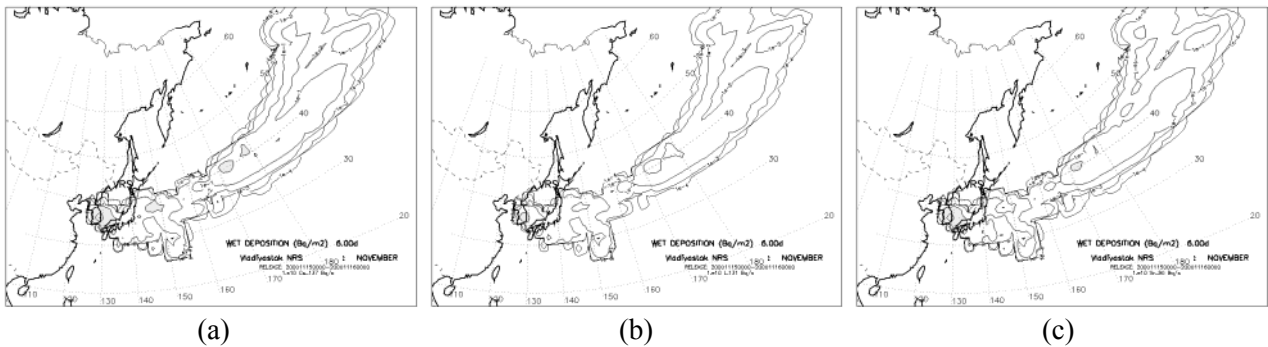


**Figure 2.7.9.** Wet deposition fields of a)  $\text{Cs}^{137}$ , b)  $^{131}\text{I}$  and c)  $^{90}\text{Sr}$  for the “unit hypothetical release” occurred at the Vladivostok NRS during 15-16 Nov, 2000, 00 UTC.

**Table 2.7.3.** Calculated deposition characteristics for the selected geographical regions of interest and locations/sites for the “unit hypothetical release” occurred at the Vladivostok NRS during 15-16 Nov, 2000, 00 UTC.

Characteristic Units Radionuclide	Integral Concentration			Dry Deposition			Wet Deposition		
	Bq·h/m <sup>3</sup>			Bq/m <sup>2</sup>			Bq/m <sup>2</sup>		
	Cs <sup>137</sup>	<sup>131</sup> I	<sup>90</sup> Sr	Cs <sup>137</sup>	<sup>131</sup> I	<sup>90</sup> Sr	Cs <sup>137</sup>	<sup>131</sup> I	<sup>90</sup> Sr
<b>Regions</b>									
<i>Alaska State</i>	-2(-4)	-3(-5)	-2(-4)	-1(-4)	-2(-4)	-1(-4)	-3(-5)	-4(-6)	-3(-5)
<i>Aleutian Islands</i>	-1(-3)	-2(-4)	-1(-3)	0(-2)	0(-2)	0(-2)	-2(-3)	-2(-4)	-2(-4)
<i>North Japan</i>	0(-1)	0(-1)	0(-1)	+1(0)	+1(0)	+1(0)	-1(-2)	-2(-2)	-1(-2)
<i>Central Japan</i>	+1(+1)	+1(0)	+1(+1)	+2(+1)	+2(+2)	+2(+2)	-1(-1)	-2(-2)	-1(-1)
<i>South Japan</i>	+1(+1)	+1(0)	+1(+1)	+2(+1)	+2(+2)	+2(+2)	0(0)	0(-1)	0(-1)
<i>North Korea</i>	+2(+1)	+1(+1)	+2(+1)	+3(+2)	+3(+2)	+3(+2)	0(-1)	-1(-2)	0(-1)
<i>South Korea</i>	+2(+1)	+1(+1)	+2(+1)	+2(+2)	+2(+2)	+2(+2)	+1(0)	0(-1)	0(0)
<i>North-East China</i>	-6(-8)	-7(-8)	-6(-8)	-5(-7)	-5(-7)	-5(-7)	-5(-7)	-6(-8)	-5(-7)
<i>Seashore China</i>	-2(-4)	-3(-5)	-2(-4)	-1(-4)	-2(-4)	-1(-4)	-6(-8)	-6(-9)	-6(-8)
<b>Sites</b>									
<i>Vladivostok NRS</i>	+1	+1	+1	+1	+2	+1	-9	-10	-9
<i>Fukuoka</i>	-1	0	+1	+1	+1	+1	0	-1	0
<i>Sapporo</i>	-2	-2	-2	-1	-1	-1	-7	-8	-7
<i>Tokyo</i>	0	0	0	+1	+1	+1	-1	-2	-1
<i>Pyongyang</i>	-1	-1	-1	0	0	0	-2	-3	-2
<i>Seoul</i>	+1	+1	+1	+2	+2	+2	0	-1	0

For the Vladivostok NRS, as shown in Table 2.7.3, the order of magnitude for the integral concentration and dry deposition is +1, although for wet deposition it is -9 (which reflects the fact that precipitation did not play a significant role near the site). For  $^{131}\text{I}$ , wet deposition is by an order

of magnitude lower than for Cs<sup>137</sup> and <sup>90</sup>Sr, but dry deposition is higher by an order of magnitude for the same two radionuclides. For all other Japanese and Korean locations/sites, the integral concentration and dry deposition patterns have the same orders of magnitude for all radionuclides, although for <sup>131</sup>I wet deposition is lower by an order of magnitude.

However, the exact values for these locations can vary significantly. For example, the integral concentration in Seoul (South Korea) is 4.5 times higher than in Fukuoka (Japan) – 6.8E+01 vs. 1.5E+01 Bq·h/m<sup>3</sup>. Therefore, if sites of interest are located not far from NRS (i.e. on a regional scale), it will be also important to consider difference in exact values of characteristics. If sites of interest are located far from NRS (i.e. on a large or global scale), then difference in orders of magnitude will be sufficient because uncertainties in modeling of transport, dispersion, and deposition will increase significantly with a time and distance from NRS.

For the locations/sites of the State of Alaska (shown in Table 2.7.1), the order of magnitude for integral concentration, dry and wet depositions is lower than -8, and therefore, should be considered as negligible.

## CONCLUSIONS

The main aim of this study is to combine atmospheric transport and dispersion modeling and statistical analyses with the radiological assessment to evaluate consequences of an accidental release at the nuclear risk sites located at the Russian Far East. The main purpose of this study is a probabilistic analysis of atmospheric transport and deposition patterns from selected nuclear risk sites for the GIS-based studies of vulnerability to radioactive deposition and risk assessment of the nuclear risk sites impact.

The nuclear risk sites of concern selected in this study are the Kamchatka (52°55'N & 158°30'E) and Vladivostok (42°55'N & 132°25'E) nuclear risk sites. The countries and geographical regions of interest are Japan, China, North and South Korea, territories of the Russian Far East, State of Alaska, and Aleutian Chain Islands.

Once the nuclear risk sites and geographical region of interest are defined, it is of particular interest to answer the following questions: Which geographical territories are at highest risk from accidental releases at NRSs? What are probabilities for radionuclide atmospheric transport and deposition on different neighbouring countries in case of accidents at NRSs?

To answer these questions we applied several research tools utilized within the Arctic Risk NARP Project (*AR-NARP, 2001-2003*). The first research tool is an isentropic trajectory model to calculate a multiyear (1987-1996) dataset of 5-day forward trajectories that originated over the NRS locations at various altitudes. The second research tool is the long-range transport model to simulate 5-day atmospheric transport, dispersion, and deposition of  $^{137}\text{Cs}$  for one-day release (at the rate of  $10^{10}$  Bq/s). As input data we used NCAR and ECMWF meteorological gridded fields for trajectory and dispersion modeling, respectively. The third research tool is a set of statistical methods (including exploratory, cluster, and probability fields analyses) for analysis of trajectory and dispersion modeling results. Additionally, several specific dates when atmospheric transport occurred towards the geographical regions of interest were also evaluated for both NRSs.

The results of probabilistic analysis of trajectory and dispersion modeling results for the selected sites are presented as a set of various indicators of the NRS possible impact on the geographical regions of interest. In this study, we calculated, constructed, and evaluated several indicators based on trajectory modeling results. They are: 1) atmospheric transport pathways, 2) airflow probability fields, 3) fast transport probability fields, 4) maximum reaching distance, 5) maximum possible impact zone, 6) relative humidity or precipitation factor fields, and 7) typical transport time fields. Similarly, we considered several indicators based on dispersion modeling results: 1) surface air concentration, 2) integrated over time concentration at the ground surface, 3) dry deposition, and 4) wet deposition. To evaluate the temporal variability of these indicators, analyses were performed on an annual, seasonal, and monthly basis.

The main results of this study are the following:

### **BASED ON TRAJECTORY MODELING RESULTS:**

**For the Kamchatka and Vladivostok NRSs,** the westerly flow is dominant throughout the year (more than 60% of the time) in the boundary layer. At altitudes of the free troposphere, the probability of transport from the west increases up to 85% of the time. The relatively rapid westerly flow toward the North American continent reaches a maximum during fall-winter (8-11% of the time) and during winter-spring (12-13% of the time) for the Kamchatka and Vladivostok NRSs, respectively.

### **For the Vladivostok NRS:**

- € The North China and North Japan regions are at the highest risk of possible impact in comparison with other regions.
- € The lower (and upper) bounds of the NRS possible impact are about of 32 (54) and 35 (87)% for the North China and North Japan regions, respectively.
- € On average, atmospheric transport to these regions could occur in 0.5 and 1.6 days, respectively. The fast transport events (in less than one day) could represent major concerns for the Japanese and North Korean regions, but such events are not common for the US territories.
- € On average, the annual typical transport times to reach the North Japan, North and South Korea are about 1, 1.5, and 2 days, respectively.
- € Although total maximum area, which might be affected during the first day of atmospheric transport after an accidental release, varies throughout the year, on average annually it is more than 5060 th.km<sup>2</sup>. From this potentially affected area, only 250 th.km<sup>2</sup> is a territory where there is the highest probability of the NRS possible impact. The area's boundaries are extended mostly in the southeastern and eastern directions from the site. Moreover, this area is a maximum in October and a minimum in January - 290 and 160 th.km<sup>2</sup>, respectively.

### **For the Kamchatka NRS:**

- € The US territories are at the highest risk compared to the rest of the regions.
- € The lower (and upper) bounds of the NRS possible impact are about of 30 (54) and 13 (32)% for the Aleutian Chain Islands and State of Alaska, respectively.
- € On average, atmospheric transport to these regions could occur in 3.0 and 5.1 days, respectively.
- € On average, annual typical transport time to reach islands of the Aleutian Chain Islands is 2.5 days, although during winter it is 1.5 days.
- € Although total maximum area, which might be affected during the first day of atmospheric transport after an accidental release, varies throughout the year, on average annually it is more than 6760 th.km<sup>2</sup>. From this potentially affected area, only 300 th.km<sup>2</sup> is territory, where there is the highest probability of the NRS possible impact. The area's boundaries are extended mostly in the eastern direction from the site. Moreover, this area is a maximum in May and a minimum in January - 340 and 190 th.km<sup>2</sup>, respectively.

### **BASED ON DISPERSION MODELING RESULTS:**

**For the Vladivostok and Kamchatka NRSs**, the integral concentration and dry deposition fields have higher values in vicinity of the sites, and it decreases significantly with a distance. Moreover, both types of fields have an elliptical form. The shape of these fields, in some way, reflects the dominating airflow patterns throughout the year. For both NRSs these fields show the prevailing atmospheric transport by westerly flows.

Although wet deposition is also high near the sites, the field is less smooth and it has a cellular structure, which is strongly dependent on irregularity of the rainfall pattern. It is interesting to note, that over some geographical areas the wet deposition is higher by an order of magnitude in comparison with dry deposition, which is also a reflection of irregularity in the rainfall patterns.

**For the Vladivostok NRS**, the integral concentration during October-November and March, at the seashore of China is  $10^{-1}$  Bq·h/m<sup>3</sup>. During March-April and October-December, along the Aleutian Chain Islands it is about  $10^{-1}$  Bq·h/m<sup>3</sup>. During October-April, over the Japanese territories it is higher than  $10^{+1}$  Bq·h/m<sup>3</sup>.

The dry deposition during October-March, over the Japanese territories is higher than  $10^{+2}$  Bq/m<sup>2</sup>. During December-February and October-November, the populated territories with deposition higher than  $10^1$  Bq/m<sup>2</sup> are situated to southeast and southwest of the site, respectively.

The total area where wet deposition is higher than  $10^0$  Bq/m<sup>2</sup> is larger during November-April in comparison with other months. The Japanese territories are minimally affected by wet deposition during July, and highly affected during September-April.

**For the Kamchatka NRS**, the integral concentration during October-March and August, at the western shore of the State of Alaska is  $10^0$  Bq·h/m<sup>3</sup>. During January-May and September, the integral concentration over the northern territories of Japan is  $10^{-1}$  Bq·h/m<sup>3</sup>, although in other months these territories appear unaffected.

The dry deposition during March, July, and September, at the western shore of the State of Alaska is  $10^{-1}$  Bq/m<sup>2</sup>. During June-August and October-November, the territory of Japan appears unaffected, although in other months there might be deposited up to  $0.5 \cdot 10^{+1}$  Bq/m<sup>2</sup> at any average given day of a month. During January, over the northeastern territories of China it is  $10^1$  Bq/m<sup>2</sup>.

The total area of the wet deposition field increases significantly during November-February reaching a maximum in December, with a flat minimum during summer months. During winter months, there are local maxima of wet deposition over the Russian Far East and State of Alaska territories. During summer months, the wet deposition field is more extended toward the northeastern direction from the site, although in other months it appeared to be more in the eastern direction. This field diminishes significantly during June-September. Moreover, during January the large area of the continental Asian part of Russia is also affected by wet deposition.

Analysis of the specific cases, when atmospheric transport from the sites toward the regions of interest occurred, showed several common peculiarities. First, shapes and magnitude of isolines are almost similar for both <sup>137</sup>Cs and <sup>90</sup>Sr time integral concentration and dry deposition fields. Both fields are relatively well correlated. Second, <sup>131</sup>I surface air concentration decreases faster with a distance from the site in comparison with <sup>137</sup>Cs and <sup>90</sup>Sr due to radioactive decay and greater propensity to serve as condensation nuclei. Third, the wet deposition fields for selected specific cases showed a similar structural irregularity of fields (as monthly and seasonal variability) in comparison with integral concentration and dry deposition fields.

### **APPLICABILITY OF RESULTS:**

The results of this study are applicable for: (i) better understanding of general atmospheric transport patterns in the event of an accidental release at NRSs, (ii) improvement of planning in emergency response to radionuclide releases from the NRS locations, (iii) studies of social and economical consequences of the NRS impact for population and environment of the neighbouring countries, (iv) multidisciplinary risk evaluation and vulnerability analysis, and (v) probabilistic assessment of radionuclide meso-, regional-, and long-range transport patterns.

The WWW-variant of this report is also available on CD (enclosed with this report with enlarged figures, if ordered) and includes archives of calculated results.

## RECOMMENDATIONS AND FUTURE STUDIES

Several concluding remarks and recommendations should be made to clarify applicability and importance of the obtained results. These results constitute initial steps to estimate atmospheric transport and deposition from two selected nuclear risk sites – Kamchatka and Vladivostok - located in the Russian Far East. In the event of an accidental release these results can be used as a preliminary estimation of likelihood and direction of the atmospheric transport, evaluation of minimum and average transport times, and identification of predominant atmospheric layer during transport reaching the borders of counties, countries, and remote geographical regions. They also can be used to estimate possible order of magnitudes for time-integrated concentration, and dry and wet deposition patterns at exact locations or for geographical territories of concern. Using calculated concentration and deposition fields it is possible to evaluate doses due to inhalation and from the underlying contaminated surfaces accumulated or averaged over the year, season, or month.

Emergency response plans to possible radionuclide releases from the nuclear risk sites could be improved by analyses of probabilities for the fast transport, airflow patterns, typical transport time, maximum reaching distance and maximum possible impact zone indicators. Valuable indicators of the NRS possible impacts will be given by the temporal variability of the radionuclide time-integrated concentration, dry, wet, and total deposition at various distances from the sites. These are input to better understanding of seriousness of possible consequences of radionuclide releases from the nuclear risk sites. This study output is valuable input data for studies of social and economical consequences for population and environment of the neighbouring countries, and especially, on a regional scale due to impact of accidents at NRSs. These results are also important data for studies of multidisciplinary risk and vulnerability, and probabilistic assessments of the radionuclide meso-, regional-, and long-range transport.

Moreover, we suggest that the developed methodology within the Arctic Risk NARP Project (*AR-NARP, 2001-2003*) and used in the RAD FARECS study might be successfully applied for other risk sites of concern such as chemical and biological.

Therefore, we recommend further studies on the following issues:

- 1) The analysis of the atmospheric transport and deposition patterns for the Vladivostok and Kamchatka NRS raises a concern of the possible fast transport as well as radionuclide deposition in the neighbouring countries such as Japan, Korea, China, Russia, and USA. Therefore, (see Appendix A) as a logical step to finalize this study we propose to evaluate: i) risks, socio-economical and geographical consequences for different geographical areas and population groups applying available demographic databases and GIS-technology, and ii) vulnerability to a radioactive deposition with a focus on the transfer of certain radionuclides into food-chains, especially for the native population, and considering risks for different geographical areas. Such analysis can provide a complete estimate of nuclear risk and regional vulnerability for geographical territories, countries, counties, and population groups in the North Pacific region due to possible accidental releases at these NRSs.
- 2) It should be mentioned that there are other nuclear risk sites in the North Pacific region: nuclear weapons-related facilities and nuclear fuel reprocessing facilities located in the northern regions of China and Japan, respectively. An approach similar to used in this study could be applied for these sites too. In addition, because there is a high monthly variability in the airflow patterns from the sites to the regions of interest, we suggest investigating

possible impacts of the NRS accidental releases using the source (nuclear risk site) vs. receptor (remote geographical location or region) relationship approach. For this purpose, the additional sensitivity of source vs. receptor indicators might be introduced (see Appendix B) for evaluation of the possible NRS impact. For example, with respect to the US concern about atmospheric transport toward the North American continent, several receptor point locations within the Pacific region north of the equator might be selected for such a study: Barrow, Nome, Anchorage, Shemya, Midway, Mauna Loa, Guam, as well as sites along the US Western Coast.

- 3) For some countries, which are located not far from the nuclear risk sites (for example, Vladivostok NRS vs. Korea, Japan, China, and Russia) another approach consisted of both the 3-d atmospheric transport, dispersion, and deposition of radionuclides model as well as statistical model might be applied (see Appendix C). The suggested approach is more useful for evaluation of the territorial risk on the local- and regional scales due to accidental releases at the nuclear risk sites.
- 4) There is a large number of radiation risk sources located in the countries of the North Pacific region. These sources represent risks of different magnitude, and their “possible danger” is highly dependent on many factors. In general, the simplest approach depends on the knowledge of the source term. But it seems reasonable to ask: What is the ranging of each radiation risk source with respect to another source as well as due to other factors? As a first step, an evaluation of the probability matrix for the transport pathways in different environments, fast transport, and removal processes might give an answer to this question. For comprehensive evaluation, the additional factors such as probabilities of the accidental releases, prevailing scenarios, accumulated activities, types of radioactive material, etc. should be considered too. Such analysis might rank the risk sources in the order of their potential danger with respect to population and environment of different territories. This allows the policy and decision makers to make an informed decision about: which sources should be considered as the first priority of study, and what measures should be taken if an accidental release will occur. Of course, for an accident, the detailed examination of the conditions at the site, the accident scenario and actual atmospheric conditions must be taken into account.

## ACKNOWLEDGMENTS

The authors are grateful to Drs. Leif Laursen (Danish Meteorological Institute, Copenhagen), Olga Rigina (Geographical Institute, Copenhagen University, Denmark), Ronny Bergman (Swedish Defence Research Authority, FOI, Umeå), Sergey Morozov (Institute of Northern Environmental Problems, Kola Science Center, Apatity, Russia), Boris Segerstahl (Thule Institute, University of Oulu, Finland), John Merrill (University of Rhode Island, Graduate School of Oceanography, Narragansett, RI, USA), Sven Nielsen (Risø National Laboratory, Denmark), Robert Andres (University of North Dakota, Space Studies Department, Grand Forks, ND, USA), and Steen C. Hoe (Danish Emergency Management Agency, DEMA) for collaboration, discussions, and constructive comments.

The computer facilities at the Danish Meteorological Institute (DMI, Copenhagen, Denmark), International Institute for Applied Systems Analysis (IIASA, Laxenburg, Austria), National Center for Atmospheric Research (NCAR, Boulder, CO, USA), and Vanderbilt University (Nashville, TN, USA) had been used extensively in the study. The meteorological data archives from the DMI, ECMWF, and NCAR facilities were used as input in the dispersion and trajectory modeling. Thanks to Dr. Bjarne Amstrup (DMI) for data preparation.

Thanks to Drs. William Hamilton (Department of Civil and Environmental Engineering, Vanderbilt University, Nashville, TN, USA) and Ann Clarke (ANC Associates, Inc., Brentwood, TN, USA) for running the cluster analysis at the Vanderbilt University computer facilities. Thank you to Ulli Neudeck (IIASA) and Bente Elise Andersen (DMI) for taking care of the administrative issues.

The authors are grateful to Dr. Jess Jørgensen (HIRLAM group, DMI), Peter Teisner (Computer Services, DMI); Assen Novatchkov, Helmut Klarn, Jaroslav Chovanec, and Serge Medow (Computer Services, IIASA), and Ginger Caldwell (Scientific Computing Division, NCAR) for the collaboration, computer assistance, and advice. Thanks to the computer consulting services at DMI, IIASA, and NCAR.

The following software products have been used in this study: IDL, Matlab, SPSS, SAS, GMT, NCAR Graphics.

The financial support for 2001 included grants of the Swedish Research Council for Environment, Agricultural Sciences and Spatial Planning (FORMAS), and the United States Department of Energy (US DOE). The financial support for 2002 included grants of the Vanderbilt University (Nashville, USA), and the United States Department of Defense (US DOD).

The views and opinions of the authors expressed in this publication do not necessarily reflect or state those of the sponsoring agencies or their institutions.

## REFERENCES

- AR-NARP, **2001-2003**: On-going Project Atmospheric Transport Pathways, Vulnerability and Possible Accidental Consequences from the Nuclear Risk Sites in the European Arctic (*Arctic Risk*) of the NARP: Nordic Arctic Research Programme. Leader: Dr. Alexander Baklanov, [alb@dmi.dk](mailto:alb@dmi.dk).
- Baker, W., ed. **1992**: Research Highlights of the NMC Development Division: 1989-1991; NOAA, 469 pp.
- Baklanov A., R. Bergman, C. Lundström and L. Thaning. **2001**: *Modeling of episodes of atmospheric transport and deposition from hypothetical nuclear accidents on the Kola peninsula*. CERUM Northern Studies No. 23. Umeå university, Sweden.
- Baklanov A., R. Bergman, B. Segerstahl, L. Thaning, **1996**: Assessment of Risk of Airborne Radioactive Contamination from Nuclear Units in North-West Russia. IIASA Research Report, XP-96-043.
- Baklanov, A. A., A. G. Mahura and S. V. Morozov, **1994**: The Simulation of Radioactive Pollution of the Environment After an Hypothetical Accident at the Kola Nuclear Power Plant. *J. Environmental Radioactivity*, **25**: 65-84.
- Baklanov, A., A. Mahura, D. Jaffe, L. Thaning, R. Bergman, R. Andres. **2001**: Atmospheric Transport Patterns and Possible Consequences for the European North after a Nuclear Accident. *Journal of Environment Radioactivity*, Vol. 60, Issue 1-2, pp. 1-26.
- Baklanov, A., A. Mahura, D. Jaffe, L. Thaning, R. Bergman, R. Andres, J. Merrill, **1998**: Atmospheric Transport Pathways and Possible Consequences after a Nuclear Accident in North-West Russia. *The 11th World Clear Air and Environment Congress*. S. Africa, Durban. 14-18 September 1998. Volume 2. E6-1: 6 pp.
- Baklanov A., Mahura A., **2001**: Atmospheric Transport Pathways, Vulnerability and Possible Accidental Consequences from Nuclear Risk Studies: Methodology for Probabilistic Atmospheric Studies. *Danish Meteorological Institute Scientific Report*, 01-09, ISBN: 87-7478-450-1, 43 p.
- Baklanov, A. and J.H. Sørensen, **2001**: Parameterisation of radionuclide deposition in atmospheric dispersion models. *Phys. Chem. Earth, (B)*, **26**, 787-799.
- Baklanov A., Mahura A., Sorensen J.H., Rigina O. **2002a**: Methodology for Risk Analysis based on Atmospheric Dispersion Modelling from Nuclear Risk Sites in Northern Europe. *Danish Meteorological Institute Scientific Report*, 55 p., (*in preparation*), Summer-Fall 2002.
- Baklanov A., Mahura A., Rigina O. **2002b**: Nuclear Risk and Vulnerability in the Arctic: New Method for Multidisciplinary Assessments. *Extended Abstracts of the Environmental Radioactivity in the Arctic & Antarctic Conference*, S-Petersburg, Russia, 16-20 June 2002, 4 p.
- Baklanov A., Mahura A., Rigina O. **2002c**: Nuclear Risk and Vulnerability: Approach for Multidisciplinary Assessments. *Extended Abstracts of the International Conference on Radioactivity in the Environment*, Principality of Monaco, 2-5 September 2002, 5 pp.
- Bergman, R., A. Baklanov, B. Segerstahl **1996**: Integrated Regional Risk Assessment: The Case of Radioactive Contamination on the Kola Peninsula. In: *Risk in a Modern Society: Proceedings of the 1996 Annual Meeting of the Society for Risk Analysis - Europe*, 3-5 June, University of Surrey, UK, pp. 221-224. (IIASA Research Report: XP-96-044)
- Bergman, R. & Baklanov, A. **1998**: *Radioactive sources in main radiological concern in the Kola-Barents region*. FRN-FOA publication, Stockholm, July 1998. 82 p.
- Bergman, R., Thaning, L. & Baklanov, A., **1998**: Site-sensitive hazards of potential airborne radioactive release from sources on the Kola Peninsula. FOA report: FOA-R—00717-861--SE, February 1998, 14 pp.
- Draxler, R. **1987**: Sensitivity of the trajectory model to the spatial and temporal resolution of the meteorological data during CAPTEX. *Journal of Climatology and Applied Meteorology*, **26**, pp. 1577-1588.
- INTAS, **2000**: Assessment of Potential Risk of Environmental Radioactive Contamination in Northern Europe from Terrestrial Nuclear Units in North-West Russia. Research Report, INTAS Project 96-1802, Research Report, 125 p., November 2000
- Jaffe, D, Mahura, A & Andres, R, **1997a**: Atmospheric Transport Pathways to Alaska from Potential Radionuclide Sites in the Former Soviet Union. *Research Report*, UAF-ADEC Joint Project 96-001, p 71.

- Jaffe, D, Mahura, A, Andres, R, Baklanov, A, Thaning, L, Bergman, R and Morozov, S, **1997b**: Atmospheric Transport from the Kola Nuclear Power Plant. *Research Report*, UAF-FOA-BECN Joint Project, BECN: Tromsø University, Norway, Fall 1997, 61 pp.
- Mahura, A., Jaffe D., Andres, R., Dasher, D., Merrill, J. **1997a**: Atmospheric Transport Pathways to Alaska from Potential Radionuclide Sites in the Former Soviet Union. Proceedings of ANS *Sixth Topical Meeting on Emergency Preparedness and Response*, San Francisco, California, April 1997, Vol 1, p 173-174.
- Mahura, A., Jaffe D., Andres, R., Dasher, D., Merrill, J. **1997b**: Atmospheric Transport Pathways from the Kola Nuclear Power Plant. Extended abstracts of Intentional Symposium on Environmental Pollution of the Arctic and The Third International Conference on *Environmental Radioactivity in the Arctic*, Tromsø, Norway, June 1-5, 1997, Vol 2, p 52-54.
- Mahura A., D.Jaffe & R.Andres **1999a**: Air Flow Patterns and Precipitation Probability Fields for the Kola NPP. Abstracts of the International Conference "*Nuclear Risks, Environmental and Development Cooperation in the North of Europe*", Apatity, Russia, 19-23 June 1999, pp. 87-93.
- Mahura, A.G., Jaffe, D., Andres, R. & Merrill, J. **1999b**: Atmospheric transport pathways from the Bilibino nuclear power plant to Alaska. *Atmospheric Environment*, 33/30, 5115-5122.
- Mahura A., Andres R., Jaffe D. **2001**: *Atmospheric transport patterns from the Kola Nuclear Reactors*. CERUM Northern Studies No. 24. Umeå university, Sweden. 33 p.
- Mahura A., **2002**: Assessment of Impact of Russian Nuclear Fleet Operations on Russian Far Eastern Coastal Regions. *IISA interim report IR-02-004*, 76 p., Jan 2002.
- Mahura, A., Baklanov, A., Sørensen, J. H., **2002a**: Methodology for Evaluation of Possible Consequences of Accidental Atmospheric Releases of Hazardous Matter. Accepted to publication in the *Rad Prot Dosim*, ref#2154.
- Mahura A., Baklanov A., Rigina O., Parker F. **2002b**: Statistical Analysis of Atmospheric Transport from the Nuclear Risk Sites in the Arctic Region. *Extended Abstracts of the Environmental Radioactivity in the Arctic & Antarctic Conference*, S-Petersburg, Russia, 16-20 June 2002, 4 p.
- Mahura A., Baklanov A., Rigina O. **2002c**: Probabilistic Analysis of Atmospheric Transport Patterns from Nuclear Risk Sites in Northern Europe. *Danish Meteorological Institute Scientific Report*, 80 p., (in preparation), Sum 2002.
- Mahura A., Baklanov A. **2002**: Evaluation of Source-Receptor Relationship for Pollutants Using Probability Fields Analysis. *Danish Meteorological Institute Scientific Report*, 67 p., (in preparation), Summer-Fall 2002.
- Merrill J., Bleck R. and Boudra D.B., **1985**: Techniques of Lagrangian Trajectory Analysis in Isentropic Coordinates. *Monthly Weather Review*, Vol 114, pp 571-581.
- Romanova V., M. Takano, **2002**: Atmospheric Transport of Radioactive Nuclides from Russia to Neighbouring Countries. *IISA interim report IR-02-010*, 26 p., Jan 2002.
- Randel, W. **1992**: Global Atmospheric Circulation Statistics, 1000-1mb; NCAR Technical Note TN-366+STR, 256 pp.
- Rigina, O. & Baklanov, A. **2002**: Regional radiation risk and vulnerability assessment by integration of mathematical modeling and GIS-analysis. *J. Environment International*, Vol. 27, No 6. pp. 1-14.
- Sass, B. H., Nielsen, N. W., Jørgensen, J.U., Amstrup, B., and Kmit, M., 2000: The operational HIRLAM system, *DMI Technical report 00-26*. Copenhagen, Denmark. <http://www.dmi.dk/f+u/publikation/tekrap/2000/Tr00-26.pdf>.
- Stohl A. **1998**: Computation, accuracy and applications of trajectories - A review and bibliography. *Atmospheric Environment*, Vol 32, Iss 6, pp. 947-966
- Sørensen, J.H. **1998**: Sensitivity of the DERMA Long-Range Gaussian Dispersion Model to Meteorological Input and Diffusion Parameters. *Atmos. Environ.* 32, 4195-4206
- Sørensen, J.H., L. Laursen and A. Rasmussen, **1994**: Use of DMI-HIRLAM for operational dispersion calculations, in: *Air Pollution Modeling and Its Application X*.
- Trenberth, K. and Olson, J. **1988**: Evaluation of NMC Global Analyses: 1979-1987; NCAR Technical Note TN-299+STR, 82 pp
- ÖCB, **2000**: Nuclear Risks, Environmental and Development Cooperation in the North of Europe. FRN publication, CERUM, University of Umea, Sweden. 240 p.

## **APPENDIXES**

- 1. MONTHLY VARIATIONS OF THE AIRFLOW PATTERNS**
- 2. MONTHLY VARIATIONS OF THE FAST TRANSPORT PATTERNS**
- 3. SEASONAL VARIATIONS OF THE TYPICAL TRANSPORT TIME PATTERNS**
- 4. MONTHLY VARIATIONS OF THE MAXIMUM POSSIBLE IMPACT ZONE AND MAXIMUM REACHING DISTANSE INDICATORS**
- 5. MONTHLY VARIATIONS OF THE AVERAGE INTEGRAL CONCENTRATION PATTERNS**
- 6. MONTHLY VARIATIONS OF THE AVERAGE DRY DEPOSITION PATTERNS**
- 7. MONTHLY VARIATIONS OF THE AVERAGE WET DEPOSITION PATTERNS**
  - A. APPROACH TO COMPLEX RADIATION RISK ASSESSMENT APPLYING GIS**
  - B. APPROACH TO PROBABILISTIC EVALUATION OF SOURCE-RECEPTOR RELATIONSHIP FOR NUCLEAR RISK SITES AND REMOTE TERRITORIES**
  - C. APPROACH TO PROBABILISTIC ASSESSMENT OF POTENTIAL TERRITORIAL RISK OF CONTAMINATION ON THE LOCAL SCALE**

# DANISH METEOROLOGICAL INSTITUTE

## Scientific Reports

Scientific reports from the Danish Meteorological Institute cover a variety of geophysical fields, i.e. meteorology (including climatology), oceanography, subjects on air and sea pollution, geomagnetism, solar-terrestrial physics, and physics of the middle and upper atmosphere.

Reports in the series within the last five years:

No. 97-1

**E. Friis Christensen og C. Skøtt:** Contributions from the International Science Team. The Ørsted Mission - a pre-launch compendium

No. 97-2

**Alix Rasmussen, Sissi Kiilsholm, Jens Havskov Sørensen, Ib Steen Mikkelsen:** Analysis of tropospheric ozone measurements in Greenland: Contract No. EV5V-CT93-0318 (DG 12 DTEE): DMI's contribution to CEC Final Report Arctic Tropospheric Ozone Chemistry ARCTOC

No. 97-3

**Peter Thejll:** A search for effects of external events on terrestrial atmospheric pressure: cosmic rays

No. 97-4

**Peter Thejll:** A search for effects of external events on terrestrial atmospheric pressure: sector boundary crossings

No. 97-5

**Knud Lassen:** Twentieth century retreat of sea-ice in the Greenland Sea

No. 98-1

**Niels Woetman Nielsen, Bjarne Amstrup, Jess U. Jørgensen:** HIRLAM 2.5 parallel tests at DMI: sensitivity to type of schemes for turbulence, moist processes and advection

No. 98-2

**Per Høeg, Georg Bergeton Larsen, Hans-Henrik Benzon, Stig Syndergaard, Mette Dahl Mortensen:** The GPSOS project Algorithm functional design and analysis of ionosphere, stratosphere and troposphere observations

No. 98-3

**Mette Dahl Mortensen, Per Høeg:** Satellite atmosphere profiling retrieval in a nonlinear troposphere Previously entitled: Limitations induced by Multipath

No. 98-4

**Mette Dahl Mortensen, Per Høeg:** Resolution properties in atmospheric profiling with GPS

No. 98-5

**R.S. Gill and M. K. Rosengren:** Evaluation of the Radarsat imagery for the operational mapping of sea ice around Greenland in 1997

No. 98-6

**R.S. Gill, H.H. Valeur, P. Nielsen and K.Q. Hansen:** Using ERS SAR images in the operational mapping of sea ice in the Greenland waters: final report for ESA-ESRIN's: pilot projekt no. PP2.PP2.DK2 and 2<sup>nd</sup> announcement of opportunity for the exploitation of ERS data projekt No. AO2..DK 102

No. 98-7

**Per Høeg et al.:** GPS Atmosphere profiling methods and error assessments

No. 98-8

**H. Svensmark, N. Woetmann Nielsen and A.M. Sempreviva:** Large scale soft and hard turbulent states of the atmosphere

No. 98-9

**Philippe Lopez, Eigil Kaas and Annette Guldborg:** The full particle-in-cell advection scheme in spherical geometry

No. 98-10

**H. Svensmark:** Influence of cosmic rays on earth's climate

No. 98-11

**Peter Thejll and Henrik Svensmark:** Notes on the method of normalized multivariate regression

No. 98-12

**K. Lassen:** Extent of sea ice in the Greenland Sea 1877-1997: an extension of DMI Scientific Report 97-5

No. 98-13

**Niels Larsen, Alberto Adriani and Guido DiDonfrancesco:** Microphysical analysis of polar stratospheric clouds observed by lidar at McMurdo, Antarctica

No.98-14

**Mette Dahl Mortensen:** The back-propagation method for inversion of radio occultation data

No. 98-15

**Xiang-Yu Huang:** Variational analysis using spatial filters

No. 99-1

**Henrik Feddersen:** Project on prediction of climate variations on seasonal to interannual timescales (PROVOST) EU contract ENV4-CT95-0109: DMI contribution to the final report: Statistical analysis and post-processing of uncoupled PROVOST simulations

No. 99-2

**Wilhelm May:** A time-slice experiment with the ECHAM4 A-GCM at high resolution: the experimental design and the assessment of climate change as compared to a greenhouse gas experiment with ECHAM4/OPYC at low resolution

No. 99-3

**Niels Larsen et al.:** European stratospheric monitoring stations in the Arctic II: CEC Environment and Climate Programme Contract ENV4-CT95-0136. DMI Contributions to the project

No. 99-4

**Alexander Baklanov:** Parameterisation of the deposition processes and radioactive decay: a review and some preliminary results with the DERMA model

No. 99-5

**Mette Dahl Mortensen:** Non-linear high resolution inversion of radio occultation data

No. 99-6

**Stig Syndergaard:** Retrieval analysis and methodologies in atmospheric limb sounding using the GNSS radio occultation technique

No. 99-7

**Jun She, Jacob Woge Nielsen:** Operational wave forecasts over the Baltic and North Sea

No. 99-8

**Henrik Feddersen:** Monthly temperature forecasts for Denmark - statistical or dynamical?

No. 99-9

**P. Thejll, K. Lassen:** Solar forcing of the Northern hemisphere air temperature: new data

No. 99-10

**Torben Stockflet Jørgensen, Aksel Walløe Hansen:** Comment on "Variation of cosmic ray flux and global coverage - a missing link in solar-climate relationships" by Henrik Svensmark and Eigil Friis-Christensen

No. 99-11

**Mette Dahl Meincke:** Inversion methods for atmospheric profiling with GPS occultations

No. 99-12

**Hans-Henrik Benzon; Laust Olsen; Per Høeg:** Simulations of current density measurements with a Faraday Current Meter and a magnetometer

No. 00-01

**Per Høeg; G. Leppelmeier:** ACE - Atmosphere Climate Experiment

No. 00-02

**Per Høeg:** FACE-IT: Field-Aligned Current Experiment in the Ionosphere and Thermosphere

No. 00-03

**Allan Gross:** Surface ozone and tropospheric chemistry with applications to regional air quality modeling. PhD thesis

No. 00-04

**Henrik Vedel:** Conversion of WGS84 geometric heights to NWP model HIRLAM geopotential heights

No. 00-05

**Jérôme Chenevez:** Advection experiments with DMI-Hirlam-Tracer

No. 00-06

**Niels Larsen:** Polar stratospheric clouds micro-physical and optical models

No. 00-07

**Alix Rasmussen:** "Uncertainty of meteorological parameters from DMI-HIRLAM"

No. 00-08

**A.L. Morozova:** Solar activity and Earth's weather. Effect of the forced atmospheric transparency changes on the troposphere temperature profile studied with atmospheric models

No. 00-09

**Niels Larsen, Bjørn M. Knudsen, Michael Gauss, Giovanni Pitari:** Effects from high-speed civil traffic aircraft emissions on polar stratospheric clouds

No. 00-10

**Søren Andersen:** Evaluation of SSM/I sea ice algorithms for use in the SAF on ocean and sea ice, July 2000

No. 00-11

**Claus Petersen, Niels Woetmann Nielsen:** Diagnosis of visibility in DMI-HIRLAM

- No. 00-12  
**Erik Buch:** A monograph on the physical oceanography of the Greenland waters
- No. 00-13  
**M. Steffensen:** Stability indices as indicators of lightning and thunder
- No. 00-14  
**Bjarne Amstrup, Kristian S. Mogensen, Xiang-Yu Huang:** Use of GPS observations in an optimum interpolation based data assimilation system
- No. 00-15  
**Mads Hvid Nielsen:** Dynamisk beskrivelse og hydrografisk klassifikation af den jyske kyststrøm
- No. 00-16  
**Kristian S. Mogensen, Jess U. Jørgensen, Bjarne Amstrup, Xiaohua Yang and Xiang-Yu Huang:** Towards an operational implementation of HIRLAM 3D-VAR at DMI
- No. 00-17  
**Sattler, Kai; Huang, Xiang-Yu:** Structure function characteristics for 2 meter temperature and relative humidity in different horizontal resolutions
- No. 00-18  
**Niels Larsen, Ib Steen Mikkelsen, Bjørn M. Knudsen m.fl.:** In-situ analysis of aerosols and gases in the polar stratosphere. A contribution to THESEO. Environment and climate research programme. Contract no. ENV4-CT97-0523. Final report
- No. 00-19  
**Amstrup, Bjarne:** EUCOS observing system experiments with the DMI HIRLAM optimum interpolation analysis and forecasting system
- No. 01-01  
**V.O. Papitashvili, L.I. Gromova, V.A. Popov and O. Rasmussen:** Northern polar cap magnetic activity index PCN: Effective area, universal time, seasonal, and solar cycle variations
- No. 01-02  
**M.E. Gorbunov:** Radiological methods for processing radio occultation data in multipath regions
- No. 01-03  
**Niels Woetmann Nielsen; Claus Petersen:** Calculation of wind gusts in DMI-HIRLAM
- No. 01-04  
**Vladimir Penenko; Alexander Baklanov:** Methods of sensitivity theory and inverse modeling for estimation of source parameter and risk/vulnerability areas
- No. 01-05  
**Sergej Zilitinkevich; Alexander Baklanov; Jutta Rost; Ann-Sofi Smedman, Vasilij Lykosov and Pierluigi Calanca:** Diagnostic and prognostic equations for the depth of the stably stratified Ekman boundary layer
- No. 01-06  
**Bjarne Amstrup:** Impact of ATOVS AMSU-A radiance data in the DMI-HIRLAM 3D-Var analysis and forecasting system
- No. 01-07  
**Sergej Zilitinkevich; Alexander Baklanov:** Calculation of the height of stable boundary layers in operational models
- No. 01-08  
**Vibeke Huess:** Sea level variations in the North Sea – from tide gauges, altimetry and modelling
- No. 01-09  
**Alexander Baklanov and Alexander Mahura:** Atmospheric transport pathways, vulnerability and possible accidental consequences from nuclear risk sites: methodology for probabilistic atmospheric studies
- No. 02-01  
**Bent Hansen Sass and Claus Petersen:** Short range atmospheric forecasts using a nudging procedure to combine analyses of cloud and precipitation with a numerical forecast model
- No. 02-02  
**Erik Buch:** Present oceanographic conditions in Greenland waters
- No. 02-03  
**Bjørn M. Knudsen, Signe B. Andersen and Allan Gross:** Contribution of the Danish Meteorological Institute to the final report of SAMMOA. CEC contract EVK2-1999-00315: Spring-to.-autumn measurements and modelling of ozone and active species
- No. 02-04  
**Nicolai Kliem:** Numerical ocean and sea ice modeling: the area around Cape Farewell (Ph.D. thesis)
- No. 02-05  
**Niels Woetmann Nielsen:** The structure and dynamics of the atmospheric boundary layer
- No. 02-06  
**Arne Skov Jensen, Hans-Henrik Benzon and Martin S. Lohmann:** A new high resolution method for processing radio occultation data
- No. 02-07  
**Per Høeg and Gottfried Kirchengast:** ACE+: Atmosphere and Climate Explorer

No. 02-08

**Rashpal Gill:** SAR surface cover classification using distribution matching

No. 02-09

**Kai Sattler, Jun She, Bent Hansen Sass, Leif Laursen, Lars Landberg, Morten Nielsen og Henning S. Christensen:** Enhanced description of the wind climate in Denmark for determination of wind resources: final report for 1363/00-0020: Supported by the Danish Energy Authority

No. 02-10

**Michael E. Gorbunov and Kent B. Lauritsen:** Canonical transform methods for radio occultation data

No. 02-11

**Kent B. Lauritsen and Martin S. Lohmann:** Unfolding of radio occultation multipath behavior using phase models

No. 02-12

**Rashpal Gill:** SAR image classification using fuzzy screening method

No. 02-13

**Kai Sattler:** Precipitation hindcasts of historical flood events

No. 02-14

**Tina Christensen:** Energetic electron precipitation studied by atmospheric x-rays

No. 02-15

**Alexander Mahura and Alexander Baklanov:** "Probabilistic analysis of atmospheric transport patterns from nuclear risk sites in Euro-Arctic Region"

No. 02-16

**A. Baklanov, A. Mahura, J.H. Sørensen, O. Rigina, R. Bergman:** Methodology for risk analysis based on atmospheric dispersion modelling from nuclear risk sites